© Copyright

by

Elizabeth Rita Hsu

2004

The Dissertation Committee for Elizabeth Rita Hsu

Certifies that this is the approved version of the following dissertation:

Fluorescence Contrast Agents and Spectroscopy for the Early Detection of Oral Cancer

Committee:

Rebecca Richards-Kortum, Supervisor

Eric Anslyn

Surangani Dharmawardhane

Ann Gillenwater

Krishnendu Roy

Fluorescence Contrast Agents and Spectroscopy for the Early Detection of Oral Cancer

by

Elizabeth Rita Hsu, B.S., M.S.

Dissertation

Presented to the Faculty of the Graduate School of
The University of Texas at Austin
in Partial Fulfillment
of the Requirements
for the Degree of

Doctor of Philosophy

The University of Texas at Austin

August, 2004

Dedication

To my family and to Micah, for their love and support through the years.

Acknowledgements

Completing a doctoral degree is not a solitary task, and there are many people who contributed to this dissertation. Heading the list is my advisor, Dr. Rebecca Richards-Kortum, who was always able to provide insight despite her busy schedule, and Dr. Ann Gillenwater, who provided tremendous clinical support. In addition, at some point in my research, I was able to turn to my remaining committee members, Drs. Eric Anslyn, Su Dharmawardhane, and Krish Roy, for advice and guidance in their area of expertise. The amount of support I received from every member of my committee is relatively unique, and a reflection of the increasing interdisciplinary nature of research

There are a number of people who provided me with technical support that I would also like to thank. Vivian Mack and Saima Ghori spent endless hours doing tissue culture to maintain cell lines for me and provided me with obscene numbers of cells on short notice. Under the guidance of Brette Luck, Jennifer Ming and Wendy Kuo wrote much of the Matlab code used for edge-detection and region-of-interest selection for mean fluorescence intensity calculations in the clinical study. Being able to conduct a clinical study in Houston from Austin was only made possible by the folks at M.D. Anderson Cancer Center, in particular Reza Alizadeh-Naderi and Dr. Qasim Hasan, who

handled many of the details. And without the training and support from John Mendenhall and Angela Bardo, I never would have been able to obtain confocal images. I also have to thank Kent Claypool, who performed the quantitative flow cytometry study, and Dr. Adel K. El-Naggar, for taking time out of his busy schedule to read the pathology for my clinical study.

I would also like to acknowledge the sources from which I received funding. These include the National Science Foundation Integrative Education and Research Traineeship, the University of Texas Continuing Fellowship, and the University of Texas College of Engineering Thrust Fellowship.

Lastly, I need to thank everyone who made the lab a fun place to work, despite the long hours in the windowless basement and late nights in the dark confocal room. This includes Kortum lab members, both past (otherwise known as the "hall of fame") and present, and other students in the Biomedical Engineering department. I fear if I attempt to list them all here, the acknowledgements section will be longer than the dissertation.

Fluorescence Contrast Agents and Spectroscopy for the Early Detection of Oral Cancer

Publication No._____

Elizabeth Rita Hsu, Ph.D.

The University of Texas at Austin, 2004

Supervisor: Rebecca Richards-Kortum

Despite advancements in treatment techniques, the five-year survival rate for oral cancer has not increased significantly over the past 40 years. This is likely due to the fact that oral cancer is generally not diagnosed until it has reached advanced stages when treatment is more difficult and debilitating and the five-year survival rate for patients is poor. Currently, diagnosis of oral cancer is achieved through visual identification and recognition, which relies on the expertise of the treating clinician.

Optical techniques could potentially improve diagnosis and detection of oral cancer by allowing objective assessment of the molecular and biochemical changes in neoplastic tissue relative to normal tissue. Successful application and validation of these

techniques will lead to better screening and early detection of premalignant lesions, reducing the incidence of cancer in high-risk individuals.

The work presented in this dissertation demonstrates the development of a molecular-specific fluorescent contrast agent in combination with fluorescence spectroscopy and confocal microscopy that could potentially be used as a diagnostic or screening technique in the oral cavity. The specificity of the contrast agent for epidermal growth factor receptor, a molecular marker overexpressed in oral cancer, was demonstrated using *in vitro* biological models, along with the ability to penetrate into multiple layers of epithelial cells using permeability-enhancing agents. The contrast agent was also evaluated in *ex vivo* biopsy samples, using fresh tissue slices from paired clinically abnormal and clinically normal biopsy samples. These experiments revealed that it may be possible to use the ratio of the mean fluorescence intensity from an abnormal to normal site or the surface mean fluorescence intensity as a diagnostic criteria to separate normal tissue from moderate dysplasia and cancer. The use of a simple spectroscopy system in conjunction with the contrast agent was also demonstrated, which would be ideal as an inexpensive diagnostic tool that could be used without specialized training. Finally, issues which must be considered for *in vivo* use of the contrast agent were explored. Together, the research presented in this dissertation lays the groundwork for the development of a tool that could be used in diagnosis of oral cancer.

Table of Contents

List of Tables xiv

List of Figures xvi

Chapter 1: Introduction 1

1.1 MOTIVATION 1

1.2 SPECIFIC AIMS 2

1.3 DISSERTATION OVERVIEW 4

Chapter 2: Background 5

2.1 INTRODUCTION 5

2.2 MOTIVATION 5

2.3 ANATOMY OF THE ORAL CAVITY 7

2.4 PATHOLOGY OF THE ORAL CAVITY 9

2.5 MOLECULAR MARKERS OF ORAL CANCER 13

2.5.1 Epidermal Growth Factor Receptor 15

2.5.2 Cytokeratins 18

2.5.3 Other Molecular Markers of Oral Neoplasia 21

2.6 CONTRAST AGENTS 23

2.6.1 Endogenous Fluorescence 23

2.6.2 Dyes 25

2.6.3 Target-specific Contrast Agents 27

2.6.4 Quantum Dots 29

2.7 OPTICAL DIAGNOSTIC TECHNIQUES OF ORAL NEOPLASIA 30

2.7.1 Optical Spectroscopy 30

2.7.2 Confocal Microscopy 35

2.8 PERMEABILITY-ENHANCING AGENTS 36

Chapter 3: A Far-Red Fluorescent Contrast Agent to Image Epidermal Growth Factor Receptor Expression 38

3.1 INTRODUCTION 38

3.2 MATERIALS AND METHODS 41

3.2.1 Contrast Agent 41

3.2.2 Cell Lines 42

3.2.3 Multilayer Tissue Constructs 43

3.2.4 Cell Monolayer Labeling 44

3.2.5 Multilayer Tissue Constructs Labeling 44

3.2.6 Fresh Tissue Slices 45

3.2.7 Imaging 45

3.2.8 Fluorometry 46

3.2.9 Quantitative Flow Cytometry 47

3.3 RESULTS 48

3.3.1 Detection of EGFR in Single Cell Monolayers 48

3.3.2 Detection of EGFR in Multilayer Tissue Constructs 51

3.3.3 Detection of EGFR in Fresh Tissue Slices 54

3.3.4 Fluorometry of Cells Labeled for EGFR 56

3.3.5 Quantitative Flow Cytometry 58

3.4 DISCUSSION 60

Chapter 4: Detection of Epidermal Growth Factor Receptor Expression in *Ex Vivo* Oral Cavity Biopsies Using a Molecular-Specific Contrast Agent **64**

4.1 INTRODUCTION 64

4.2 MATERIALS AND METHODS 66

4.2.1 Contrast Agent 66

4.2.2 Fresh Tissue Slices 66

4.2.3 Imaging 67

4.2.4 Image Processing 68

4.2.5 Diagnosis Using Mean Fluorescence Intensity 68

4.3 RESULTS 70

4.3.1 Overview of Patients 70

4.3.2 Fluorescence Confocal Imaging 72

4.3.3 Image Processing Example 80

4.3.4 Diagnosis Using Mean Fluorescence Intensity 83

4.4 DISCUSSION 87

Chapter 5: A Simple and Inexpensive Fluorescence Spectroscopy System Capable of Detecting a Molecular-Specific Contrast Agent for Diagnosis of Oral Neoplasia **94**

5.1 INTRODUCTION 94

5.2 MATERIALS AND METHODS 97

5.2.1 Spectroscopy System 97

5.2.2 Contrast Agent 100

5.2.3 Pre-labeled Mutlilayer Tissue Constructs 100

5.2.4 Multilayer Tissue Constructs Labeled in the Presence of Permeability-Enhancing Agents 101

5.2.5 Fresh Tissue Slices 101

5.2.6 Spectroscopy Measurements 102

5.2.7 Signal-to-Noise Ratio 103

5.3 RESULTS 103

5.3.1 System Characterization 103

5.3.2 Spectroscopy Measurements of Pre-labeled Multilayer Tissue Constructs 105

5.3.3 Spectroscopy Measurements of Multilayer Tissue Constructs Labeled in the Presence of Permeability-Enhancing Agents 109

5.3.4 Spectroscopy Measurements of Fresh Tissue Slices 114

5.4 DISCUSSION 116

Chapter 6: Considerations for *in vivo* Use of the Fluorescent Contrast Agent _ 122

6.1 INTRODUCTION _____ 122

6.2 MATERIALS AND METHODS _____ 123

6.2.1 Cytotoxicity, Two Day Incubation _____ 123

6.2.2 Cytotoxicity, Eleven Day Incubation _____ 124

6.2.3 Cytotoxicity, Recovery After Exposure _____ 124

6.2.4 Performance of Contrast Agent under Physiological Temperature _ 125

6.3 RESULTS _____ 125

6.3.1 Cytotoxicity of Alexa Fluor® 660 Streptavidin, Two Day Incubation 125

6.3.2 Cytotoxicity, Eleven Day Incubation _____ 125

6.3.3 Recovery After Exposure_____ 128

6.3.4 Performance of Contrast Agent under Physiological Temperature _ 129

6.4 DISCUSSION _____ 132

Chapter 7: Summary and Conclusions _____ 139

7.1 SUMMARY OF RESULTS _____ 139

7.2 FUTURE DIRECTIONS _____ 141

References _____ 145

Vita _____ 163

List of Tables

Table 2-1 Five-year survival rate of oral cancer as related to stage of tumor. 6

Table 2-2 Incidence of SCC by location in the oral cavity (3). 13

Table 2-3 Cytokeratins (CK) associated with different tissue types according to different studies. Results sited include Ogden *et al* (40), Sawaf *et al* (39), Morgan *et al* (41), Vaidya *et al* (42), Xu *et al* (43), Cema *et al* (44), and Kannan *et al* (45). An author's name in the + column indicates that the cytokeratin was associated with the tissue type by their study. An author's name in the – column indicates that the cytokeratin showed decreasing amounts or was not associated with the tissue type by their study. 20

Table 2-4 Summary of results of studies reviewed by Ramanujam evaluating fluorescence spectroscopy in the oral cavity for distinguishing carcinoma and dysplasia from normal tissue. The table includes the excitation and emission wavelengths used in analysis, the sample size (normal N and abnormal A samples), and the resulting sensitivity (SE) and specificity (SP). Table modified from (81).. 34

Table 4-1 Summary of patients in clinical study, site of biopsy, and pathological diagnosis of the clinically abnormal and normal biopsy. Abbreviations used include floor of mouth (FOM), buccal mucosa (BM), differentiated (diff), and moderate (mod). No diagnosis occurs when there is no epithelium in the sample and a pathological diagnosis cannot be made. A site in the center of the "site" column indicates that both the abnormal and normal biopsy were from the same site. 71

Table 4-2 Breakdown of biopsy samples by pathological diagnosis. 72

Table 5-1 Power in system after each optical component. 104

List of Figures

Figure 2-1 Cartoon drawing of the regions of the oral cavity. Figure modified from (10). 7

Figure 2-2 Progression from normal epithelium to invasive SCC. Recognized precursors include dysplasia and carcinoma in situ. The significance and relationship of benign keratosis in the transformation process is less well understood (3). 11

Figure 2-3 Cartoon of progression from normal through the stages of dysplasia to invasive carcinoma. Modified from (14). 12

Figure 2-4 Cancer development and progression. Identification of molecular makers early in the progression of cancer increases intervention efficacy and survival. Figure modified from (16). 14

Figure 2-5 Fluorescence excitation (a) and emission (b) spectra of various endogenous tissue fluorophores. From (55). 24

Figure 3-1 Confocal images of SqCC/Y1 and MDA-MB-435S cells taken with a 40x oil immersion objective. (a), (c), (e), and (g) are false color fluorescence images obtained at 50

Figure 3-2 False color confocal images of SqCC/Y1 tissue constructs labeled with anti-EGFR and Alexa Fluor® 660 streptavidin in the presence of permeability-enhancing 52

Figure 3-3 False color confocal images of SqCC/Y1 tissue constructs labeled with anti-human IgG and Alexa Fluor® 660 streptavidin in the presence of permeability-

enhancing agents taken with a 10x objective. The scale bar in both images is 100 μm. (a) Tissue construct labeled in the presence of 10% PVP. (b) Tissue construct labeled in the presence of 4% BSA. 53

Figure 3-4 Confocal images of SqCC/Y1 tissue constructs labeled with anti-EGFR and Alexa Fluor® 660 streptavidin taken with a 40x oil immersion objective. (a) and (c) are false color fluorescence images obtained at excitation 647 nm with a 665 nm longpass filter. (b) and (d) are transmitted DIC images. Scale bar in all images is 25μm. (a) and (b) Tissue constructs labeled in the presence of PBS only. (c) and (d) Tissue constructs labeled in the presence of 5% DMSO. 54

Figure 3-5 Confocal images of tissue slices from a (a) clinically abnormal and (b) clinically normal biopsy pair and corresponding H&E images ((c) and (d) respectively). Confocal images taken with a 40x oil immersion objective; scale bar is 25 μm. H&E images taken with a 10x objective. Abnormal biopsy taken from the retromolar trigone. Diagnosis of (c) was moderate dysplasia in the epithelium with foci of moderately-differentiated cancer. Normal biopsy taken from the pharyngeal wall. Diagnosis of (d) was normal with mild hyperkeratosis. 55

Figure 3-6 (a) Fluorescence intensities for SqCC/Y1 cells labeled for various incubation times using a 1:10 antibody dilution averaged over three trials. (b) Fluorescence intensities for SqCC/Y1 cells labeled with different dilutions of antibody using a 60 min incubation time averaged over three trials. In both graphs, the PBS background and background produced by the supernatant of the cell suspension has been

corrected for in all samples. The squares are cells labeled using EGFR, corrected for the background intensity of cells by subtraction of the IgG sample. The diamonds are cells labeled using the IgG control. 57

Figure 3-7 Fluorescence intensities for SqCC/Y1 cells labeled with the contrast agent in the presence of no EGF, 0.0133 μM EGF, 0.133 μM EGF, and 1.33 μM EGF averaged over three trials. All samples are corrected for the PBS background and background produced by the supernatant of the cell suspension. 58

Figure 3-8 Standard curve generated by quantitative flow cytometry data, plotting the number of monoclonal antibody immobilized on the bead versus the mean fluorescence intensity determined by flow cytometry (black diamonds). The mean fluorescence intensity for each of the cells lines, SqCC/Y1 (pink square), UMSCC-22A (yellow triangle), and A253 (blue circle) is plotted along the standard curve, and the number of EGFR/cell interpolated from the standard curve. 59

Figure 4-1 Images for patient 4. Left column images are from the clinically abnormal biopsy, which was diagnosed as moderate dysplasia with underlying foci of moderate to poorly-differentiated cancer. Right column images are from the clinically normal biopsy, ... 74

Figure 4-2 Images for patient 6. Abnormal biopsy was diagnosed as invasive moderately differentiated cancer. Normal biopsy was diagnosed as hyperplasia and hyperkeratosis. (a) False color fluorescence confocal image from abnormal biopsy, laser power 6 μW. 76

Figure 4-3 Images from patient 10. A mixed pathological diagnosis was obtained for the clinically abnormal biopsy, with one tissue slice from the biopsy containing only hyperplastic and hypkeratotic tissue and the second tissue slice containing mild dysplasia. (a-c) Left column images are from the tissue slice from the clinically abnormal biopsy diagnosed as hyperplasia and hyperkeratosis. (a) False color fluorescence confocal 78

Figure 4-4 Images from patient 8. Both the clinically abnormal and clinically normal were diagnosed as hyperplasia and hyperkeratosis (i.e., pathologically normal). (a) False color fluorescence confocal image from clinically abnormal biopsy, laser power 13 μW. (b) False color fluorescence confocal image from clinically normal biopsy, laser power 8 μW. The white line in (a) and (b) indicates the basement membrane. Fluorescence images taken with 40x objective, scale bar 25 μm. 80

Figure 4-5 Example of edge detection and mask determined using Matlab code from three successive images from a z-series stack of the abnormal biopsy from patient 4. (a)-(c) Red lines indicate edges chosen. (d)-(f) Mask created using the detected edges. 82

Figure 4-6 Plot of the ratio of the mean fluorescence intensity from the clinically abnormal to clinically normal biopsy from the same patient. Patient 3 is not included since no diagnosis was obtained for the clinically normal biopsy. Diagnosis for each patient is based on the diagnosis from the clinically abnormal biopsy since all clinically normal biopsies were confirmed to be pathologically normal (hyperplasia

and hyperkeratosis). Biopsies classified as normal and cancer or normal and dysplasia had a mixture of both normal and cancerous or dysplastic tissue in the H&E sections. 84

Figure 4-7 Diagnosis using the mean fluorescence intensity from the surface epithelium. In three cases, only one biopsy is shown per patient (patients 8,9, and 12). Both the clinically abnormal and clinically normal biopsies from patient 5 are also omitted. 86

Figure 4-8 Plot of the ratio of the mean fluorescence intensity from the surface layer to basal layer versus the mean fluorescence intensity for the entire epithelium for normal, hyperplasia, hyperkeratosis, and dysplasia biopsies..... 87

Figure 5-1 Block diagram of spectroscopy system. 99

Figure 5-2 Photo of spectroscopy system..... 99

Figure 5-3 Power as a function of separation distance from the probe..... 105

Figure 5-4 Spectra from multilayer tissue constructs prepared using SqCC/Y1 cells labeled using the EGFR contrast agent at various separation distances from the surface. Cells labeled using the EGFR contrast agent (blue) have a stronger optical signal than those labeled using the IgG control (red), Alexa Fluor® 660 (AFS) dye only (green), and unlabeled cells (pink), which have virtually no optical signal. (a) Probe touching surface (b) 1 mm separation between probe and surface (c) 2 mm (d) 3 mm (e) 4 mm and (f) 5 mm..... 107

Figure 5-5 (a) Overlay plot of multilayer tissue constructs prepared using SqCC/Y1 cells labeled using the EGFR contrast agent. (b) Maximum intensity at each separation

distance. Signal increases with increasing separation distance up to 2 mm and then decreases. 108

Figure 5-6 (a) and (c) Original (blue) and smoothed (red) spectra used to calculate SNR for multilayer tissue constructs prepared using SqCC/Y1 cells labeled using the EGFR contrast agent. (b) and (d) SNR as a function of wavelength. (a) and (b) are for a separation distance of 2 mm, which had the strongest optical signal. (c) and (d) are for the probe touching the multilayer tissue construct, which had the weakest optical signal. 109

Figure 5-7 Spectra from multilayer tissue constructs labeled using in the presence of the permeability-enhancing agent, 5% DMSO. Multilayer tissue constructs were labeled using the EGFR contrast agent in the presence of 5% DMSO (blue) and PBS (green), using the IgG control in the presence of 5% DMSO (red) and PBS (pink), and left unlabeled (black). The optical signal from the two samples labeled using the EGFR contrast agent is higher than those labeled using the IgG control or left unlabeled, with the multilayer tissue construct labeled in the presence of 5% DMSO having a stronger signal than that labeled in the presence of PBS. (a) Probe touching surface (b) 1 mm separation between probe and surface (c) 2 mm (d) 3 mm (e) 4 mm and (f) 5 mm. 111

Figure 5-8 Overlay plot of multilayer tissue constructs labeled in the presence of 5% DMSO (a) and PBS (c) using the EGFR contrast agent. Maximum intensity at each

separation distance for the 5% DMSO sample (b) and PBS sample (d). The signal increases until a separation distance of 3 mm and then decreases in both cases. ... 112

Figure 5-9 (a) and (c) Original (blue) and smoothed (red) spectra used to calculate SNR for multilayer tissue constructs labeled in the presence of 5% DMSO using the EGFR contrast agent. (b) and (d) SNR as a function of wavelength. (a) and (b) are for a separation distance of 3 mm, which had the strongest optical signal. (c) and (d) are for the probe touching the multilayer tissue construct, which had the weakest optical signal. 113

Figure 5-10 (a) and (c) Original (blue) and smoothed (red) spectra used to calculate SNR for multilayer tissue constructs labeled in the presence of PBS using the EGFR contrast agent. (b) and (d) SNR as a function of wavelength. (a) and (b) are for a separation distance of 3 mm, which had the strongest optical signal. (c) and (d) are for the probe touching the multilayer tissue construct, which had the weakest optical signal..... 114

Figure 5-11 Spectra from tissue slices prepared from abnormal and normal biopsies from the oral cavity. Signal from both the abnormal (blue) and normal (red) tissue slices labeled using the EGFR contrast agent is higher than the IgG control samples from the abnormal (green) and normal (pink) tissue slices. Measurements taken at a 3 mm separation distance. 115

Figure 5-12 (a) and (c) Original (blue) and smoothed (red) spectra used to calculate SNR for abnormal and normal tissue slices using the EGFR contrast agent. (b) and (d)

SNR as a function of wavelength. (a) and (b) are from the abnormal tissue slice. (c) and (d) are from the normal tissue slice. 116

Figure 6-1 Results of two day cytotoxicity experiment. (a) Percent viability of the cells. (b) Concentration of cells in number of cells/mL. 125

Figure 6-2 Results of eleven day cytotoxicity experiment. (a) Viability on day three, relatively comparable among all samples. (b) Cell concentration on day three. (c) Viability on day seven. (d) Cell concentration on day seven. Significantly lower for cells grown in the presence of dye. (e) Viability on day eleven. (f) Cell concentration on day eleven. The poor reattachment of cells grown with dye is reflected in the low cell count. 127

Figure 6-3 Results of recovery after exposure experiment. (a) Viability on day seven. (b) Cell concentration on day seven. (c) Viability on day eight after recovery. (d) Cell concentration on day eight after recovery. 129

Figure 6-4 SqCC/Y1 cells labeled at room temperature and at 37ºC. Left column are fluorescence confocal images, right column are DIC transmitted images. (a) EGFR 131

Chapter 1

Introduction

1.1 MOTIVATION

The use of molecular-specific contrast agents in combination with noninvasive optical detection has the potential to significantly improve early diagnosis and treatment of oral cancer. Molecular-specific contrast agents not only provide increased specificity for precancer and cancer by targeting markers which are specific to precancer and cancer, but also have the potential to aid early detection by targeting markers which are expressed early in the transformation process. Optical methods allow for noninvasive detection of the optical signature provided by the contrast agents, providing real-time diagnosis and eliminating the need for painful biopsies. Fluorescence spectroscopy is a noninvasive, near real-time method of providing quantitative standard for cancer detection. In addition to contributing to patient comfort, the use of spectroscopy eliminates the subjectivity of visual recognition for diagnosis and the need for clinical expertise in detection of oral cancer. In this dissertation, I will show that the combination of molecular-specific contrast agents and noninvasive optical detection increases optical contrast between normal and neoplastic tissue and aids in early detection of oral cancer. Besides prevention, early diagnosis is one of the most important elements in treatment of cancer as it greatly improves the five-year survival rate of patients and minimizes the severity of treatment necessary to eradicate the cancer. The development of effective

screening techniques in the oral cavity is particularly critical since there are currently no methods of screening for oral cancer beyond visual recognition.

1.2 SPECIFIC AIMS

The primary goal of my research was to develop a potential tool for screening or diagnosis of oral cancer using a molecular-specific fluorescence contrast agent that would preferentially target precancerous and cancerous tissue and a fluorescence spectroscopy system. In order to accomplish this, I set the following as my specific aims:

(1) Investigate potential markers specific to oral precancer and cancer and develop methods of specifically targeting these markers. Two markers in particular were focused on for targeting: cytokeratins, as an intracellular marker, and epidermal growth factor receptor (EGFR), as an extracellular marker. Other markers of oral cancer were also investigated as potential alternatives.

(2) Develop contrast agents based on probe molecules specific to the markers for oral precancer and cancer conjugated to fluorescent markers. The probe molecules were antibodies against the marker of interest. The fluorescent marker was a long-wavelength fluorescent dye.

(3) Design and build a simple and inexpensive spectroscopy system to detect the fluorescence emission spectra from the contrast agent. The spectroscopy system targeted the wavelength specific to the fluorescent marker, and measured the emission spectra of the marker. The system consisted of a light source which provided the proper

wavelength light for excitation of the fluorescent contrast agent, a miniature spectrometer from Ocean Optics, and a fiber optic probe.

(4) Validate the contrast agent in two biological models. First, monolayers of cancerous oral epithelial cells were used to test the specificity and relative binding efficiencies of the contrast agents. Second, three-dimensional multilayer tissue constructs consisting of multiple layers of epithelial cells embedded in collagen were used as a model system for tissue *in vivo* to determine the binding efficiencies and penetration depth of the contrast agent. In the penetration depth studies, the need for permeability-enhancing agents was investigated. Permeability-enhancing agents which could be added to the contrast agent to improve penetration depth include dimethyl sulfoxide (DMSO), polyvinylpyrroliodone (PVP), and bovine serum albumin (BSA). The ability of the spectroscopy system to detect the contrast agents in the multilayer tissue construct was also investigated.

(5) Test the contrast agent and spectroscopy system were in living normal and neoplastic oral tissue using fresh transverse sections of biopsies obtained from consenting patients at the University of Texas M.D. Anderson Cancer Center. The sections, known as fresh tissue slices, were maintained in culture until application of the contrast agents so that the binding in living tissue could be studied.

(6) Investigate the possibility of *in vivo* use of the contrast agent. In addition to investigating previous *in vivo* work done by other investigators using similar systems,

physiological labeling and standard cytotoxicity assays with the contrast agent were performed.

1.3 DISSERTATION OVERVIEW

The second chapter provides the motivation and background for this dissertation, including an overview of the anatomy and pathology of the oral cavity and a summary of molecular markers of oral neoplasia, contrast agents currently in use, optical diagnostic techniques of oral neoplasia, and permeability-enhancing agents. The third chapter includes portions of a paper published in *Photochemistry and Photobiology*, demonstrating the efficacy of the contrast agent in *in vitro* cell monolayer models, multilayer tissue constructs in the presence of permeability-enhancing agents, and its potential to distinguish abnormal from normal tissue in fresh tissue slices prepared from paired biopsy samples from the oral cavity. The fourth chapter expands on the possibility of using the fluorescence intensity of the contrast agent in diagnosing oral cancer using paired biopsies obtained from 17 consenting patients at the University of Texas M.D. Anderson Cancer Center. The fifth chapter describes a simple and inexpensive fluorescence spectroscopy system that can be used to detect the optical signature of the contrast agent from labeled cells in multilayer tissue constructs. The sixth chapter explores issues which must be considered for *in vivo* use of the contrast agent, including cytotoxicity of the fluorescent dye. The last chapter will provide summary and conclusions for the dissertation.

Chapter 2

Background

2.1 INTRODUCTION

This chapter will provide the necessary context to understand this dissertation. First, the motivation for the research presented in the dissertation will be discussed. Second, an overview of the anatomy and the pathology of the oral cavity will be provided. Molecular markers that could be used to detect precancerous and cancerous lesions will then be discussed. Contrast agents currently in use for detection of neoplasia will then be reviewed. Finally, an overview of optical diagnostic techniques and permeability enhancing agents will be presented.

2.2 MOTIVATION

In the United States, it is predicted that approximately 30,000 new cases of oral cancer are diagnosed each year (1, 2), with approximately 7,200 deaths due to oral cancer in the year 2003 (1). Despite the fact that the oral cavity is in an easily accessible area for screening, the mortality due to oral cancer accounts for approximately 1.7% of mortality due to cancer overall (3). Worldwide, the problem is even greater, with oral and pharyngeal cancers ranking fifth in prevalence (4) and accounting for approximately 50% of all cases of cancers in males in India (5). The five-year survival rate for patients diagnosed with oral cancer at all stages is approximately 50% (1, 6); however, this number dramatically shifts depending on the stage of the cancer at the time of diagnosis.

The five-year survival rate varies from 9-100% depending on the invasion and metastasis of the tumor (2, 3). Table 2-1 summarizes the five-year survival rate as a function of tumor stage.

Table 2-1 Five-year survival rate of oral cancer as related to stage of tumor.

Tumor Stage	Five-year survival rate
0	100%
I	64-85%
II	55-66%
III	33-41%
IV	9%
Five-year survival rates complied from (2, 3)	

Early diagnosis not only improves the five-year survival rate of patients, but also results in less radical and debilitating treatments, thus improving the quality of life for patients (2). Over the past 40 years, the five-year survival rate for oral cancer has not significantly increased although treatment techniques have advanced (7, 8). Further, the five-year survival rate for oral cancer is among the lowest of the major cancers worldwide (8). This is likely due to the fact that oral cancer is generally not diagnosed until it has reached advanced stages when treatment is more difficult and debilitating and the five-year survival rate for patients is poor. Currently, diagnosis of oral cancer is achieved through visual identification and recognition, which relies on the experience of the treating clinician.

Optical techniques could potentially improve diagnosis and detection of oral cancer by allowing objective assessment of the molecular and biochemical changes in neoplastic tissue relative to normal tissue. Successful application and validation of these

techniques will lead to better screening and early detection of premalignant lesions, reducing the incidence of cancer in high-risk individuals.

2.3 ANATOMY OF THE ORAL CAVITY

Anatomically, the oral cavity can be divided into two major regions, the oral vestibule and the oral cavity proper. The vestibule is the opening to the oral cavity and consists of the space between the teeth and buccal gingiva and the lips and cheeks. The oral cavity proper consists of the hard and soft palate, which form the roof of the oral cavity, and the tongue, which forms the floor of the oral cavity (9). Figure 2-1 illustrates the regions of the oral cavity.

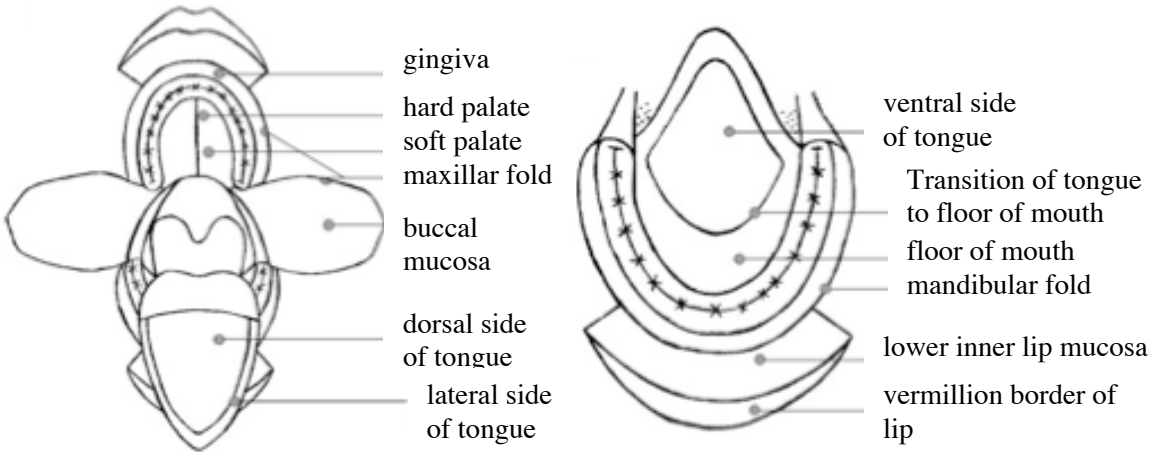

Figure 2-1 Cartoon drawing of the regions of the oral cavity. Figure modified from (10).

The oral cavity is lined by a mucosal membrane that consists of an outer layer of stratified squamous epithelium and an underlying layer of dense connective tissue known as the lamina propria (11). A submucosa beneath the connective tissue can also occur, consisting of blood vessels, fat, and glands (11). Depending on the site within the oral

cavity and the function of the site, structural modifications occur in the epithelium and connective tissue. There are three histological types of epithelia in the oral cavity: masticatory mucosa, which is a tough mucosa found in the gingiva and hard palate, lining mucosa, which is a flexible mucosa found in the lips, cheek, vestibule, alveolar mucosa, soft palate, floor of mouth, and inferior surface of the tongue, and specialized mucosa, which is a mix of the masticatory and lining mucosa found on the dorsum of the tongue (11).

The epithelium of the oral cavity can be either keratinized, as with the masticatory mucosa, or nonkeratinized, as with the lining mucosa, and provides protection against mechanical, microbial, and chemical damage (11). The epithelium can further be broken down in more layers. From the basement membrane to the superficial epithelium, this consists of the basal layer, spinous layer, granular layer, and keratinized layer for keratinized epithelium and the basal layer, spinous layer, intermediate layer, and superficial layer for nonkeratinized epithelium (11). The basal layer consists of two to three layers of the least-differentiated cells that are responsible for cell division and production and are cuboidal or columnar in shape. As the cells progress superficially in the epithelium, they begin to express more keratins and increase in size. In the granular layer, the cells assume a flattened shaped with densely packed keratin filaments. The cells in the intermediate layer of nonkertanized epithelium also assume a flattened shape and express increased keratin compared to basal cells. Finally, at the most superficial keratinized layer, the cells have thickened plasma membranes and contain densely packed

keratin filaments and no organelles. In the oral cavity, there tends to be a higher rate of cell production but a reduced turnover time in both keratinized and nonkeratinized epithelium as compared to the epidermis (11).

Within the oral cavity, the structure and appearance of the mucosa differs depending on the exact site and the function of the site. For example, an area exposed to the functional demands of mechanical stress will be lined with masticatory mucosa while an area which needs to withstand distention will be lined with lining mucosa. The difference in clinical appearance of the oral mucosa varies depending on the distribution of superficial blood vessels, the type and thickness of the epithelium, composition of the submucosa, pigmentation and appendages, surface features of the mucosa, functional adaptations, and disease (11). The thickness of the epithelial layer depends on the site within the oral cavity, ranging from the thin layer of 190 μm +/- 40 μm of the floor of the mouth to the thick layer of 580 μm +/- 90 μm of the buccal mucosa (11).

2.4 PATHOLOGY OF THE ORAL CAVITY

Diagnosis of disease in the oral cavity depends on clinical suspicion based visual assessment and subsequent microscopic assessment after biopsy (12). There is a deficiency in the recognition of early lesions in the oral cavity, and this may be due to the fact that the oral cavity is tended to by two different types of clinicians (13). The dentist is the primary clinician seen for routine treatment in the oral cavity and is familiar with the anatomical region, but may not have specialized training in recognizing early cancer.

By the time a lesion is recognized as cancer by a clinician without specialized training, it generally has reached advanced stages.

Oral premalignancies often present as leukoplakia or erythroplakia. Leukoplakia, the most common form of oral precancer (2), is due to the biochemical process of hyperkeratosis (12, 13) and is defined as a clinical white patch on the oral mucous membrane that cannot be removed and cannot be classified as another disease entity. Leukoplakia, however, can represent either a benign hyperkeratotic lesion or a dysplastic changes indicative of a pre-invasive or invasive cancer (2) and red inflammation known as erythroplakia exhibits the most significant cellular changes indicative of early cancer (13). Erythroplakia may be present with or without the keratinization that produces the white leukoplakia and is often disregarded as innocuous because of lack of keratinization. At time of clinical identification, erythroplakia is almost always associated with dysplasia or carcinoma (2) and is the most common and primary color presentation of early squamous cancer (13).

The development of invasive squamous cell carcinoma (SCC) can be outlined using the progression of carcinoma in the cervix as a model as shown in Figure 2-2 (3). Keratosis is caused by increased keratin production and commonly occurs in the oral cavity due to irritation. While keratosis is often a feature of early malignancy, the relationship between benign keratosis and eventual development of carcinoma is uncertain (3).

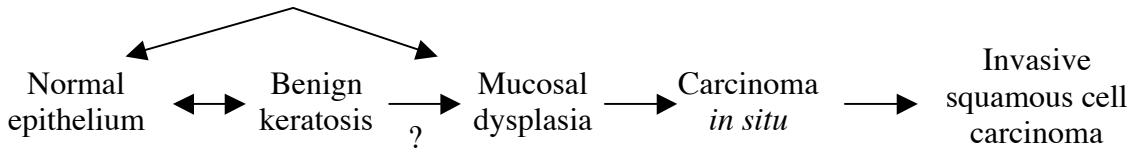

Figure 2-2 Progression from normal epithelium to invasive SCC. Recognized precursors include dysplasia and carcinoma in situ. The significance and relationship of benign keratosis in the transformation process is less well understood (3).

In the oral cavity, dysplasia and carcinoma *in situ* are well-recognized precursors of invasive SCC, though there are various degrees of dysplasia that must be distinguished when considering treatment options. Mild dysplasia is not highly indicative of an early malignant process and has the potential to resolve without treatment while severe dysplasia can often coexist with carcinoma *in situ* and invasive carcinoma and could be considered early malignancy rather than precancer (13). The progression from normal tissue through the various stages of dysplasia to invasive SCC is illustrated in Figure 2-3.

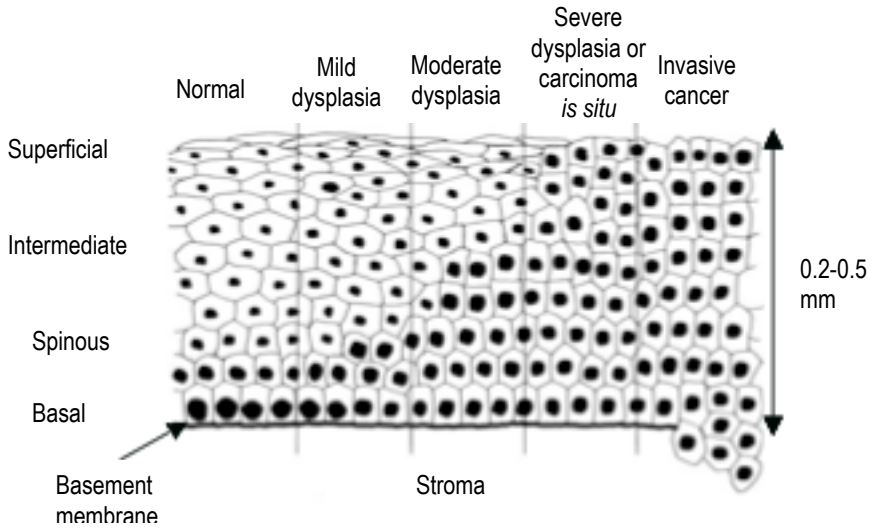

Figure 2-3 Cartoon of progression from normal through the stages of dysplasia to invasive carcinoma. Modified from (14).

When severe dysplasia or carcinoma has been diagnosed in the oral cavity, the possibility of field cancerization or field changes in the remaining oral mucosa must be considered. The concept of field cancerization was developed when it was observed that there is a high incidence of second primary cancers in patients with oral SCC, with 2-7% of patients developing a second cancer within a year of initial treatment (12, 15). The development of multiple primary tumors can be explained by the etiology of oral cancer. Large regions of the oral mucosa are exposed to the etiological agents that cause cancer in the oral cavity, such as tobacco and alcohol, allowing for the possibility of independent transformation of single epithelial cells in multiple locations (12, 15). There is also the possibility of a clonal cluster of cancer cells spreading within the oral cavity, either through saliva or regional blood vessels, resulting in geographically distinct but clonal

cancers. Tumor tissue may also have a paracrine effect on adjacent normal tissue, increasing its susceptibility to future development of carcinoma (12).

Molecular changes in the oral mucosa that may predispose the patient to the development of additional primary cancers are known as field changes (12). Identification of predictive markers based on these molecular changes would have significant prognostic and patient management implications.

SCC does not affect all areas of the oral cavity equally, with the lateral surfaces and the underside of the tongue being the most often affected (3). The high-risk areas of oral SCC are the lateral tongue, the ventral tongue, the floor of the mouth, the soft palate, and the tonsilar pillars (3). The incidence of SCC by location is outlined in Table 2-2.

Table 2-2 Incidence of SCC by location in the oral cavity (3).

General Location	Incidence	Specific Location
Tongue	26%	• Lateral surface • Ventral surface
Oral pharynx	23%	• Soft palate • Tonsillar pillars
Lip	20%	• Vermilion surface
Floor of mouth	17%	• Floor of mouth
Gingiva	9%	• Gingiva
Buccal mucosa	3%	• Buccal mucosa
Hard Palate	2%	• Hard palate

2.5 MOLECULAR MARKERS OF ORAL CANCER

Current pathological techniques involve microscopic examination of tissue, such that detection and identification of cancer only occurs after disease onset (16) and requires biopsy. Molecular markers, however, can potentially act as early indicators of

disease or the progression of disease (16). In order to be effective, a molecular marker must meet the following criteria: easily detectable, relevant across populations, and useful in either early detection, identification of high-risk individuals, early detection of recurrence, or as intermediate endpoints in chemoprevention (16). As illustrated in Figure 2-4, identifying a molecular marker early in the transformation process can improve intervention efficacy and increase survival.

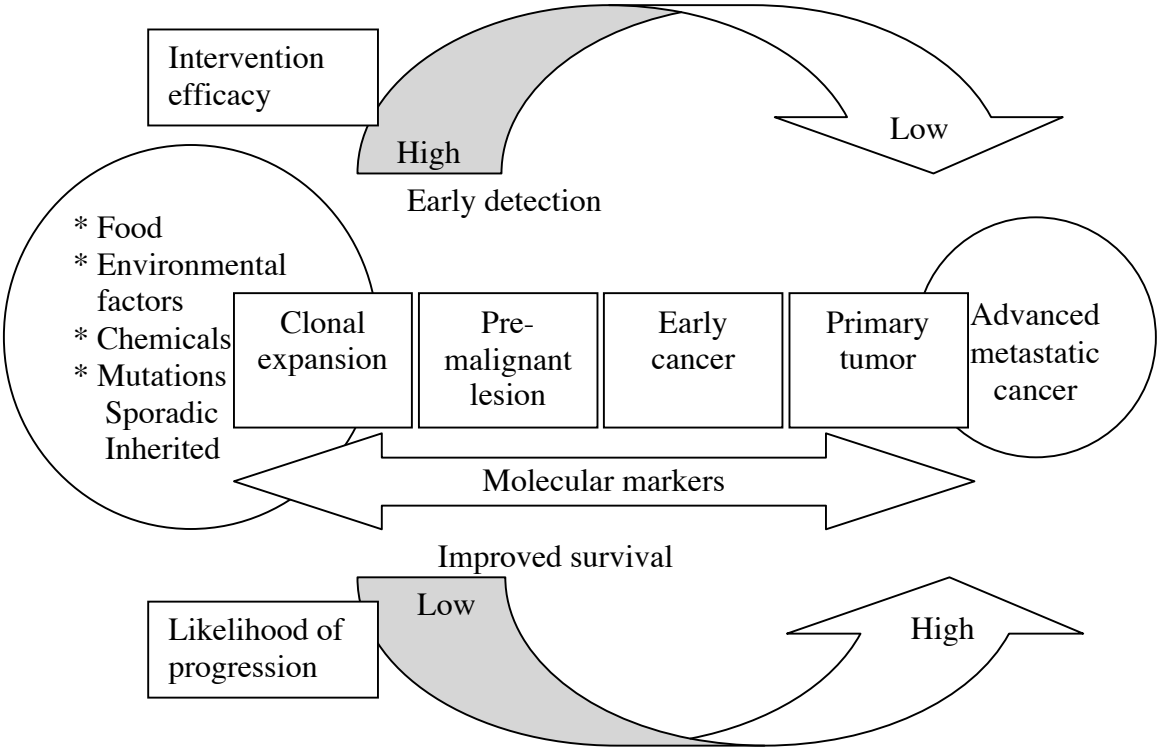

Figure 2-4 Cancer development and progression. Identification of molecular makers early in the progression of cancer increases intervention efficacy and survival. Figure modified from (16).

Molecular markers can be broadly classified into genetic markers and their protein products, proliferative markers, differentation markers, angiogenic markers, apoptosis markers, migration markers, and extracellular and serum markers (15-20). Genetic markers and their protein products can be further broken down into oncogenes, tumor suppressors, genetic instability makers, and cell cycle regulation makers (15, 16, 18, 19).

Of course, the biology of tumor progression is not so simple that a single marker can be used as an absolute positive indication for cancer; tumor progression is unique to each individual and the specific type of tumor. It is more likely that a set of molecular markers will be needed for screening and early diagnosis of most cancers (17, 19). However, even the use of a single molecular maker has the potential to aid early diagnosis, reduce the subjectivity often associated with pathological diagnosis, and reduce the need for clinical expertise in diagnosis. Further, because of the probability of field cancerization in oral cancer, molecular markers can be used to monitor patients for second primary tumors after initial treatment.

2.5.1 Epidermal Growth Factor Receptor

An extracellular target which has been studied extensively in tumor progression is epidermal growth factor receptor (EGFR). EGFR is a 170 kDa transmembrane tyrosine kinase receptor, part of the *erb*B subfamily of receptors. The extracellular ligand binding domain is anchored by a single transmembrane domain and intracellularly, EGFR contains a juxta-membrane region, protein kinase domain, and carboxy-terminal region

(21). Six ligands bind EGFR: epidermal growth factor (EGF), transforming growth factor-alpha (TGF-α), amphiregulin (AR), heparin-binding EGF-like growth factor, betacellulin, cripto, and epiregulin (21). These ligands have distinct expression patterns during development and distinct isoelectric points, which suggests multiple functions of EGFR that could be modulated by the environment (21). A number of cellular events are mediated by the activated receptor, including ion fluxes, phosphorylation events, gene expression, DNA synthesis, and malignant transformation (21).

Malignant transformation is usually associated with overexpression of both EGFR and its ligands; overexpression of ligand alone with normal receptor expression results in hyperproliferation but not transformation (21). Overexpression of EGFR has been associated with a number of human malignancies including bladder, breast, cervix and vulva, glioma, lung, and head and neck tumors (22-24). EGFR mRNA expression can be increased approximately 69-fold in malignant versus normal oral cavity tissue (21, 22); however, elevated mRNA expression is not always seen (25) and increased mRNA may instead be due to transcriptional or post-transcriptional modifications (24). Further, overexpression of EGFR is generally not due to amplification of the EGFR gene, which is only seen in 5-20% of patients overexpressing EGFR (26-28). This suggests that gene amplification is not the only mechanism of EGFR overexpression, and the major mechanism of overexpression develops post-transcriptionally or post-translationally (26-28).

Nouri *et al* found that 73% of the invasive oral squamous cell carcinomas they studied showed strong expression of EGFR (23). Other reports have estimated that 50-98% of tumors in the oral cavity overexpress EGFR (27-31). EGFR expression is detected at all stages of carcinogenesis, from normal-early hyperplasia, dysplasia, and invasive carcinoma (32, 33). EGFR expression is elevated during the progression from hyperplasia to dysplasia and increases during progression from dysplasia to invasive squamous cell carcinoma (34). Further, EGFR expression is elevated in normal epithelium which is adjacent to tumor (34), regardless of tobacco and alcohol abuse (35). EGFR expression is about 2-fold higher in histologically normal epithelia adjacent to head and neck tumors than normal control epithelia from nonsmokers (34). EGFR expression in normal epithelia adjacent to tumor in patients who smoke and drink excessively is higher than that in patients who do not smoke or drink (35). Overexpression of EGFR in malignancy appears to be related to high rates of cell growth and proliferation rather than DNA repair (22).

The correlation between EGFR expression and tumor staging, prognosis, and relapse has also been investigated. Overexpression of EGFR may not correlate strongly with tumor staging, with a number of studies reporting no significant correlation between receptor levels and tumor stage (27, 28, 36). However, some studies have found that tumor EGFR levels are correlated to the size of tumor (30, 31) and have shown that mean values of EGFR increased with tumor size and advanced clinical stage (28). In a correlative study of patients with advanced head and neck squamous cell carcinoma

(HNSCC) enrolled in a radiotherapy study, EGFR expression was a strong prognostic indicator for overall survival and disease-free survival and was highly predictive for the probability of local-regional relapse but not distant metastasis (36).

EGFR has been targeted for use in cancer therapeutic agents, with the belief that inhibiting the tyrosine kinase receptor will inhibit cancer growth and terminal differentiation (21) and possibly cause regression of precancerous lesions (37). Targeting generally involves the use of monoclonal antibodies which target the receptor and prevent binding of ligand (21). Soukos *et al* expanded on this by conjugating the antibody to a photoactive molecule and demonstrated regression of premalignant lesions in the Syrian golden hamster cheek model after i.v. injection of the conjugate and exposure to therapeutic light (37). In addition, they were able to visualize dysplasia in their model using a conjugate of the antibody and fluorescent dye.

2.5.2 Cytokeratins

Cytokeratins are the intermediate filaments of epithelial cells, and are broken down into two subclasses, acidic and neutral to basic. The expression pattern of intermediate filaments during embryologic development and differentiation parallels the appearance of histologically distinct cell types in the embryo and adult, indicating that cell types can be characterized based on their intermediate filament expression pattern (38). The cytokeratin profile of a tissue depends on the developmental stage, cell type, tissue differentiation, and pathological modifications, making cytokeratins an excellent marker for differentiation state (39), with rapidly proliferating cells expressing

characteristic cytokeratins. Intermediate filament typing is potentially useful in tumor diagnosis, particularly in cases where tumors cannot be classified by conventional procedures, and metastases appear to retain the intermediate filament expression typical of the primary tumor (38). All carcinoma cells contain cytokeratins regardless of degree of differentiation, with different types of tumors expressing different amounts, types, and arrangements of cytokeratins (38). This indicates that the cytokeratin expression pattern can be used to distinguish and even classify tumors. However, the situation is more complicated than simply typing for a single cytokeratin, since conflicting studies have associated various cytokeratins with different stages of oral cancer. Table 2-3 lists cytokeratins by their association with tissue type according to the findings of different groups.

Table 2-3 Cytokeratins (CK) associated with different tissue types according to different studies. Results sited include Ogden *et al* (40), Sawaf *et al* (39), Morgan *et al* (41), Vaidya *et al* (42), Xu *et al* (43), Cema *et al* (44), and Kannan *et al* (45). An author's name in the + column indicates that the cytokeratin was associated with the tissue type by their study. An author's name in the – column indicates that the cytokeratin showed decreasing amounts or was not associated with the tissue type by their study.

CK	Well differentiated oral SCC		Moderately differentiated oral SCC		Poorly differentiated oral SCC		Oral dysplasia		Oral hyperplasia	
	+	-	+	-	+	-	+	-	+	-
1	Sawaf Morgan Vaidya			Morgan				Xu		
4			Sawaf	Morgan						
5							Cema			
6							Cema			
7	Ogden		Sawaf		Morgan Sawaf					
8	Ogden		Sawaf		Morgan Sawaf		Xu			
10		Ogden		Morgan		Ogden		Cema, Kannan		
13	Sawaf Morgan	Ogden	Sawaf	Morgan		Ogden		Cema Kannan		
16	Vaidya									
17			Vaidya					Cema		Cema
18	Ogden		Sawaf Vaidya		Morgan Sawaf			Cema		Cema
19	Ogden		Sawaf		Morgan Sawaf			Cema	Xu	Cema

As is evident in Table 2-3, there is no universal agreement as to the type of cytokeratin associated with oral cancer, regardless of stage. There are probably a number of reasons for these conflicting results. First, the tissue type will determine the

cytokeratins expressed, and the oral cavity has numerous tissue types, including cornifying stratified epithelia, noncornifying stratified epithelia, pseudostratified columnar epithelia, junctional epithelia, and salivary glands (46). In addition, the location of the tissue within the oral cavity may affect cytokeratin expression. Further, the actual type of tumor will influence how the cytokeratin pattern changes with tumorigenesis, with pre-neoplasia, squamous cell carcinoma, adenocarcinoma, and odontogenic tumors showing differing expression patterns (46). Finally, the different antibodies used to probe the tissue and the various preparation techniques of the tissue before histological examination by different researchers could affect the cytokeratins detected.

It does appear, however, that cytokeratin 8 could be used in distinguishing malignancy in the oral cavity, as it has been shown not to be present in normal tissue (40, 47) and has been associated with malignancy (39, 43, 47, 48). Cytokeratin 18 could be used in order to distinguish carcinoma from dysplasia and hyperplasia, as it has been associated with all stages of carcinoma (39-42) and not with dysplasia or hyperplasia (44). However, the biggest challenge with using cytokeratins as a molecular marker for living cells and tissue is that it is an intracellular target. There is an inherent resistance to transport of high molecular weight markers (49), and uptake relies on non-specific cell endocytosis or permeablization of the cell membrane.

2.5.3 Other Molecular Markers of Oral Neoplasia

Some molecular markers associated with oral cancer include p53, ras, myc, matrix metalloproteinases (MMP), galectins, Ki-67, and the argyrophilic nucleolar organizer region (AgNOR). p53, ras, and myc are three examples of genetic markers which have been associated with oral neoplasia. p53 is a well-known tumor suppressor and in oral cancer, p53 has been found to be mutated in up to 80% of cancers and the mutation may occur before or during the transition period from precancer to SCC (12). Further, the p53 gene is targeted either directly or indirectly by tobacco carcinogens (50). Ras is a potential oncogene whose protein product ras^{p21} is expressed in oral leukoplakias and carcinomas but not in normal tissue (32). Myc is another oncogene whose protein product is increased in dysplasia and remained elevated throughout tumorigenesis (33). p53, ras, and myc are only a small subset of genes implicated in the tumorigenic process upon some form of mutation.

MMPs and galectins are two examples of extracellular and serum markers associated with oral neoplasia. MMPs appear to be important extrinsic regulators of tissue remodeling that occurs when tumors acquire invasive characteristics (51). MMP-1 expression increases during SCC progression and MMP-1 mRNA is detected in early stages of SCC (52). Further, MMPs are also required during angiogenesis, which is a necessary step for continued tumor growth. Aberrant expression of glycoproteins and carbohydrate-binding molecules could affect interactions with the extracellular matrix and basement membrane and may also occur in head and neck tumors (53, 54). Galectin-

1 and galectin-3 are expressed in head and neck squamous cell carcinoma lines and tumor specimens and may play a role in cellular adhesion and recognition (53).

In addition to EGFR, Ki-67 and AgNOR are two examples of proliferative markers. In immunohistochemical analysis of oral cavity tissue, Ki-67-positive cells and higher AgNOR numbers were found at the invasive tumor front (50). An increase in proliferative markers indicates an increase in cellular metabolic activity in the tumorigenic progression.

2.6 CONTRAST AGENTS

2.6.1 Endogenous Fluorescence

Tissue will autofluoresce due to endogenous fluorophores, including the reduced form of nicotinamide adenine dinucleotide (NADH), flavins (FAD^+, FMN, and riboflavin), aromatic amino acids (tryptophan, tyrosine, and phenylalanine), collagen crosslinks, and elastin crosslinks. In addition, hemoglobin absorption also contributes to fluorescence spectra by attenuating the excitation and emission wavelengths that overlap with hemoglobin absorption, which is strongest at 420, 540, and 580 nm. Changes in tissue architecture and intrinsic fluorophores in malignant tissue from its normal counterparts are reflected in their autofluorescence spectra. These changes can be in fluorophore concentration or spatial distribution, the metabolic status of a fluorophore, the biochemical and biophysical microenvironment of the tissue, the tissue architecture, or the distribution of non-fluorescent chromophores that attenuate light through

absorption of the excitation or emission light (55). Each of the intrinsic fluorophores has a distinct excitation and emission spectra, as illustrated in Figure 2-5.

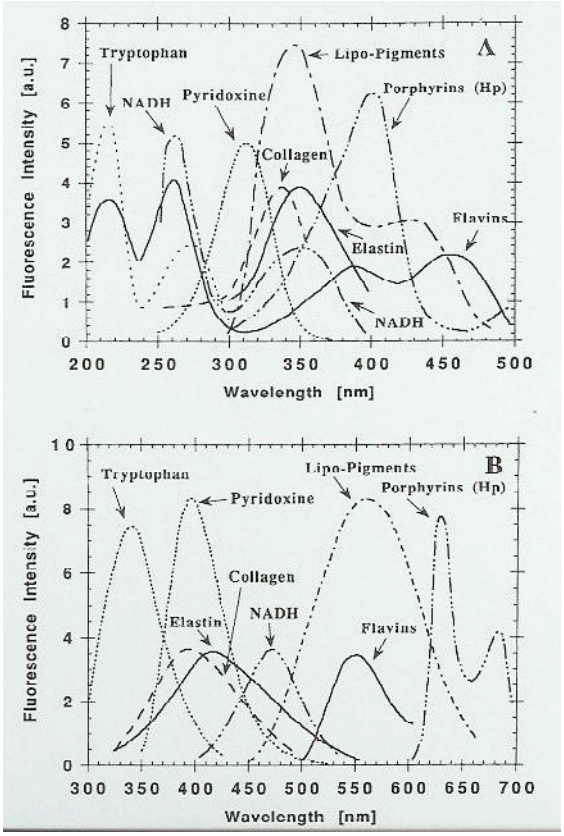

Figure 2-5 Fluorescence excitation (a) and emission (b) spectra of various endogenous tissue fluorophores. From (55).

However, the primary drawback to the use of autofluorescence is that the optical excitation wavelengths are relatively short, limiting penetration depth into the tissue due to increased scattering and absorption. Therefore, deeper lesions cannot be easily diagnosed. Autofluorescence signals also tend to be relatively weak, photobleach rapidly, and are subject to a low signal-to-noise ratio (SNR). Finally, the exact nature of the biological changes which drive the differences in fluorescence spectra between

normal and abnormal tissue are not known. The differences may be due to changes in tissue architecture, such as thickening of the mucosa or loss of layered structure (55, 56), and/or due to a combination of changes in both the concentration, form, and distribution of endogenous fluorophores and the absorption properties of normal versus neoplastic tissue (55, 57, 58).

The effectiveness of autofluorescence can be increased by the addition of 5-aminolevulinic acid (ALA), which is a precursor to the endogenous fluorophore protoporphyrin IX (PP IX) that accumulates in certain premalignant tissues (49, 59). Exogneous addition of ALA bypasses the normal feedback control production of PP IX (59), increasing the concentration of PP IX and leading to a better SNR. In addition to the tendency to accumulate PP IX and a higher rate than normal tissue, malignant cells also convert ALA to PP IX at different rates and intensities than normal cells (59). While PP IX emits in the 600 nm range, it excites at 450 nm, so penetration depth is still limited and absorption of hemoglobin could reduce the excitation efficiency of PP IX. In addition, Heintzelman *et al* found that while PP IX was associated with a larger number of abnormal samples, it was not diagnostically useful for discriminating neoplastic tissue in the oral cavity (58).

2.6.2 Dyes

In order to improve diagnostic accuracy and improve contrast, a number of studies have been performed using vital dyes such as toluidine blue (molecular weight 305.83) and Lugol's iodine solution (a solution of 5% iodine, molecular weight

126.90447, and 10% potassium iodine, molecular weight 166.0 in water) as staining agents. These dyes are taken up by neoplastic tissue due to increased permeability of the cell membrane. However, tissue which has undergone trauma also displays increased permeability and will show increased uptake of the dye relative to normal tissue even though it has not undergone malignant transformation (49). This contributes to the lack of specificity associated with detection mediated solely by vital dyes. A study which determined the reliability of staining with toluidine blue *in vivo* to detect oral epithelial dysplasia, *in situ* carcinoma, and squamous cell carcinoma associated with potentially malignant epithelial lesions found a high sensitivity of 84% to 100% but a greatly variable specificity of 44% to 100% (60). Toluidine blue has been incorporated into a commercially available ready-to-use kit (OraTest®, Zila Inc, Phoenix, AZ, known as OraScan® in some countries) as a 1% toluidine blue solution for staining and a 1% acetic acid solution for pre- and post-rinsing. As with toluidine blue studies, the OraScan® kit showed a relatively high sensitivity of 79.5% but a low specificity of 62% (61). The low specificity associated with toluidine blue staining is attributed to inflammation and trauma areas which retained the stain (60), illustrating the major drawback to vital staining.

Fluorescent molecules have also been used to detect tumors *in vivo*. As with the vital stains, the fluorescent molecules are not designed to be target-specific but show increased uptake in tumor tissue as compared to normal tissue. Aromatic lanthanide chelates are examples of fluorescent molecules which have been used in rat models to

detect colon cancer (49). The near-infrared dye indocyanine green (ICG) has also been used as a non-specific dye for *in vivo* imaging in cerebral pathways, mammary disease and reactive lymph nodes, angiography in ophthalmology, hepatic function, and detection of tumor margins in gliomas (49, 62-64). The stability and intensity of ICG has also shown to be increased by complexation to silver island films through human serum albumin (63).

2.6.3 Target-specific Contrast Agents

Target-specific contrast agents have the advantage of increased molecular specificity as compared to vital dyes. Instead of simply relying on increased permeability of the cell membranes of malignant tissue, target-specific contrast agents use molecular markers which are associated specifically with neoplasia or are overexpressed in neoplasia relative to normal tissue. This has the potential to provide high detection specificity due to enhanced accumulation of the contrast agent. In addition, the use of molecular markers that are expressed early in the transformation process could greatly aid early detection.

The use of a fluorophore conjugated to a probe of the molecular marker would further improve imaging by providing better optical properties and increased SNR compared to autofluorescence. By choosing a fluorophore with an excitation wavelength above 600 nm, a high quantum yield, and a large Stokes shift, a target-specific contrast agent can be designed with increased penetration depth into the tissue and a strong signal that can be easily filtered from excitation light. Probes that can be used in target-specific

contrast agents include antibodies or antibody fragments against the molecular marker or if the marker is a receptor, ligands for the receptor or short peptide sequences of the ligand. Contrast agents based on near infrared dyes conjugated to peptides for the somatostatin receptor have been show to localize to tumors which overexpress the receptor *in vivo* in rodent models (65, 66). Localization to tumors *in vivo* in rodent models has also been achieved by targeting the bombesin receptor (66) and the epidermal growth factor receptor (37). The cyanine family of dyes has been used as fluorescent markers in target-specific contrast agents, using antibodies, antibody fragments, and peptide platforms to localize to the tumor (49, 62, 67, 68). Licha *et al* conjugated cyanine dyes to somatostatin receptor-specific peptides and showed intracellular localization in cell models (68). Cyanine dyes with longer excitation and emission wavelengths were shown to be more effective in visualizing tumors in deeper tissue than their shorter-wavelength counterparts (62, 67).

A variation of target-specific contrast agents are those that are biologically activated by proteases or reporter genes (49, 69). These contrast agents are activated by proteases, and generally contain fluorophores which are self-quenched until cleaved by tumor-specific proteases. This suppresses the fluorescent signal until it has localized to the tumor, thereby amplifying the signal and SNR. Weissleder *et al* bound near-infrared fluorescence probes to a long circulating graft polymer, which quenched the signal until cleavage by lysosomal proteases in tumor cells, and demonstrated a 12-fold increase in signal between protease-activated and unactivated probes (69). Reporter genes can also

contain an optical signature, which can be used to monitor cellular events *in vivo*. This can be used to monitor tumor growth and progression and optimize treatment regimens (49).

2.6.4 Quantum Dots

Quantum dots are seminconductor nanoparticles which are photochemically stable with narrow, symmetric emission spectra and absorbance maxima that shift to higher energy with decreasing particle size (70). This results in tunable fluorophores that can be excited at any wavelength shorter than the emission peak, but still emit the same characteristic spectra regardless of excitation wavelength (70). A spectral range from 400 nm to 2 μm with 20 to 30 nm FWHM can be achieved using various materials and sizes for nanocrystals (70). The ability to excite multiple types of quantum dots with a single excitation wavelength facilitates multi-color fluorescent labeling, which can be used in biological systems to specifically label multiple targets simultaneously. The optical properties of quantum dots are potentially advantageous over traditional fluorescent dyes, which require multiple excitation wavelengths, are more difficult to resolve in multi-color labeling experiments, and tend to photobleach more quickly than quantum dots. The biggest challenge to using quantum dots in biological systems is their lack of water solubility and potential toxicity. This has been overcome by adding an outer shell to the quantum dots, which makes them water-soluble without changing their optical properties (70, 71). In addition, this outer coating can be modified with various chemical groups that allow covalent attachment to various biomolecules (70, 71) such

that quantum dots can be used in place of fluorescent dyes in target-specific contrast agents. Silica-coated CdSe-CdS quantum dots have been used to specifically label actin and nuclei of mouse 3T3 fibroblasts (70) while transport inside of HeLa cells was demonstrated with zinc-capped CdSe quantum dots coated with mercaptoacetic acid conjugated to transferrin (71). These examples illustrate that quantum dots can be made biocompatible and have the potential to be used in *in vivo* as part of target-specific contrast agents.

2.7 OPTICAL DIAGNOSTIC TECHNIQUES OF ORAL NEOPLASIA

Optical techniques have the potential to provide near real-time diagnosis information noninvasively. In addition to greatly increasing patient comfort and reducing loss to follow-up, cost-savings could also be realized by the medical industry by eliminating unnecessary biopsies and reducing patient follow-up time (72). Numerous *in vivo* optical techniques have been developed including multi-spectral fluorescence imaging, multi-spectral reflectance imaging with polarized and unpolarized light, confocal microscopy (73, 74), reflectance spectroscopy with polarized and unpolarized light (75, 76), and fluorescence spectroscopy (57).

2.7.1 Optical Spectroscopy

Optical spectroscopy techniques have the ability to provide quantitative information of underlying biochemical and morphological changes that occur during

tumorigenesis. Because the information is quantitative, diagnosis becomes less subjective and could potentially be performed by less specialized personnel.

As discussed previously, fluorescence spectroscopy can be used to distinguish malignancy in the oral cavity based on autofluorescence. A number of studies in *in vitro* cell models, *ex vivo* tissue samples, and *in vivo* in patients have interrogated the ability to use changes in autofluorescence as a distinguishing characteristic of neoplasia.

Sacks *et al* showed that the differentiation state of terminally differentiated cells compared to less differentiated cells can be distinguished based on autofluorescence at excitation wavelengths of 300 and 380 nm with emission at 450 and 510 nm respectively (77). In addition, Kolli *et al* determined the correlation between mean epithelial thickness and changes in autofluorescence. Comparing *in vivo* tumor sites to contralateral normal sites, a correlation of 40% to the mean epithelial thickness of the site was achieved using the ratio of fluorescence intensities at 290/330 nm in an excitation scan from 200 to 360 nm measured at an emission wavelength of 380 nm and the ratio of fluorescence intensities at 390/450 nm in an emission scan from 360 to 600 nm excited at 340 nm (78). A correlation of only 40% between the fluorescence intensity ratios and the mean epithelial thickness indicates that other factors are contributing to the observed fluorescence (78). Abnormal differentiation and epithelial thickening are hallmarks of neoplasia, and these results suggest that autofluroescence can be used to distinguish alterations in tissue which could be indicative of neoplasia.

Studies investigating the changes in autofluorescence between normal and abnormal tissue found that the differences in the fluorescence spectra can be used as criteria to diagnose malignancy (55, 58, 79-81). In the oral cavity, the optimal excitation wavelengths for distinguishing oral neoplasia range from 300-400 nm (58, 81-85).

In a study using normal and cancerous *ex vivo* oral tissue samples, Wang *et al* were able to use two excitation wavelengths to achieve a sensitivity of 81.25%, specificity of 93.75%, and positive predictive value of 92.86% (56). In this study, they compared the performance of diagnostic classifications using single excitation wavelengths by calculating the ratio of the area under the curve at emission wavelengths of 330 +/- 5 nm and 470 +/- 5 nm (using excitation wavelengths of 280, 290, and 300 nm) and the ratio of the area under the curve at emission wavelengths of 380 +/- 5 nm and 460 +/- 5 nm (using excitation wavelengths of 320, 330, and 340 nm) to the performance of a classification scheme which paired the two ratios. While the sensitivity was the same for the single or two excitation wavelength classification, the two excitation wavelength classification showed approximately a 30% increase in specificity and 20% increase in positive predictive value compared to the single excitation wavelength method.

In an *in vivo* study that consisted of a training set of 9 normal volunteers and 11 patients with suspected cancer and a validation set of 56 normal volunteers and 3 patients with suspected cancer, Heintzelman *et al* were able to achieve 90% specificity and 90% sensitivity in separating dysplasia and cancer from normal tissue using three excitation

wavelengths (350, 380, and 400 nm) and an algorithm based on four emission intensities (58). When the algorithm was simplified to use a single emission wavelength at 472 nm at all three excitation wavelengths, sensitivity remained at 90% and specificity dropped only 2% to 88%. They were further able to simplify their diagnostic algorithm using a ratio of fluorescence intensities at two excitation wavelengths (400 and 350 nm) and at a single emission wavelength (472 nm) and achieve an average sensitivity of 95 +/- 7% and specificity of 93 +/- 6% for the training and validation sets.

In a 2000 review article on fluorescence spectroscopy, Ramanujam summarized studies evaluating the performance of fluorescence spectroscopy for detecting invasive carcinoma, early carcinoma, and dysplasia of the oral cavity (81). Table 2-4 provides an overview of spectroscopy studies based on autofluorescence. Overall, the lowest sensitivity achieved using fluorescence spectroscopy was 81.25% and the lowest specificity was 87.5%.

Table 2-4 Summary of results of studies reviewed by Ramanujam evaluating fluorescence spectroscopy in the oral cavity for distinguishing carcinoma and dysplasia from normal tissue. The table includes the excitation and emission wavelengths used in analysis, the sample size (normal N and abnormal A samples), and the resulting sensitivity (SE) and specificity (SP). Table modified from (81).

Group	Excitation wavelength (nm)	Measurement type	Emssion wavelengths (nm)	Sample size (N; A)	SE;SP
Dhingra *et al* (86)	370 410	Spectra	490 640	14; 10	100; 87.5
Gillenwater *et al* (57)	337 410	Spectra	Peak 635, 490	17; 11	94; 100
Kulapaditharom and Boonkitticharoan (87)	442	Images	Red, green	16; 16	100; 87.5
Betz *et al* (85)	375-440	Images Spectra	> 515 nm	36; NA 36; NA	43.3; NA 94.4; NA
Wang *et al* (56)	280, 290, 300 320,330, 340	Spectra	330/460 380/460	16; 16	81.25; 93.75
Heintzelman *et al* (58)	350 380 400	Spectra	418 and 470 448 400	56; 3	90; 90

The performance of fluorescence spectroscopy can be further improved by combining it with diffuse reflectance spectroscopy and light scattering spectroscopy in a technique known as trimodal spectroscopy. Each mode of spectroscopy provides different information about the tissue; fluorescence spectroscopy provides direct biochemical information, diffuse reflectance spectroscopy provides information on tissue absorption and structure, and light scattering spectroscopy provides information on the

size distribution of cell nuclei within the tissue (82). In an *in vivo* study of 15 patients with various degrees of malignancy and 8 normal volunteers, Müller *et al* were able to achieve a sensitivity and specificity of 96%, a positive predictive value of 0.93, and negative predictive value of 0.98 in distinguishing dysplasia and cancer from normal tissue (82). Further, they were able to achieve a sensitivity of 64%, specificity of 90%, positive predictive value of 0.9, and negative predictive value of 0.64 in distinguishing dysplasia from cancerous tissue.

2.7.2 Confocal Microscopy

In vivo imaging techniques, such as confocal microscopy, have the ability to provide the intracellular detail used in histological analysis without removing or physically sectioning the tissue (73). Further, with the development of fiber-based confocal microscopy (88-93), the possibility of imaging tissue in real time *in vivo* as a means of diagnosis is a reality.

In a study of normal subjects comparing reflectance confocal images from the tongue and lip to histology images, confocal images correlated well to histology both qualitatively and quantitatively (74). Clark *et al* were also able to use reflectance confocal microscopy to image excised biopsies from the oral cavity and identify nuclear and cellular changes characteristic of carcinoma (94). *In vivo* confocal imaging of tooth structure, cells of the gingival, and mucosal membrane as far back as the premolar teeth has been performed by Watson *et al* (95).

2.8 PERMEABILITY-ENHANCING AGENTS

In order for exogenous contrast agents to be effective *in vivo* in targeting neoplasia in tissue, it may be necessary to penetrate through multiple layers of epithelial cells. While contrast agents could be injected via i.v. or i.p. injection, topical application would be preferable in order to minimize systemic exposure to the contrast agent. In addition, topical application is probably the most effective way to target an epithelial cancer in the oral cavity. However, in order to label deeper tumors, the contrast agent will have to pass either intercellularly or intracellularly to reach cells near the basement membrane or those which have invaded into the stroma, which may require that the contrast agent be applied in conjunction with a permeability-enhancing agent.

Dimethyl sulfoxide (DMSO) is widely used in cell biology and medical applications. It has uses as a drug adjuvant, cryoprotective agent, free radical scavenger, membrane fusogen, membrane permeabilizer, and inducer of cell differentation (96, 97). DMSO itself is readily permeable through biological membranes, including human skin, and can also enhance the permeability of low molecular weight solutes or increase their penetration into the deeper layers of the skin (97). The mechanism behind the ability of DMSO to permeabilize biomembranes may be related to its ability to reduce the distance separating lipid bilayers, allowing an increase in the flux of solutes across lipid bilayers (96). It may also reduce the energy required for a molecule to passively diffuse across the cell membrane by removing the waters of hydration at the membrane interface (96).

Pyrroliodones are also known permeability enhancers (98). By combining polymers, which are often used in drug delivery, particularly for sustained release, with pyrroliodones, drug permeation across a barrier can be improved, with polyvinylpyrroliodone (PVP) being an effective combination (98). 4% bovine serum albumin (BSA) has shown to improve recovery of lipophilic compounds across a cell monolayer by reducing retention of the highly lipophilic compounds due to non-specific binding and providing an absorptive driving force (99).

Chapter 3

A Far-Red Fluorescent Contrast Agent to Image Epidermal Growth Factor Receptor Expression[1]

3.1 INTRODUCTION

Advances in optical technologies which offer novel noninvasive tools to improve the screening and diagnosis of cancer and its precursors have recently generated much excitement. These methods have the potential to provide diagnostic information in near real-time without the need for biopsy and with minimal patient discomfort and cost. Numerous optical techniques have been developed and tested *in vivo* in pilot studies, including multi-spectral fluorescence imaging (100, 101), multi-spectral reflectance imaging with polarized and unpolarized light (101, 102), confocal microscopy (73, 74), reflectance spectroscopy with polarized and unpolarized light (75, 76, 103), and fluorescence spectroscopy (55, 57, 81, 103).

The oral cavity is an ideal site for the application of optical techniques because of accessibility and convenient visualization. Currently, diagnosis of oral cancer is achieved through visual identification and recognition, which relies on the experience of the treating clinician. Optical techniques could potentially improve diagnosis and detection

[1] Portions of this chapter have been published previously in Hsu, E.R., E.V. Anslyn, S. Dharmawardhane, R. Alizadeh-Naderi, J.S. Aaron, K.V. Sokolov, A.K. El-Naggar, A.M. Gillenwater, and R.R. Richards-Kortum, 2004. A far-red fluorescent contrast agent to image epidermal growth factor receptor expression. *Photochem. Photobiol.* **79(3)**, 272-279.

of oral cancer by allowing objective assessment of the molecular and biochemical changes in neoplastic tissue relative to normal tissue. Successful application and validation of these techniques will lead to better screening and early detection of premalignant lesions, reducing incidence of cancer in high-risk individuals.

Recently, *in vivo* studies have demonstrated the ability of fluorescence spectroscopy to distinguish neoplasia in the oral cavity based on autofluorescence. Excitation wavelengths optimal for diagnosis of invasive carcinoma, early carcinoma, and dysplasia lie within the range of 300-440 nm (58, 81-85). While preliminary results with autofluorescence are promising, there are several limitations. First, autofluorescence signals tend to be relatively weak, photobleach rapidly, and are subject to low signal-to-noise ratio (SNR). Second, the penetration depth of the near UV and blue excitation wavelengths are relatively limited, implying that deeper lesions or deeper margins of superficial tumors cannot be easily evaluated.

Molecular-specific, exogenous optically active contrast agents that bind to biomarkers modified early during neoplastic transformation may facilitate the detection of early neoplastic lesions (16) and improve diagnostic accuracy and contrast. The use of a highly stable, high quantum yield fluorophore conjugated to a molecular-specific probe of the biomarker would also allow increased SNR compared to autofluorescence. In addition, using an exogenous fluorophore with excitation and emission wavelengths in the red to near infrared region increases the penetration depth.

Several studies have shown overexpression of epidermal growth factor receptor (EGFR) in premalignant and invasive oral squamous epithelial lesions. EGFR expression is detected at all stages of carcinogenesis, from normal-early hyperplasia, dysplasia, and invasive carcinoma (32, 33). EGFR expression is elevated during the progression from hyperplasia to dysplasia and increases during progression from dysplasia to invasive squamous cell carcinoma (SCC) (34). Moreover, EGFR expression is elevated in normal epithelium which is adjacent to tumor (34), regardless of tobacco and alcohol abuse (35). Nouri *et al* found that 73% of the invasive oral SCC they studied showed strong expression of EGFR (23). Other reports have estimated overexpression of EGFR in all oral cancers at 50-98% (21).

Soukos *et al* targeted SCC by conjugating an EGFR antibody to a photoactive molecule and demonstrated regression of premalignant lesions in the Syrian golden hamster cheek model after i.v. injection of the conjugate and exposure to therapeutic doses of light (37). In addition, they were able to visualize dysplasia in their model using a conjugate of the antibody and a fluorescent dye three days after i.v. injection of the antibody-dye conjugate. However, for diagnostic purposes, topical application of the contrast agent would be preferable in order to minimize patient discomfort, systemic exposure to the contrast agent, and possible immunogenic effects.

The purpose of the present study is to develop and evaluate a molecular-specific contrast agent to EGFR using a monoclonal antibody and far-red fluorescent dye which could be applied topically for detection of oral cavity neoplasia in humans. The first

steps in the development of a contrast agent for potential use in *in vivo* detection of oral cancer are to test the efficacy of the contrast agent in *in vitro* and *ex vivo* models. In this study, we demonstrate the specificity of the agent for imaging EGFR in cancer cell lines and the ability to penetrate throughout 500 μm thick multilayer epithelial tissue constructs when applied topically with permeability-enhancing agents such as dimethyl sulfoxide (DMSO), polyvinylpyrrolidone (PVP), and bovine serum albumin (BSA). In order to test the penetration depth of the contrast agents across multiple layers of epithelial cells, mutilayer tissue constructs which have been shown to mimic the optical properties of the epithelial layer *in vivo* were used (104). Finally, we demonstrate the potential use of the fluorescence intensity of the contrast agent to distinguish abnormal tissue from normal tissue using fresh tissue slices prepared from biopsy samples from the oral cavity. We conclude that this contrast agent could potentially be used in conjunction with fluorescence spectroscopy and/or imaging to improve quantitative, objective tumor detection and demarcation.

3.2 MATERIALS AND METHODS

3.2.1 Contrast Agent

The antibody used in the contrast agent was a biotinylated mouse monoclonal anti-human EGFR (clone 111.6, 200 mg/ml, LabVision NeoMarkers, Fremont, CA) and was used at a 1:10 dilution. The antibody is targeted against the extracellular domain of EGFR and blocks the binding of epidermal growth factor (EGF) to the receptor. Alexa

Fluor® 660 streptavidin (Molecular Probes, Eugene, OR) was used as the far-red fluorescent marker. Alexa Fluor® 660 streptavidin has a broad absorption peak with a maximum at 669 nm, but can also be excited at 633 nm or 647 nm. Its emission maximum is at 690 nm with a relative quantum yield of 0.88 compared to 7-hydroxy-9H-(1, 3-dichloro-9, 9-dimethylacridin-2-one) (DDAO). Alexa Fluor® 660 streptavidin has a degree of labeling of 4.7 moles of dye per mole of protein using an e of 110,000 cm^{-1} M^{-1} at the absorbance maximum (all information on Alexa Fluor® 660 streptavidin as reported by Molecular Probes in the Certificate of Analysis for lot #65C1). The dye was provided as a 1 mg lyophilized powder and reconstituted in 1 ml of deionized water and stored in frozen aliquots. For use in labeling, it was diluted to 250 mg/ml in PBS and used at a 1:8 dilution.

3.2.2 Cell Lines

Six human cell lines were tested: MDA-MB-468 (American Type Culture Collection, Manassas, VA), an adenocarcinoma of the mammary gland known to overexpress EGFR at ~$1x10^6$ receptors/cell (receptor number/cell from American Type Culture Collection and (105)), MDA-MB-435S (American Type Culture Collection), a ductal adenocarcinoma of the breast which expresses no EGFR (105), SiHa (American Type Culture Collection), a squamous cell carcinoma of the cervix, SqCC/Y1 (kindly provided by Reuben Lotan, at the University of Texas M.D. Anderson Cancer Center), a squamous cell carcinoma of the buccal mucosa, UMSCC-22A (kindly provided by Reuben Lotan), derived from a primary tumor of the hypopharynx, and A253 (American

Type Culture Collection), an epidermoid carcinoma of the submaxillary salivary gland . MDA-MB-468 and MDA-MB-435S cells were grown in minimal essential media (Invitrogen, Carlsbad, CA) with 10% fetal bovine serum (FBS) (Hyclone, Logan, UT), penicillin, streptomycin, glutamine, sodium pyruvate, non-essential amino acids, and vitamins (Invitrogen). SiHa, SqCC/Y1, and UMSCC-22A cells were grown in Dulbecco's modified essential media/F12 (Invitrogen) with 5% FBS, penicillin, streptomycin, and glutamine. A253 cells were grown in McCoy's 5A (Invitrogen) with 5% FBS, penicillin, streptomycin, and glutamine. To grow monolayers of cells for imaging, small wells were created using adhesive CoverWell imaging chambers (Grace Bio-Labs, Bend, OR) with a 25 mm diameter and 0.5 mm depth secured to a No. 1 24x40 mm glass coverslip. Cells were plated at a density of 0.2 million cells/ml in the chambers, and allowed to grow for 3-4 days in a 37ºC incubator with 5% CO_2 until 60-90% confluency.

3.2.3 Multilayer Tissue Constructs

Multilayer tissue constructs representing the structure of oral dysplasia were created using SqCC/Y1 cells. A collagen solution was prepared by combining collagen (Roche Applied Science, Indianapolis, IN) reconstituted in 0.2% sterile acetic acid, 0.2 M HEPES, 10x phosphate buffered saline (PBS), and 1x PBS, final pH 7.4. SqCC/Y1 cells were resuspended in the collagen solution at a density of 80 million cells/ml. Tissue constructs were formed by pipetting 100 μl of the cell-collagen solution into Costar Transwell inserts (VWR, West Chester, PA), 6.5 mm diameter with an 8 μm pore size,

allowing the tissue constructs to gel, and adding media in the insert on top of the tissue construct and to the bottom well. PBS was added to empty wells to increase humidity within the plate. The tissue constructs were allowed to grow for 14-21 hours in a 37ºC incubator with 5% CO_2.

3.2.4 Cell Monolayer Labeling

Three samples were prepared: cells labeled for EGFR using the biotinylated EGFR antibody and two sets of control cells, one labeled using a biotinylated anti-human IgG (goat monoclonal, Vector Laboratories, Burlinghame, CA) and one not exposed to any antibody but labeled with the Alexa Fluor® 660 streptavidin dye only. Between all changes of solution, cells were washed 2x with 1x PBS. The media was removed from the wells and cells were blocked for endogenous biotin using an Avidin/Biotin blocking kit (Vector Laboratories). Cells were successively incubated with the primary EGFR or IgG antibody and the Alexa Fluor ® 660 streptavidin for 1 hour at room temperature. After the final washes, PBS was added to the chambers and sealed using a microscope slide.

3.2.5 Multilayer Tissue Constructs Labeling

Multilayer tissue constructs were labeled in a similar fashion to the cells with either the EGFR antibody or anti-human IgG antibody. In addition, the blocking agents, antibodies, and dye were added in permeability-enhancing solutions of 5% DMSO, 10% PVP, or 4% BSA in addition to a PBS control. After labeling in the Transwells, the

tissue constructs were removed, embedded in 3% agarose, and sliced transversely into 250 mm sections using a Krumdieck tissue slicer (MD 1000-A1, Alabama Research and Development, Munford, AL) which is designed to cut fresh tissue with minimal damage. Three replicates of each experiment were performed.

3.2.6 Fresh Tissue Slices

Paired clinically abnormal and clinically normal biopsies were obtained from consenting patients at the University of Texas M.D. Anderson Cancer Center. The clinical protocols were approved by the Institutional Review Boards at the University of Texas M.D. Anderson Cancer Center and the University of Texas at Austin. Biopsies were immediately placed and remained in chilled culture media until they were sectioned into 200 μm transverse slices using a Krumdieck tissue slicer. After slicing, biopsies were labeled as above. The avidin and biotin blocking solutions were added in a 5% BSA solution in PBS. A biotinylated normal mouse IgG (Vector Laboratories) was used as a control. H&E stained sections were obtained for each biopsy and the slices that were labeled for EGFR and imaged.

3.2.7 Imaging

Optically sectioned fluorescence images of the samples were obtained using an inverted Lecia TCS 4D laser scanning confocal microscope, equipped with a Kr/Ar laser providing excitation at 647 nm and a 665 nm long-pass filter. Images were acquired with a 10x objective with a numerical aperture of 0.3 and working distance of 11000 μm or

40x oil-immersion objective with a numerical aperture of 1.0 and working distance of 80 μm. The laser power for image acquisition varied between 3-30 μW. Stacks of images were obtained, with a z-step of 1.5-3 μm and 5-30 images per stack. The contrast, brightness, line averaging, integration time, and pinhole size remained constant for all images in a single experiment.

3.2.8 Fluorometry

Fluorometry was used in order to determine the efficacy of binding using various primary antibody concentrations, incubation times, and the specificity of binding of the contrast agent. Fluorescence emission spectra of suspensions of SqCC/Y1 cells labeled for EGFR were measured in a Spex Fluorolog (JY Horiba, Edison, NJ). Approximately 8-9 million cells were harvested for each sample and resuspended in phenol red-free DMEM with 5% FBS, penicillin, streptomycin, and glutamine. Labeling was performed as for cell monolayers, with the cells centrifuged at 1000 rpm for 3 min in order to change solutions and wash. After labeling, the cells were washed in PBS and resuspended in 3 ml of PBS for the emission scans. Fluorescence emission spectra were measured at an excitation wavelength of 633 nm and emission wavelengths from 643-700 nm at 5 nm increments with a 1 s integration time. Background fluorescence emission spectra were determined by pelleting the cells and measuring the supernatants of the cell suspensions. PBS was also measured as a background. The fluorescence intensity was determined by calculating the area under the emission curve after subtracting the background PBS and/or supernatant.

In order to test the efficacy of labeling at various antibody concentrations and incubation times, cells were labeled using various dilutions of biotinylated EGFR antibody and biotinylated normal mouse IgG of 1:4, 1:10, 1:50, and 1:100 with a 60 min incubation time and using various incubation times of 5, 15, 30, and 60 minutes with a 1:10 antibody dilution.

The specificity of the contrast agent for EGFR was tested in a competitive binding study with EGF. Lyophilized EGF (Sigma Aldrich, St. Louis, MO) was reconstituted in 0.2 μm-filtered 10 mM acetic acid with 0.1% BSA. Cells were labeled as above, with either no, 0.0133 μM, 0.133 μM, or 1.33 μM EGF added in addition to the anti-EGFR antibody.

3.2.9 Quantitative Flow Cytometry

Quantitative flow cytometry was performed on the SqCC/Y1 to determine how many receptors per cell were being labeled. Standard beads from a QIFI kit (Dako Cytomation, Carpinteia, CA) with known amounts of mouse monoclonal anti-CD5 immobilized on the surface produced a calibration curve from which the number of labeled receptors on the cells could be interpolated. Cells were harvested at 70% confluency or less and resuspended at a concentration of 1 million cells/ml in 1 ml of PBS with 5% BSA. Cells were labeled for EGFR using the unbiotinylated version of the same EGFR antibody used in the contrast agent at a 1:10 dilution in phenol red-free DMEM with 5% FBS, penicillin, streptomycin, and glutamine for 1 hour at room temperature with constant shaking. A secondary antibody of goat anti-mouse $F(ab')_2$-

FITC (Dako Cytomation) at a concentration of 1 mg/ml was added at a 1:10 dilution to detect the EGFR antibody. Three control samples were also prepared: cells labeled with normal mouse IgG (Vector Laboratories), cells labeled with the secondary antibody only, and unlabeled cells. MDA-MB-468 cells were also labeled for EGFR as a positive control. In addition, a second quantitative flow cytometry experiment was performed using SqCC/Y1, UMSCC-22A, and A253 cells. Quantitative flow cytometry was performed on a Coulter EPICS Elite flow cytometer with a 15 mW argon laser source at 488 nm.

3.3 RESULTS

To determine the efficacy of using a molecular-specific far-red fluorescent contrast agent to EGFR to detect oral cavity neoplasia, we labeled unfixed monolayers of malignant cells, multilayer tissue constructs, and fresh tissue sections from oral cavity biopsies.

3.3.1 Detection of EGFR in Single Cell Monolayers

Fluorescence images of SqCC/Y1 cells labeled with biotinylated anti-EGFR conjugated to Alexa Fluor® 660 streptavidin obtained with a 40x objective are shown in Fig. 1 along with images of appropriate controls and images of MDA-MB-435S cells. Clear fluorescence is seen for SqCC/Y1 cells labeled with the anti-EGFR in Figure 3-1 (a) with the corresponding transmitted DIC image in Figure 3-1 (b). No fluorescence is seen with either the anti-IgG (Figure 3-1 (c) and (d)) or dye-only control (Figure 3-1 (e)

and (f)). Similar results are seen for MDA-MB-468, SiHa, UMSCC-22A, and A253 cells with the MDA-MB-468 cells showing a much greater fluorescence intensity than the SqCC/Y1 cells (images not shown). MDA-MB-435S cells, which do not express EGFR, show very little fluorescence when labeled with the anti-EGFR (Figure 3-1 (g)).

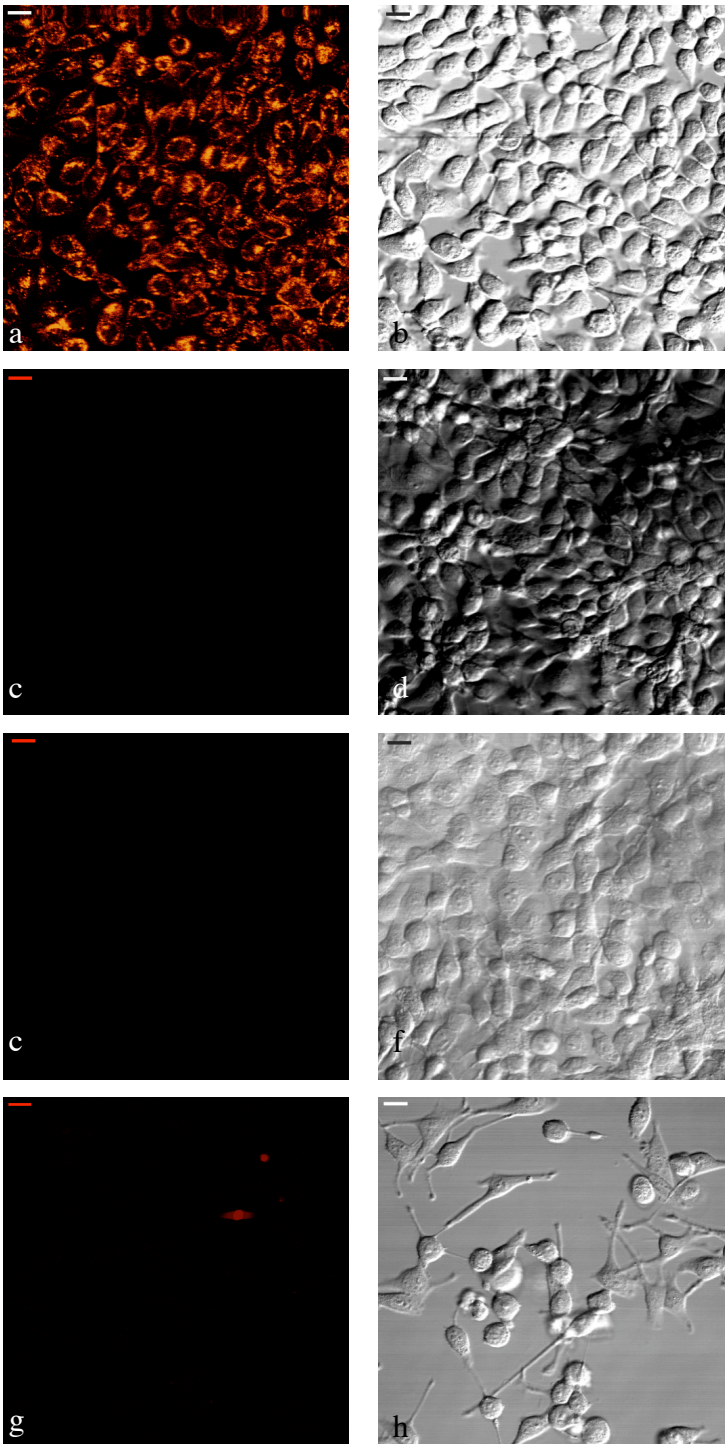

Figure 3-1 Confocal images of SqCC/Y1 and MDA-MB-435S cells taken with a 40x oil immersion objective. (a), (c), (e), and (g) are false color fluorescence images obtained at

excitation 647 nm with a 665 nm longpass filter. (b), (d), (f), and (h) are transmitted DIC images. Scale bar in all images is 25μm. (a) SqCC/Y1 cells labeled with anti-EGFR and Alexa Fluor® 660 streptavidin. (b) Corresponding transmitted DIC image. (c) SqCC/Y1 cells labeled with anti-human IgG and Alexa Fluor® 660 streptavidin. (d) Corresponding transmitted DIC image. (e) SqCC/Y1 cells labeled with Alexa Fluor® 660 streptavidin only, no antibody. (f) Corresponding transmitted DIC image. (g) MDA-MB-435S cells labeled with anti-EGFR and Alexa Fluor® 660 streptavidin. (h) Corresponding transmitted DIC image.

3.3.2 Detection of EGFR in Multilayer Tissue Constructs

Fluorescence images of SqCC/Y1 tissue constructs obtained with a 10x objective are shown in Fig. 2. Tissue constructs labeled in the presence of 5% DMSO Figure 3-2 (b)), 10% PVP (Fig. 2 (c)), and 4% BSA (Fig. 2 (d)) demonstrate labeling through a greater depth than those labeled in PBS only Figure 3-2 (a)). For the corresponding anti-human IgG controls of the tissue constructs, some non-specific labeling is seen with 10% PVP (Figure 3-3 (a)) and 4% BSA (Figure 3-3 (b)). The image shown in Figure 3-3 (b) for the 4% BSA IgG control showed the most fluorescence of all 3 trials, but it appears the labeling is non-specific when compared to the contrast agent in Figure 3-2 (d) where individual cells can be clearly seen. The 10% PVP IgG control shown in Figure 3-3 (a) has a relative fluorescence intensity less than with the contrast agent shown in Figure 3-2 (c). Fluorescence images of the same tissue constructs labeled in the presence of PBS and 5% DMSO obtained with a 40x objective are shown in Figure 3-4. Cell membrane EGFR labeling of cells embedded in collagen is clearly evident in both cases, though labeling is more intense in the presence of 5% DMSO (Figure 3-4 (c)).

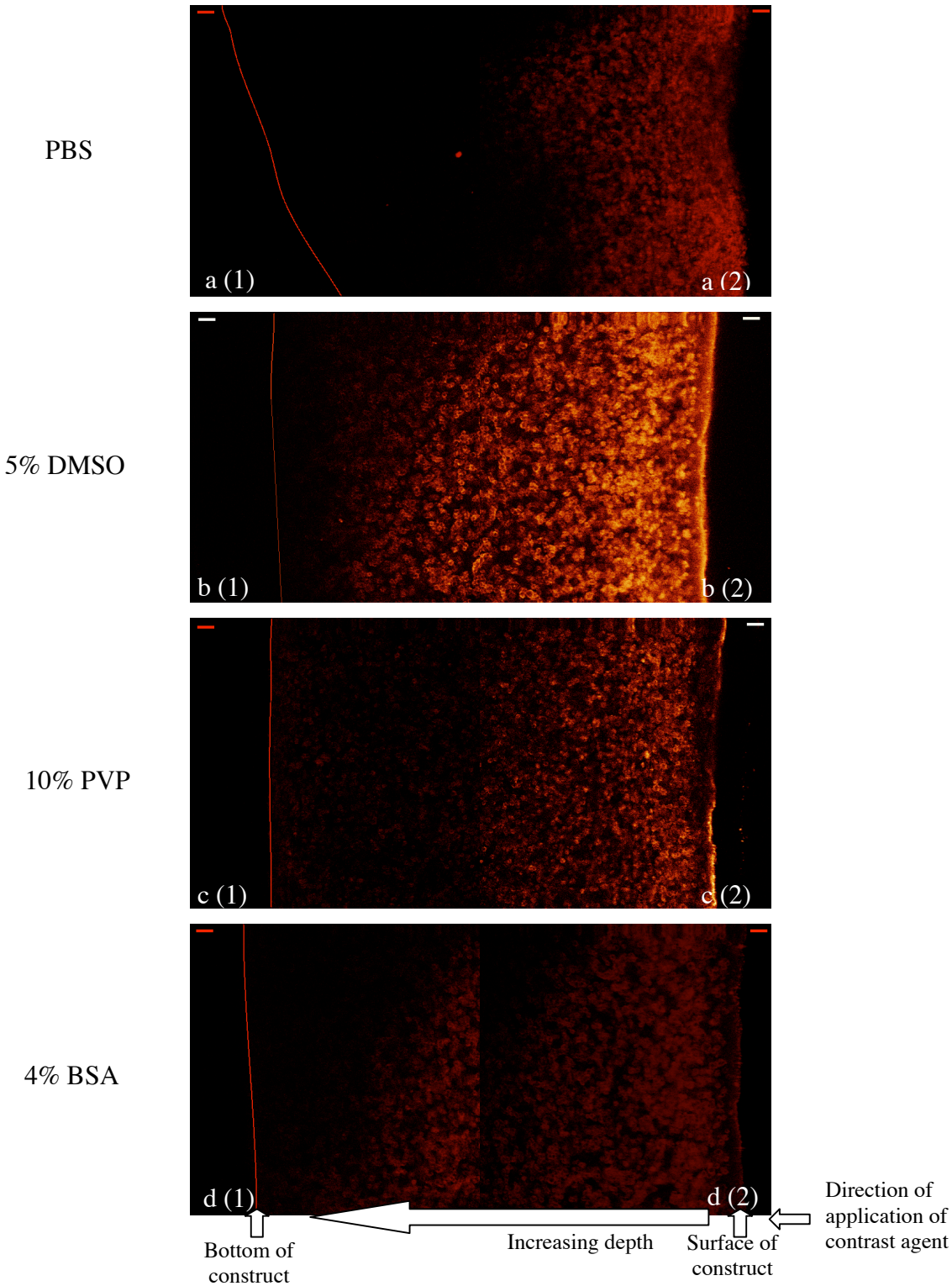

Figure 3-2 False color confocal images of SqCC/Y1 tissue constructs labeled with anti-EGFR and Alexa Fluor® 660 streptavidin in the presence of permeability-enhancing

agents taken with a 10x objective. The scale bar in all images is 100 μm. (2) images are the top of the constructs with the contrast agent applied from the right. (1) images are the bottom of the tissue construct, with the line representing the approximate location of the bottom of the construct. (a) Tissue constructs labeled in the presence of PBS only. (b) Tissue constructs labeled in the presence of 5% DMSO. (c) Tissue constructs labeled in the presence of 10% PVP. (d) Tissue constructs labeled in the presence of 4% BSA.

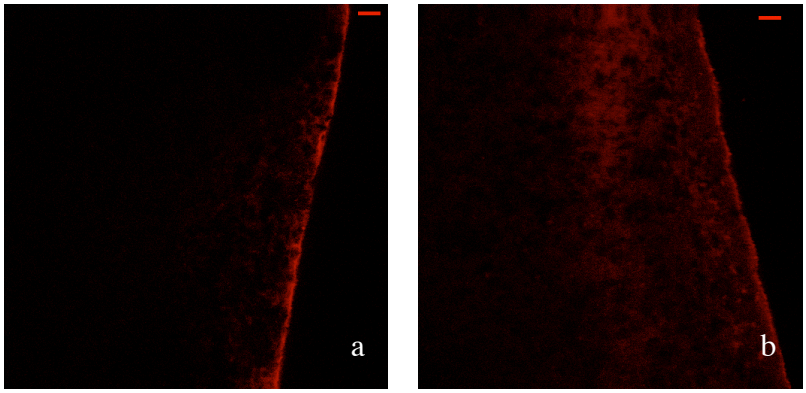

Figure 3-3 False color confocal images of SqCC/Y1 tissue constructs labeled with anti-human IgG and Alexa Fluor® 660 streptavidin in the presence of permeability-enhancing agents taken with a 10x objective. The scale bar in both images is 100 μm. (a) Tissue construct labeled in the presence of 10% PVP. (b) Tissue construct labeled in the presence of 4% BSA.

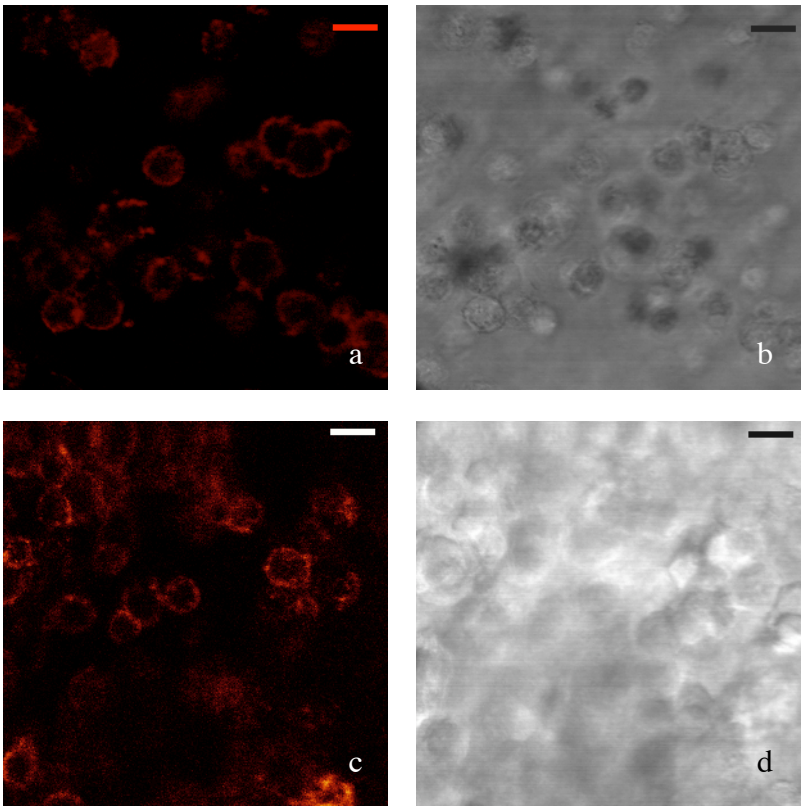

Figure 3-4 Confocal images of SqCC/Y1 tissue constructs labeled with anti-EGFR and Alexa Fluor® 660 streptavidin taken with a 40x oil immersion objective. (a) and (c) are false color fluorescence images obtained at excitation 647 nm with a 665 nm longpass filter. (b) and (d) are transmitted DIC images. Scale bar in all images is 25μm. (a) and (b) Tissue constructs labeled in the presence of PBS only. (c) and (d) Tissue constructs labeled in the presence of 5% DMSO.

3.3.3 Detection of EGFR in Fresh Tissue Slices

Fluorescence images from a clinically abnormal and clinically normal biopsy pair are shown in Figure 3-5 (a) and (b), labeled for EGFR using the contrast agent obtained with a 40x objective. Figure 3-5 (c) and (d) show the corresponding H&E images for the clinically abnormal and clinically normal biopsy respectively. The abnormal biopsy was

obtained from the retromolar trigone and diagnosed as moderate dysplasia of the squamous epithelium with underlying foci of invasive squamous carcinoma. The normal biopsy was obtained from the pharyngeal wall and diagnosed as normal with mild hyperkeratosis. The fluorescence intensity is considerably higher in the abnormal sample (Figure 3-5 (a)) than in the normal sample (Figure 3-5 (b)), by an average factor of 5x.

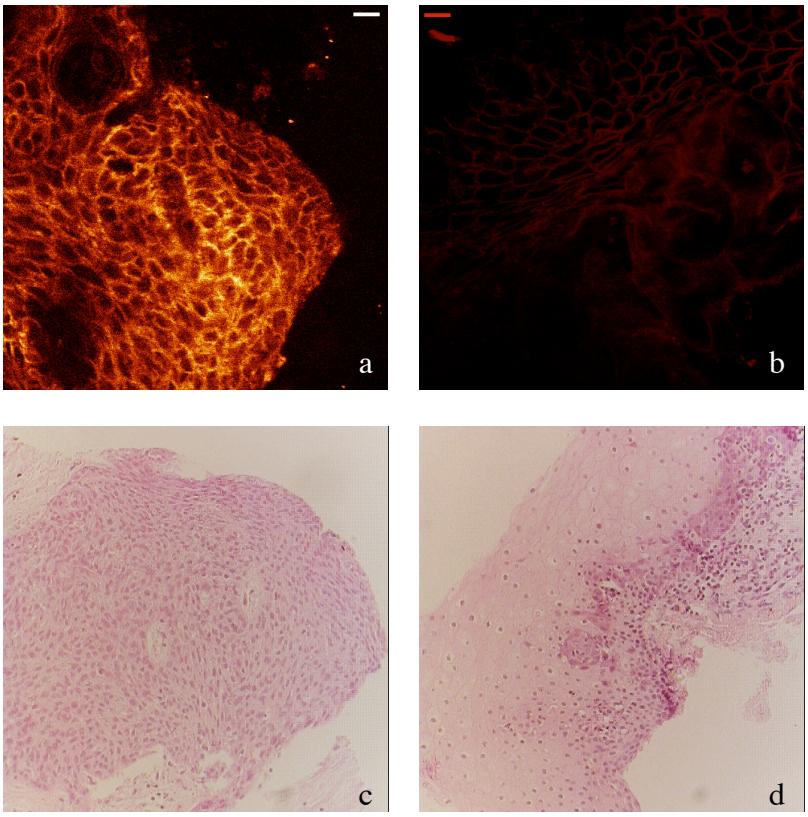

Figure 3-5 Confocal images of tissue slices from a (a) clinically abnormal and (b) clinically normal biopsy pair and corresponding H&E images ((c) and (d) respectively). Confocal images taken with a 40x oil immersion objective; scale bar is 25 μm. H&E images taken with a 10x objective. Abnormal biopsy taken from the retromolar trigone. Diagnosis of (c) was moderate dysplasia in the epithelium with foci of moderately-differentiated cancer. Normal biopsy taken from the pharyngeal wall. Diagnosis of (d) was normal with mild hyperkeratosis.

3.3.4 Fluorometry of Cells Labeled for EGFR

The mean fluorescence intensities of SqCC/Y1 cells labeled for various incubation times and with various dilutions of EGFR antibody are shown in Fig. 6. In Fig. 6, the squares are cells labeled for EGFR corrected for background intensity by subtracting IgG and the diamonds are cells labeled using the IgG control. Cells labeled for various incubation times of 5, 15, 30, and 60 min showed a linear increase in fluorescence with increasing incubation time as shown in Figure 3-6 (a). Cells labeled using various dilutions of the EGFR antibody of 1:4, 1:10, 1:50, and 1:100 also showed a linear increase in fluorescence with increasing antibody concentration as shown in Figure 3-6 (b). In both cases, the shortest incubation time and the lowest antibody dilution still demonstrated a significant increase in fluorescence compared to the control. Cells labeled in the presence of 0.0133 μM EGF did not show a significant difference in fluorescence intensity compared to those labeled in the presence of no EGF. However, the cells labeled in the presence of increasing concentrations of EGF showed a linear decrease in fluorescence intensity with increase in EGF concentration as shown in Figure 3-7.

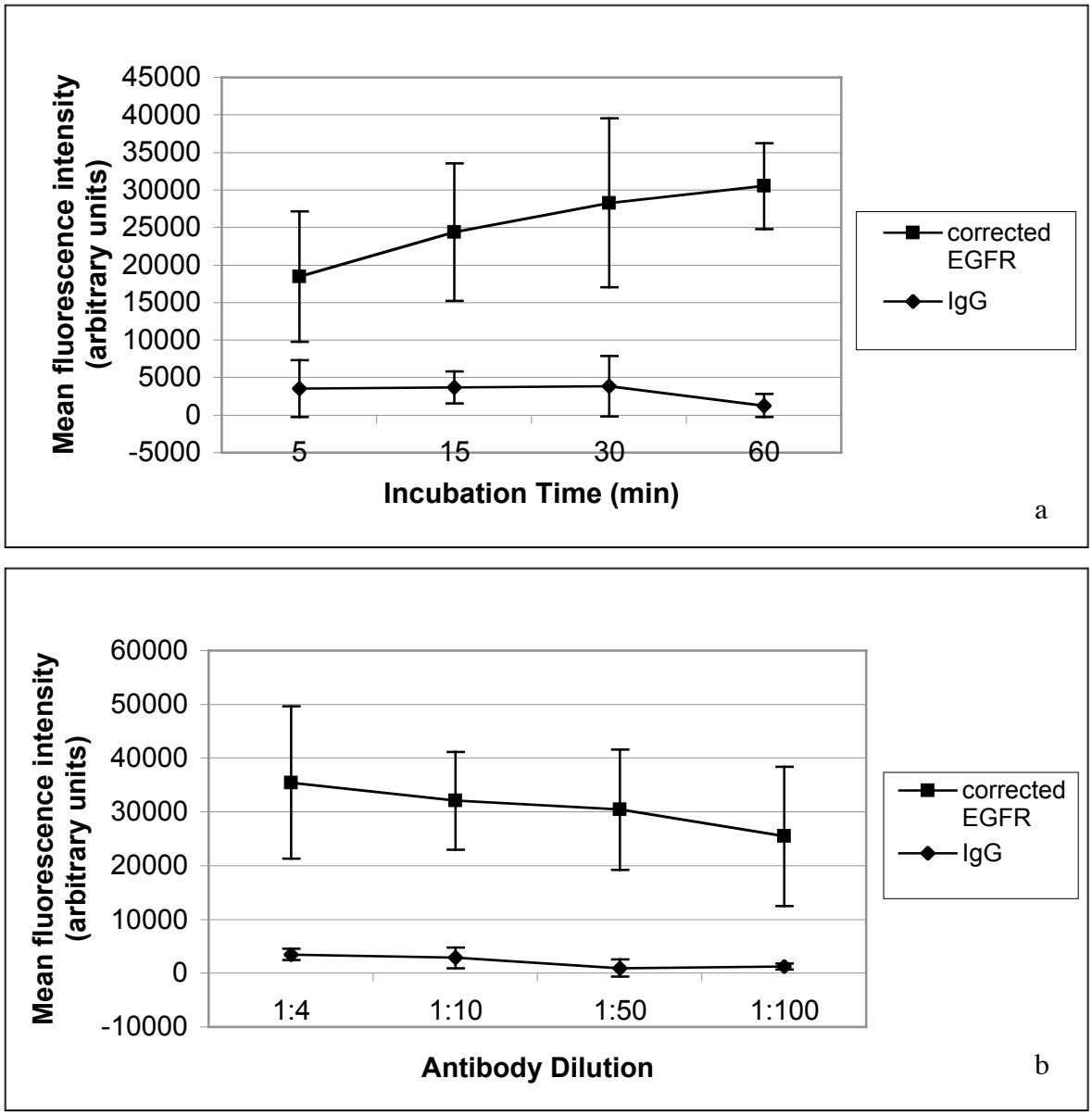

Figure 3-6 (a) Fluorescence intensities for SqCC/Y1 cells labeled for various incubation times using a 1:10 antibody dilution averaged over three trials. (b) Fluorescence intensities for SqCC/Y1 cells labeled with different dilutions of antibody using a 60 min incubation time averaged over three trials. In both graphs, the PBS background and background produced by the supernatant of the cell suspension has been corrected for in all samples. The squares are cells labeled using EGFR, corrected for the background intensity of cells by subtraction of the IgG sample. The diamonds are cells labeled using the IgG control.

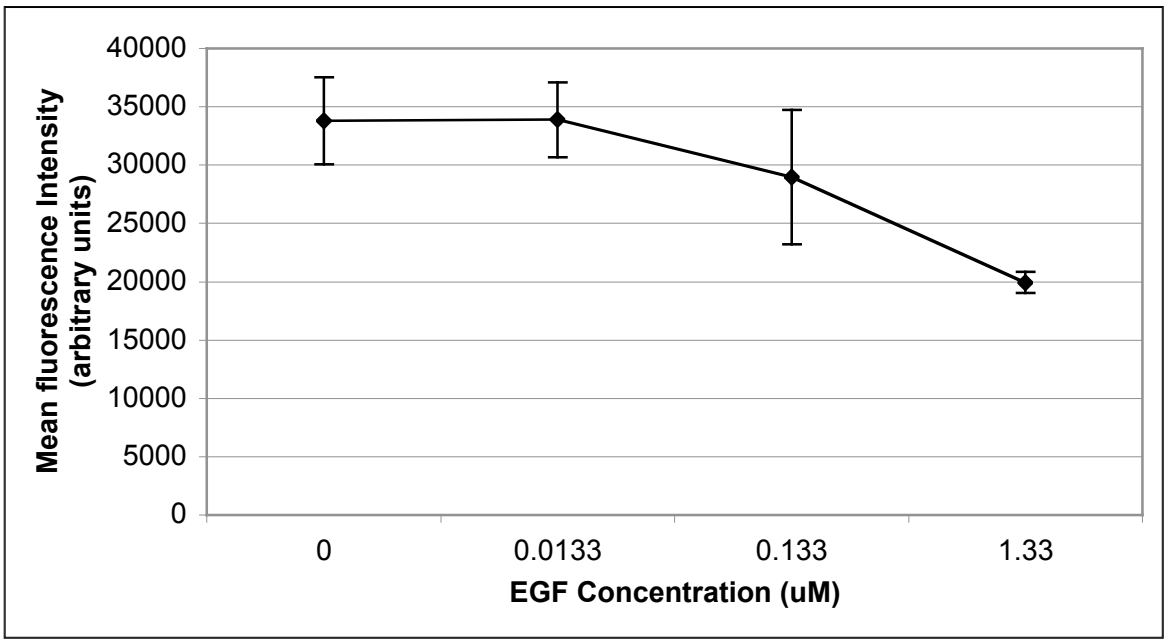

Figure 3-7 Fluorescence intensities for SqCC/Y1 cells labeled with the contrast agent in the presence of no EGF, 0.0133 μM EGF, 0.133 μM EGF, and 1.33 μM EGF averaged over three trials. All samples are corrected for the PBS background and background produced by the supernatant of the cell suspension.

3.3.5 Quantitative Flow Cytometry

The number of EGFR per cell was determined for SqCC/Y1 cells using the QIFI kit analysis. Approximately 300,000 receptors per cell were labeled in the first experiment (data not shown). Other investigators reported the number of EGF receptors per cell as 4.70-8 x 10^5 (26, 106), similar to that reported here.

The second quantitative flow cytometry experiment using the three cell lines from the oral cavity demonstrated that labeling could be achieved on cell lines with various levels of EGFR expression.

The standard curve generated by the QIFI calibration beads is illustrated in Figure 3-8, with the mean fluorescence intensity from each of the cell lines plotted along the standard curve. The number of EGFR per SqCC/Y1 cell from this experiment was approximately 200,000, slightly less than in the first experiment. A253 cells were calculated to have approximately 100,000 EGFR per cell, which agrees with reported literature of 0.51×10^5 and 1.15×10^5 low and high affinity EGFR binding sites per cell (26). The UMSCC-22A cells were determined to have an intermediate number of EGFR at approximately 160,000 per cell.

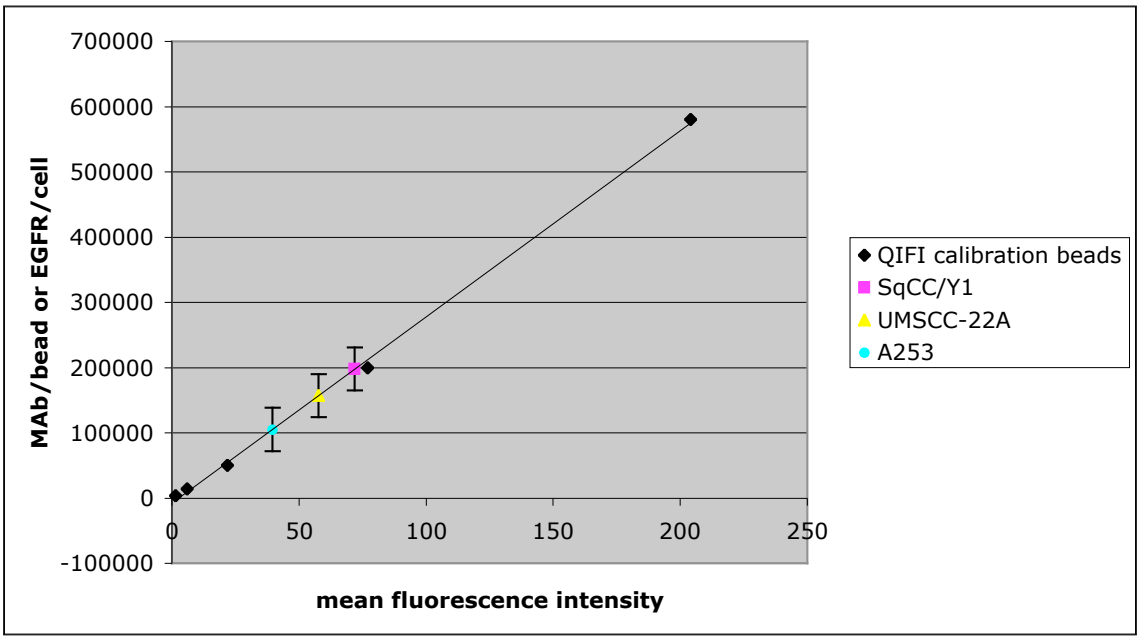

Figure 3-8 Standard curve generated by quantitative flow cytometry data, plotting the number of monoclonal antibody immobilized on the bead versus the mean fluorescence intensity determined by flow cytometry (black diamonds). The mean fluorescence intensity for each of the cells lines, SqCC/Y1 (pink square), UMSCC-22A (yellow triangle), and A253 (blue circle) is plotted along the standard curve, and the number of EGFR/cell interpolated from the standard curve.

3.4 DISCUSSION

In vitro experiments with cell cultures demonstrate that the contrast agent specifically targets the extracellular membrane of neoplastic cells and suggests specific targeting of EGFR. EGFR is a transmembrane protein, thus as expected, fluorescence is seen primarily at the cell membrane, where the EGF receptor is located, and little to no fluorescence is seen with controls. The fluorometry competitive binding studies with EGF demonstrate the contrast agent binds to a much lower degree in the presence of EGF, also suggesting that it is specifically targeting EGFR.

An advantage of using Alexa Fluor® 660 streptavidin is that it has a broad absorption peak, allowing it to be efficiently excited between 633-660 nm with emission at 690 nm. The broad excitation range allows the contrast agent to be used readily with the 633 nm laser line of a HeNe or the 647 nm laser line of a krypton-ion laser while still maintaining a relatively long Stokes shift for easy rejection of elastically scattered excitation. An excitation wavelength greater than about 600 nm allows for increased penetration depth into tissue with substantially reduced interference from autofluoresence of endogenous fluorophores and scattering and absorption from tissue structures.

Fluormetry experiments with varying dilutions of the EGFR antibody and varying the incubation time indicate that the antibody can be used in relatively low concentrations and only short incubation times are required to achieve a detectable fluorescence signal. The use of low antibody concentrations is critical in the development of the contrast agent to minimize the possibility for immunogenic effects and to keep costs low. In

addition, for clinical applications of the contrast agent, a short incubation time is critical in order to achieve expedient diagnosis with minimal patient discomfort and waiting time.

Numerous studies have achieved localization of target-specific NIR fluorescent contrast agents to tumors using monoclonal antibodies or peptide delivery platforms *in vivo* in animal models (37, 62, 65-67), however in all cases, the conjugate was delivered via i.v. or i.p. injection. In contrast, we are exploring methods to achieve labeling through topical application of the contrast agent. Topical application of the contrast agent is ideal to reduce systemic exposure to the contrast agent and minimize the discomfort associated with i.v. injection. However, in order to label deeper lesions through topical application, the contrast agent may have to be applied in conjunction with permeability-enhancing agents in order to increase the penetration depth through multiple layers of epithelial cells. DMSO, PVP, and BSA have all been applied as penetration enhancers across biomembranes, cell monolayers, and multiple layers of epithelial cells (96-99, 107). All three permeability-enhancing agents tested here, 5% DMSO, 10% PVP, and 4% BSA, increased penetration of the contrast agent relative to PBS in tissue constructs. Tissue constructs labeled in the presence of either DMSO or PVP demonstrated fluorescence to the bottom of the tissue construct, approximately 500 μm.

The ability to distinguish abnormal from normal tissue based on fluorescence intensity of the contrast agent was achieved. In the biopsy pair presented here, the dysplastic slice had a fluorescence intensity 5x greater than that of the normal slice.

Histologically, the abnormal slice contained both dysplasia in the epithelium and foci of moderately-differentiated cancer while the normal slice was normal with mild hyperkeratosis. Although EGFR is expressed in normal tissue, the likelihood is that overexpression of EGFR in abnormal tissue provides sufficiently increased fluorescence intensity to discriminate abnormal from normal tissue. In addition, while the elevation of EGFR in normal-early hyperplasia and in normal tissue adjacent to tumor may lead to false positive diagnoses, it also has the possibility to facilitate early detection by providing a marker for tissue which is likely to undergo carcinogenesis and should be monitored. A preliminary clinical study testing at least 20 pairs of abnormal and normal biopsies from the oral cavity is currently in progress to determine the efficacy of distinguishing abnormal from normal tissue based on the fluorescence intensity of the contrast agent.

Fluorescence spectroscopy and/or imaging could be used in order to detect the signal of the contrast agent *in vivo* and localize potential tumors or tumor margins. In addition, with the development of fiber-based *in vivo* confocal microscopes (88-93), including the commercially available fiber-based confocal fluorescence microscopes produced by OptiScan Imaging Limited (Victoria, Australia) and Mauna Kea Technologies (Paris, France), the contrast agent could be used to provide additional signal for imaging applications to the epithelial layer *in vivo* to allow for diagnosis of abnormal tissue.

A number of significant issues must be addressed prior to performing clinical trials with this contrast agent. Issues which must be considered are toxicity of the Alexa Fluor® 660 dye, possible immunogenic effects of the antibody, optimal time for localization of the contrast agent to neoplasia and subsequent imaging, and clearance of the contrast agent from the tissues. While these pharmokinetic issues will need to be addressed, we have demonstrated that the contrast agent has the ability to target EGFR-positive cells in viable *in vitro* biological models of cell monolayers and cell suspensions, that deeper labeling is possible through topical application and the use of permeability-enhancing agents, and that there is the potential to distinguish abnormal from normal tissue based on fluorescence intensity in *ex vivo* biopsy samples.

Chapter 4

Detection of Epidermal Growth Factor Receptor Expression in *Ex Vivo* Oral Cavity Biopsies Using a Molecular-Specific Contrast Agent

4.1 INTRODUCTION

Over the past 40 years, the five-year survival rate for oral cancer has not significantly increased although treatment techniques have advanced (7, 8). This is most likely due to the fact that oral cancer is generally not diagnosed until it has reached later stages, when treatment is more debilitating and prognosis is poor. Failure to recognize oral cancer in its early stages is primarily because detection of oral cancer relies entirely upon recognition and suspicion by the treating clinician. The oral cavity is tended to by two different types of clinicians and this split in professional responsibility may lead to a deficiency in the recognition of suspicious lesions and diagnosis of disease (13). The dentist, who is most familiar with this anatomical region, most often treats the oral cavity, but may not have specialized training in recognizing early cancer. This may result in a lack of diagnosis until a lesion has reached advanced stages when it is easily identifiable as cancer.

Detection of early cancer in the oral cavity could be greatly improved through the use of molecular markers that are indicative of the transformation process. Molecular markers can act as early indicators of disease or progression of disease (16), and possibly permit detection of cancer before a clinician would recognize the lesion. One method of

utilizing molecular markers as an indicator of disease is to develop fluorescent contrast agents which specifically target the molecular marker and can be interrogated *in vivo* using optical techniques such as spectroscopy or confocal microscopy. Optical techniques have the advantage of the potential to provide near real-time information non-invasively, while most current diagnostic methods in the oral cavity require biopsy and microscopic examination of tissue.

Epidermal growth factor receptor (EGFR) is a promising molecular target for detection of oral cancer because various studies have estimated that 50-98% of tumors in the oral cavity overexpress EGFR (27-31). EGFR is expressed in normal tissue in cells that are undergoing proliferation (24), with elevated expression during the progression to dysplasia and cancer (34). Researchers have also investigated the correlation between EGFR expression and tumor staging, prognosis, and relapse. Studies have found that tumor EGFR levels are correlated to the size of tumor (30, 31) and that mean values of EGFR increase with tumor size and advanced clinical stage (28). In a correlative study of patients with advanced head and neck squamous cell carcinoma (HNSCC) enrolled in a radiotherapy study, EGFR expression was a strong prognostic indicator for overall survival and disease-free survival and was highly predictive for the probability of local-regional relapse but not distant metastasis (36). Other studies, however, have reported no significant correlation between EGFR levels and tumor staging (27, 28, 36).

Previously, we demonstrated the efficacy of a far-red fluorescence contrast agent targeted against EGFR in squamous carcinoma cells of the buccal mucosa in monolayer

culture and in 500 μm thick multilayer tissue constructs (108). In this study, we are further exploring the use of the contrast agent by testing it in *ex vivo* paired normal and abnormal biopsy samples obtained from consenting patients at the University of Texas M.D. Anderson Cancer Center.

4.2 MATERIALS AND METHODS

4.2.1 Contrast Agent

The contrast agent is described in detail in (108), but will be briefly reviewed here. The antibody used in the contrast agent was a biotinylated mouse monoclonal anti-human EGFR (clone 111.6, 200 mg/ml, LabVision NeoMarkers, Fremont, CA) and was used at a 1:10 dilution. Alexa Fluor® 660 streptavidin (Molecular Probes, Eugene, OR) was used as the far-red fluorescent marker. For use in labeling, it was diluted from a 1 mg/ml stock to 250 mg/ml in PBS and used at a 1:8 dilution.

4.2.2 Fresh Tissue Slices

Paired clinically abnormal and clinically normal biopsies were obtained from consenting patients at the University of Texas M.D. Anderson Cancer Center. The clinical protocols were approved by the Institutional Review Boards at the University of Texas M.D. Anderson Cancer Center and the University of Texas at Austin. Biopsies were immediately placed and remained in chilled culture media (phenol-red free, Dulbecco's modified essential media/F12 with high glucose, Invitrogen, Carlsbad, CA) until they were sectioned into 200-400 μm transverse slices using a Krumdieck tissue

slicer (MD 1000-A1, Alabama Research and Development, Munford, AL) which is designed to cut fresh tissue with minimal damage. After slicing, biopsies were labeled using the contrast agent. The tissue slices were first blocked for endogenous biotin using an Avidin/Biotin blocking kit (Vector Laboratories, Burlinghame, CA) in a 5% bovine serum albumin (BSA) solution in PBS. The tissue slices were successively incubated with the primary EGFR antibody or a biotinylated normal mouse IgG (Vector Laboratories) and the Alexa Fluor® 660 streptavidin for 30 min. at room temperature with constant shaking. All dilutions were prepared in a 1.25% BSA solution in PBS. Between all changes of solution, the tissue slices were washed in PBS for 5 min. two times with constant shaking. Hematoxylin and eosin (H&E) stained sections and EGFR immunohistochemistry (IHC) was obtained for each biopsy and the slices that were labeled for EGFR and imaged. H&E stained sections were examined by a board-certified pathologist and diagnosis was assessed using standard histopathological criteria as follows: normal, hyperplasia, hyperkeratosis, dysplasia (mild, moderate, or severe), and *in situ* or invasive cancer (well-, moderate-, or poorly-differentiated).

4.2.3 Imaging

Optically sectioned fluorescence images of the samples were obtained using an inverted Lecia TCS 4D laser scanning confocal microscope, equipped with a Kr/Ar laser providing excitation at 647 nm and a 665 nm long-pass filter. Images were acquired with a 40x oil-immersion objective with a numerical aperture of 1.0 and working distance of 80 μm. The laser power for image acquisition varied between 3-30 μW. Z-series stacks

of images were obtained, with a z-step of 1.5-3 μm and 5-30 images per stack. The contrast, brightness, line averaging, integration time, and pinhole size remained constant for all acquisitions.

4.2.4 Image Processing

MATLAB (the MathWorks, Inc, Natick, MA) code was written to detect the fluorescently-labeled edges of the epithelium in the images and convert the edges into a mask. This mask was then applied to the original image so only information from the fluorescently-labeled epithelium was obtained. The mean fluorescence intensity (MFI) for the fluorescent portions of each image in each stack was obtained by dividing the image by the laser power at the time of acquisition. In cases where fluorescently-labeled cells occupied the entire field of view, the MFI was calculated for the entire image without using edge detection.

4.2.5 Diagnosis Using Mean Fluorescence Intensity

MFI was used to determine if there was a correlation between fluorescence and pathological diagnosis. In addition, the epithelium was broken down into three layers, basal, intermediate, and surface, to determine if MFI by epithelial layer would be a more effective means for diagnosis. If an image stack contained the basement membrane or was within approximately 50 μm of the basement membrane, it was classified as basal. If it contained the superficial epithelium, epithelial-surface transition, or was within 50 μm of the surface, it was classified as surface. If no basement membrane or obvious

superficial epithelium was present, it was classified as intermediate. If the image stack contained the entire epithelial layer, from the basement membrane to surface, its MFI was added to all three categories. In cases of invasive carcinoma, cells at the surface of the tissue slice or within 50 μm of the surface were classified as surface. Cells which were obviously embedded in the stroma were classified as basal. If the cells were not near the surface or obviously invaded into the stroma, the image stack was classified as intermediate.

The tissue slices prepared from the biopsies obtained from the first three patients were labeled using a stock of the Alexa Fluor® 660 dye that was weighed out to prepare the 1 mg/ml stock solution instead of reconstituting the entire vial in 1 ml of dH_2O, as was done with the remaining stocks of dye. Due to the sensitivity of the scale and small amounts of dye being weighed, the solution prepared using dye that was weighed in this manner was less concentrated than dye prepared by using the entire contents of the vial. In order to correct for this difference, a scaling factor was determined using the ratio of the optical densities of two solutions, one prepared in each manner. The fluorescence intensities calculated for the first three patients were multiplied by this scaling factor.

In assigning a classification to a biopsy, hyperkeratosis and/or hyperplasia were considered normal. In addition, when a diagnosis of varying degrees of severity occurred for dysplasia or cancer, either from different sections from the same biopsy having a different diagnosis or a single section having focal areas of a different diagnosis, then the biopsy was classified according to the most severe of the diagnoses. For example, a

biopsy that had mild to moderate dysplasia was classified as moderate dysplasia and a biopsy that had moderately-differentiated cancer and moderate dysplasia was classified as moderately-differentiated cancer. However, if a biopsy contained both benign and malignant tissue, it was noted as containing both rather than being classified by only the malignant diagnosis. For example, a biopsy containing invasive carcinoma with overlying normal epithelium was classified as normal and cancer.

4.3 RESULTS

4.3.1 Overview of Patients

A total of 17 patients participated in this study. Table 4-1 provides an overview of the patients obtained in the study, with the site of biopsy and pathological diagnosis of the clinically abnormal and normal biopsy. The number of biopsies by pathological diagnosis is listed in Table 4-2.

Table 4-1 Summary of patients in clinical study, site of biopsy, and pathological diagnosis of the clinically abnormal and normal biopsy. Abbreviations used include floor of mouth (FOM), buccal mucosa (BM), differentiated (diff), and moderate (mod). No diagnosis occurs when there is no epithelium in the sample and a pathological diagnosis cannot be made. A site in the center of the "site" column indicates that both the abnormal and normal biopsy were from the same site.

Patient Number	Site		Pathology Diagnosis	
	Abnormal	Normal	Clinically Abnormal	Clinically Normal
1	Tongue		Well diff. cancer	Normal
2	Gingiva		Mild-moderate dysplasia	Hyperplasia, hyperkeratosis
3	Tongue		Hyperkeratosis, mild-moderate dysplasia	No diagnosis
4	Retromolar trigone	Pharyngeal wall	Mod. dysplasia, moderate-poor diff. cancer	Mild hyperkeratosis
5	Floor of mouth		Hyperkeratosis	Hyperplasia, hyperkeratosis
6	Mandibular gingival FOM	Buccal mucosa	Invasive moderate diff. cancer	Hyperplasia, hyperkeratosis
7	BM anterior margin	Right lateral tongue	Hyperplasia, hyperkeratosis	Hyperplasia, hyperkeratosis
8	Left lateral tongue	Right lateral tongue	Hyperkeratosis, hyperplasia	Hyperplasia, hyperkeratosis
9	Base of tongue	Buccal mucosa	Invasive moderate diff. cancer	Hyperplasia, hyperkeratosis
10	Buccal mucosa		Hyperplasia, hyperkeratosis, mild-mod dysplasia	Hyperplasia, hyperkeratosis
11	Left lateral tongue		Invasive moderate diff. cancer	Hyperplasia, hyperkeratosis
12	Right tongue	Right BM	Normal, moderate diff. cancer	Hyperplasia, hyperkeratosis
13	Right BM	Left BM	Hyperkeratosis, mild dysplasia	Hyperplasia, hyperkeratosis
14	Left buccal mucosa	Anterior BM (lower lip)	Hyperkeratosis, mild dysplasia	Hyperplasia, hyperkeratosis
15	Right lateral tongue		Hyperkeratosis, mild dysplasia	Hyperplasia, hyperkeratosis
16	Gingiva near buccal mucosa		Normal, mod. dysplasia, invasive mod. diff cancer	Hyperplasia, hyperkeratosis
17	Gingiva	Gingiva-BM junction	Invasive well diff. cancer	Hyperkeratosis

Table 4-2 Breakdown of biopsy samples by pathological diagnosis.

Pathological Diagnosis	Number of biopsy samples
Normal	1
Hyperkeratosis and/or hyperplasia	18
Mild dysplasia	3
Mild-moderate dysplasia	2
Well-differentiated cancer	2
Moderately-differentiated cancer	3
Moderate dysplasia and moderate to poorly-differentiated cancer	1
Hyperplasia, hyperkeratosis and dysplasia	1
Normal and cancer	2
No diagnosis	1

As is evident in Table 4-1, some of the clinically abnormal biopsies were found to be pathologically normal, which reduced the number of overall abnormal samples in the study. Three of the clinically abnormal biopsies were found to be pathologically normal, resulting in a specificity of 85% and sensitivity of 100% based on clinical impression.

4.3.2 Fluorescence Confocal Imaging

Figure 4-1 illustrates fluorescence confocal, H&E, and EGFR IHC images from patient 4. The clinically abnormal biopsy was from the retromolar trigone and diagnosed as moderate dysplasia with underlying foci of moderate to poorly-differentiated cancer. The clinically normal biopsy was from the pharyngeal wall and diagnosed as hyperplasia and hyperkeratosis, conditions considered as normal in the oral cavity. Figure 4-1 (a) is representative of the fluorescence throughout the entire epithelium of the abnormal biopsy. The stromal to epithelial transition in a normal biopsy is shown in Figure 4-1 (b). Fluorescence is evident near the basement membrane of epithelium from this normal

biopsy. The corresponding EGFR IHC sections are shown in Figure 4-1 (e) and (f) for the abnormal and normal biopsy. EGFR staining is strong throughout the epithelium of the abnormal biopsy, which corresponds to what was seen in the fluorescence confocal imaging. In the normal biopsy, EGFR staining is strong near the basement membrane and decreases superficially, with virtually no staining in the most superficial layer. This also corresponds to what was observed in confocal imaging of normal biopsies.

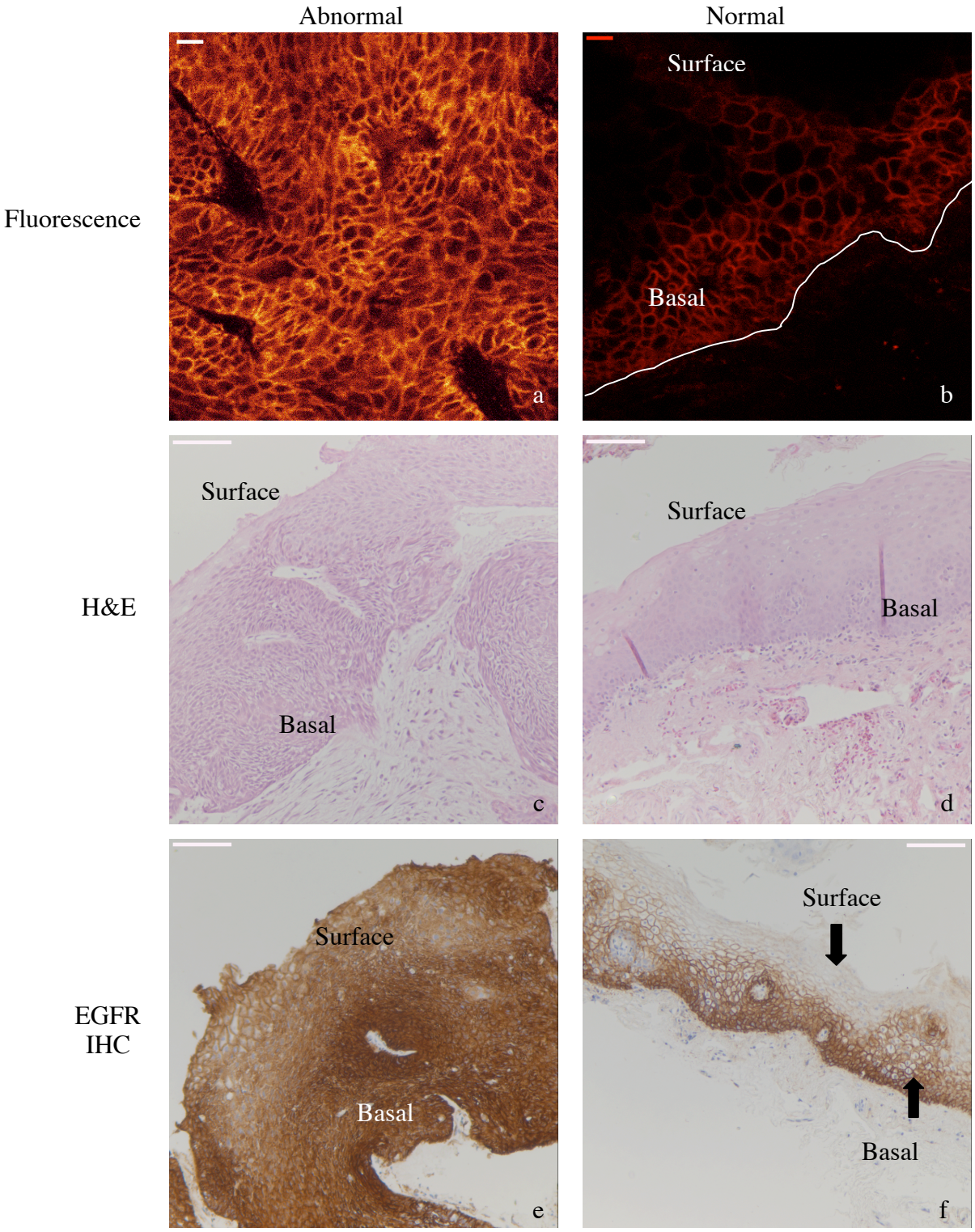

Figure 4-1 Images for patient 4. Left column images are from the clinically abnormal biopsy, which was diagnosed as moderate dysplasia with underlying foci of moderate to poorly-differentiated cancer. Right column images are from the clinically normal biopsy,

which was diagnosed as hyperplasia and hyperkeratosis. (a) False color fluorescence confocal image from abnormal biopsy, laser power 4 μW. (b) False color fluorescence confocal image from normal tissue biopsy, laser power 9 μW. The white line indicates the basement membrane. (c) and (d) Corresponding H&E images for abnormal and normal biopsies, respectively. (e) Abnormal EGFR IHC. Staining is present throughout the entire epithelium. (f) Normal EGFR IHC. Staining is strong near the basement membrane and decreases to virtually no staining in the superficial epithelium. Fluorescence images taken with 40x objective, scale bar 25 μm. H&E and EGFR IHC images taken with 10x objective, scale bar 100 μm.

Images from an invasive moderately-differentiated cancer from patient 6 are shown in Figure 4-2. The clinically normal biopsy was diagnosed as hyperplasia and hyperkeratosis. No clear epithelium could be distinguished in the abnormal biopsy, with labeled cells fluorescing throughout the section (Figure 4-2 (a)). This morphology was confirmed by the H&E section (Figure 4-2 (b)), which revealed an invasive cancer, such that no clear epithelium existed in the biopsy. Figure 4-2 (c) and (d) show fluorescence confocal images from the basement membrane and superficial layer of the normal biopsy respectively. As is evident from these images, fluorescence was strong near the basement membrane and decreased in the superficial layer, which correlates well to expected EGFR expression in normal epithelium. The corresponding transmitted image of the normal superficial epithelium is shown in Figure 4-2 (f).

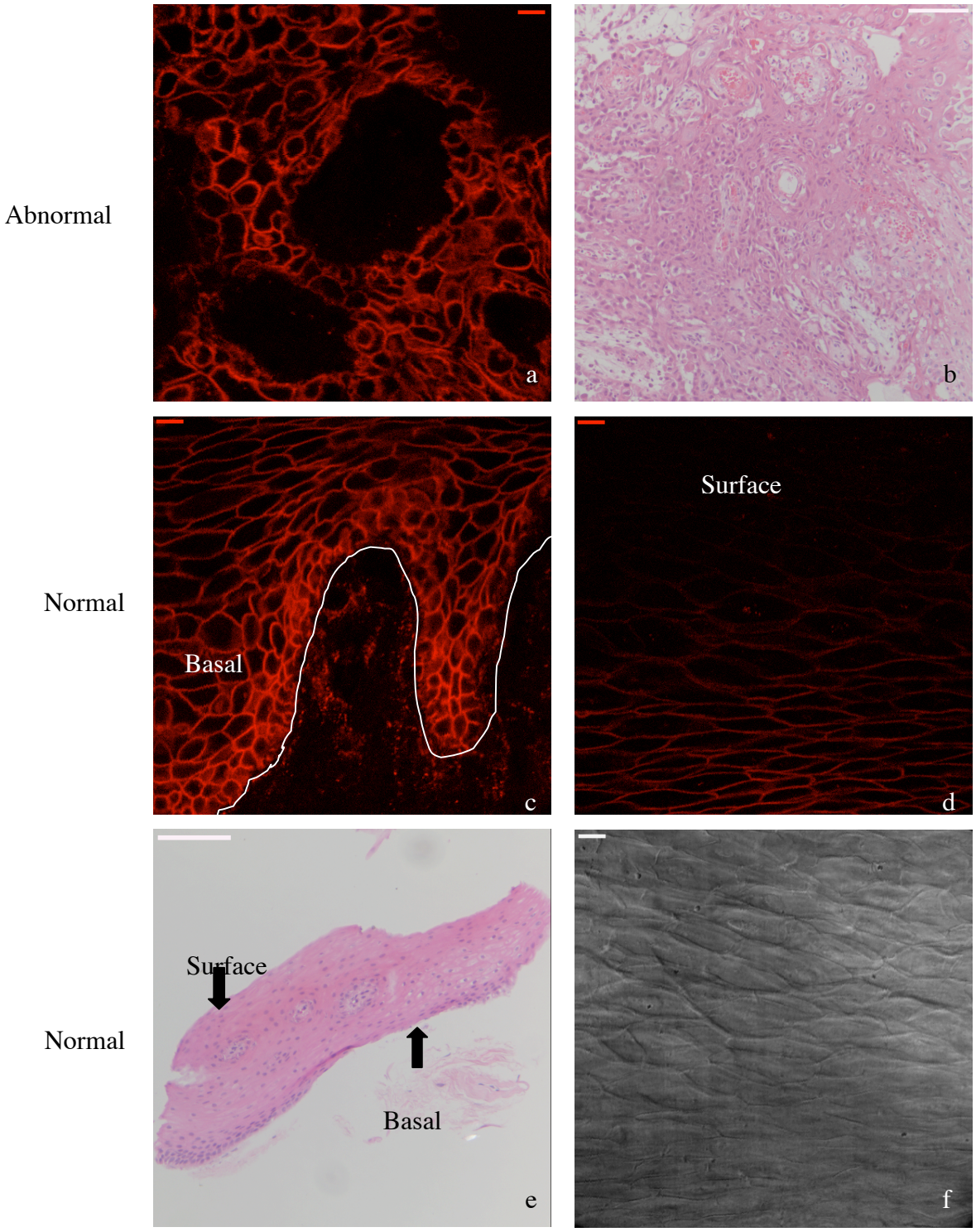

Figure 4-2 Images for patient 6. Abnormal biopsy was diagnosed as invasive moderately differentiated cancer. Normal biopsy was diagnosed as hyperplasia and hyperkeratosis. (a) False color fluorescence confocal image from abnormal biopsy, laser power 6 μW.

(b) Corresponding H&E. Invasive cancer cells are present throughout the section. (c) False color fluorescence confocal image from basal layer of the normal biopsy, laser power 7 μW. Fluorescence is strong near the basement membrane, which is indicated by a white line. (d) False color fluorescence confocal image from the superficial layer of the normal biopsy, laser power 9 μW. Fluorescence decreases in superficial layers. (e) Corresponding H&E. (f) Corresponding transmitted image of the superficial layer of the normal biopsy. Fluorescence images taken with 40x objective, scale bar 25 μm. H&E images taken with 10x objective, scale bar 100 μm.

An example of a clinically abnormal biopsy with mixed pathological diagnosis of hyperplasia and hyperkeratosis for one tissue slice and mild dysplasia for the second tissue since is illustrated in Figure 4-3 along with the corresponding clinically normal biopsy, which was also pathologically normal. Figure 4-3 (a) through (c) are the fluorescence confocal, H&E, and EGFR IHC images for the clinically abnormal and pathologically normal tissue slice. Strong EGFR labeling near the basement membrane is evident in both the IHC and fluorescence images. Figure 4-3 (d) through (f) are the fluorescence confocal, H&E, and EGFR IHC images for the clinically abnormal tissue slice that was diagnosed as mild dysplasia. Fluorescence is strong near the basement membrane (Figure 4-3 (d)). Thickening of the epithelial layer with dysplastic cells is evident in the H&E image (Figure 4-3 (e)). These same cells also stain for EGFR in the IHC image (Figure 4-3 (f)). Figure 4-3 (g) though (i) are the fluorescence confocal, H&E, and EGFR IHC images for the clinically and pathologically normal biopsy. Fluorescence is again evident in the basal layers (Figure 4-3 (g)). The relative amount of EGFR staining in the IHC image (Figure 4-3 (i)) is similar to that in Figure 4-3 (c).

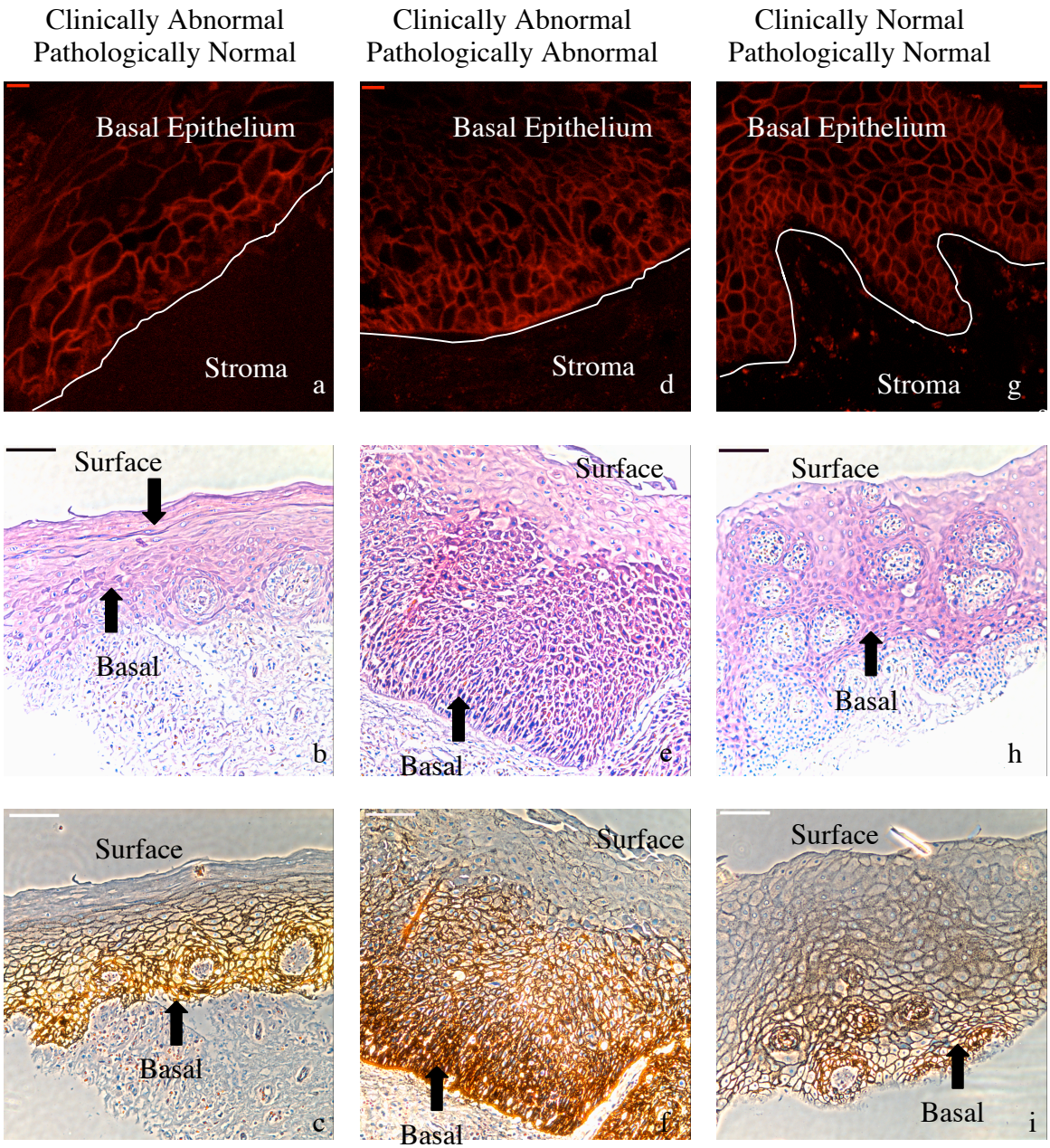

Figure 4-3 Images from patient 10. A mixed pathological diagnosis was obtained for the clinically abnormal biopsy, with one tissue slice from the biopsy containing only hyperplastic and hypkeratotic tissue and the second tissue slice containing mild dysplasia. (a-c) Left column images are from the tissue slice from the clinically abnormal biopsy diagnosed as hyperplasia and hyperkeratosis. (a) False color fluorescence confocal

image, laser power 16 μW. White line indicates basement membrane. (b) Corresponding H&E. (c) EGFR IHC. Strong staining near basement membrane and little to no staining in the superficial layers. (d-f) Center column images are from the tissue slice from the clinically abnormal biopsy diagnosed as mild dysplasia. (d) False color fluorescence confocal image, laser power 9 μW. White line indicates basement membrane. (e) Corresponding H&E. Thickening of the epithelial layer with dysplastic cells is evident. (f) EGFR IHC. Staining stronger near basement membrane than either pathologically normal tissue slice (c and i). (g-i) Right column images are from the clinically normal biopsy diagnosed as hyperplasia and hyperkeratosis. (g) False color fluorescence confocal image, laser power 9 μW. White line indicates basement membrane. (h) Corresponding H&E. (i) EGFR IHC. Strong staining near basement membrane with very little staining in superficial layers. Fluorescence images taken with 40x objective, scale bar 25 μm. H&E and EGFR IHC images taken with 10x objective, scale bar 100 μm.

Figure 4-4 (a) and (b) demonstrate the typical amount of non-specific fluorescence seen in the stroma. The white line in both images indicates the basement membrane. Some non-specific fluorescence is present in the stroma, but it is clearly not indicative of any cellular structure, while the staining in the epithelial layer is consistent with a cellular pattern.

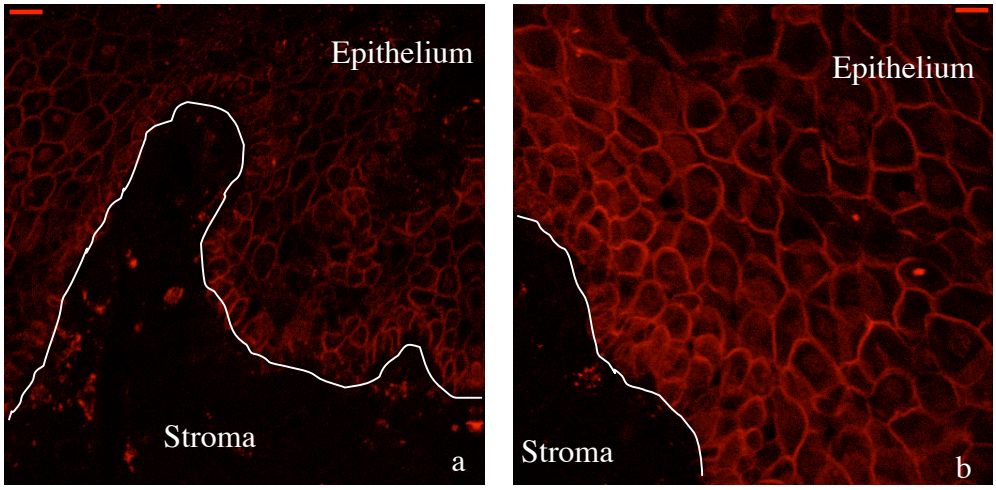

Figure 4-4 Images from patient 8. Both the clinically abnormal and clinically normal were diagnosed as hyperplasia and hyperkeratosis (i.e., pathologically normal). (a) False color fluorescence confocal image from clinically abnormal biopsy, laser power 13 μW. (b) False color fluorescence confocal image from clinically normal biopsy, laser power 8 μW. The white line in (a) and (b) indicates the basement membrane. Fluorescence images taken with 40x objective, scale bar 25 μm.

4.3.3 Image Processing Example

The results of the Matlab code used to determine the edge of the fluorescently-labeled epithlieum and the mask created using these edges are illustrated in Figure 4-5 for three successive images in a z-series stack from the abnormal biopsy for patient 4. In Figure 4-5 (a) through (c), the white lines indicate the edges chosen by the Matlab code. The region determined by those edges was converted to a mask as shown in Figure 4-5 (d) through (f). The solid red region indicates the pixels that were assigned a value of 1 in the mask and the pixels in the black region were assigned a value of 0 in the mask.

When the mask was multiplied with the original image, only fluorescence information from the labeled epithelial region was considered for MFI calculations.

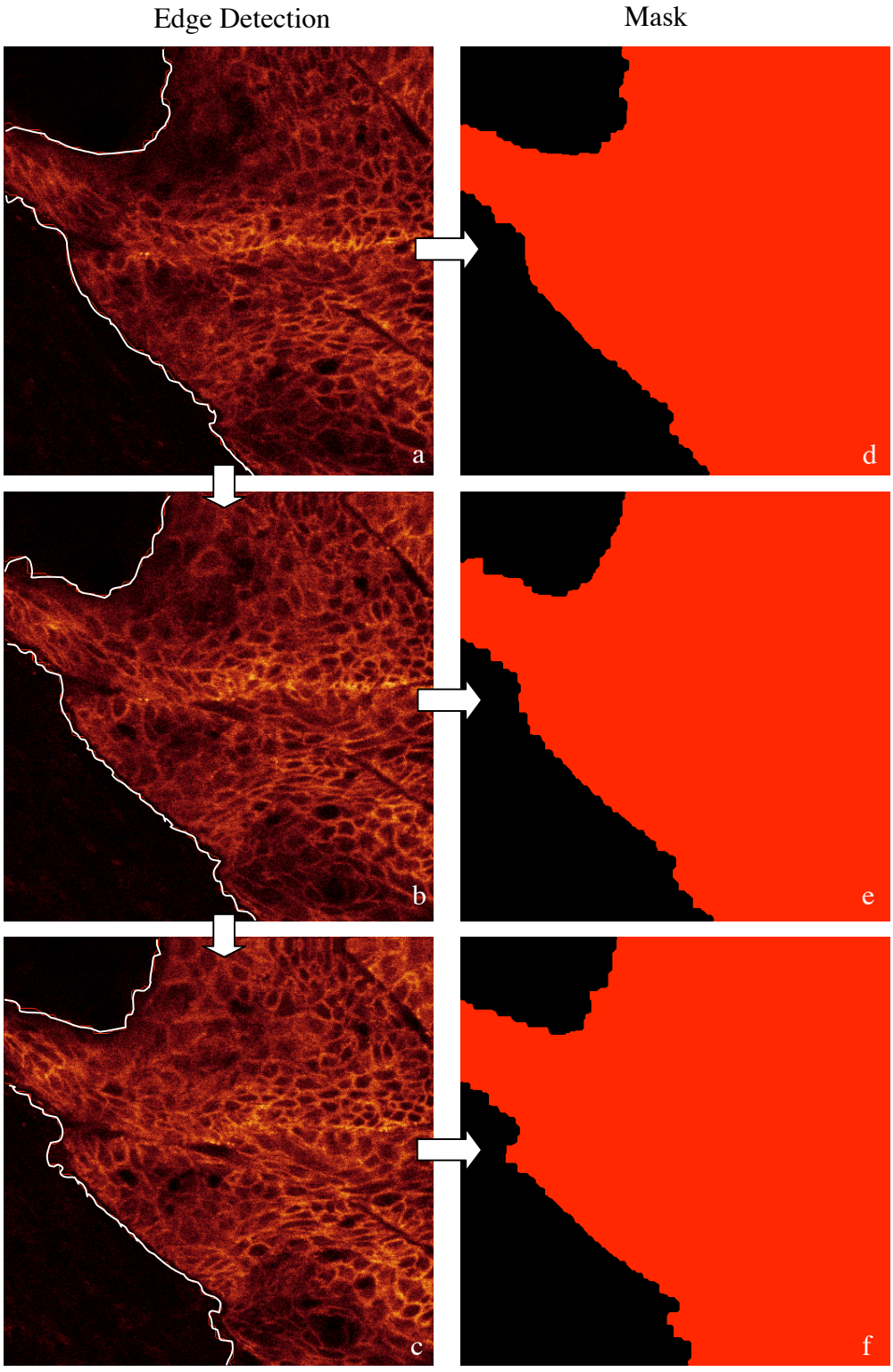

Figure 4-5 Example of edge detection and mask determined using Matlab code from three successive images from a z-series stack of the abnormal biopsy from patient 4. (a)-(c) Red lines indicate edges chosen. (d)-(f) Mask created using the detected edges.

4.3.4 Diagnosis Using Mean Fluorescence Intensity

In order to illustrate interpatient variation, the ratio of the MFI of all image stacks from the clinically abnormal and normal biopsies from each patient was determined. This ratio was then plotted using the pathological diagnosis of the clinically abnormal biopsy. In cases where both the clinically abnormal and clinically normal biopsy were pathologically normal, the ratio was still calculated by dividing the MFI of the clinically abnormal biopsy by the MFI of the clinically normal biopsy and this ratio plotted using the normal pathological diagnosis of the clinically abnormal biopsy. The plot of the ratio of the MFI of the clinically abnormal to clinically normal biopsy by diagnosis of the clinically abnormal biopsy and patient number as shown in Figure 4-6. Patient 3 is omitted from this plot because no diagnosis was obtained for the clinically normal biopsy so a ratio could not be calculated. The ratio for moderate dysplasia and cancer was typically greater than 2, except for patient 17, which had a pathological diagnosis of well-differentiated cancer and a ratio slightly less than 2. Patients with mixed diagnosis of normal and cancer (patients 12 and 16) or normal and dysplasia (patient 10) also had a ratio less than 2. The presence of normal tissue in the abnormal biopsy may have resulted in the lower ratio. A diagnosis of mild dysplasia (patients 13-15) also had a ratio less than 2.

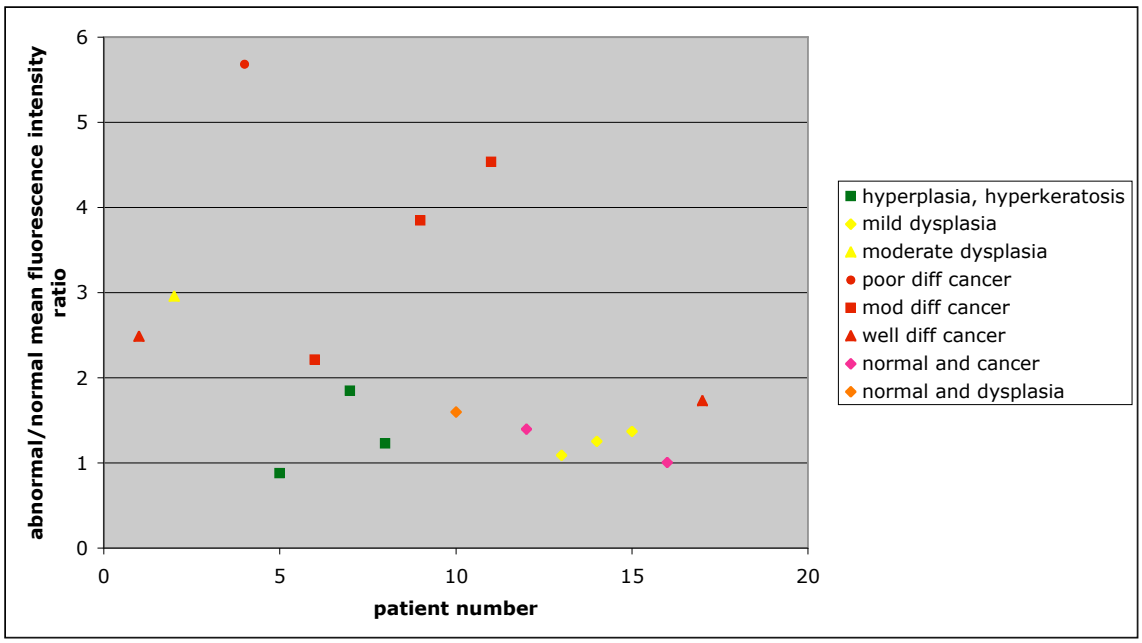

Figure 4-6 Plot of the ratio of the mean fluorescence intensity from the clinically abnormal to clinically normal biopsy from the same patient. Patient 3 is not included since no diagnosis was obtained for the clinically normal biopsy. Diagnosis for each patient is based on the diagnosis from the clinically abnormal biopsy since all clinically normal biopsies were confirmed to be pathologically normal (hyperplasia and hyperkeratosis). Biopsies classified as normal and cancer or normal and dysplasia had a mixture of both normal and cancerous or dysplastic tissue in the H&E sections.

Based on the confocal images and EGFR IHC stained sections, it became evident EGFR expression varied based on location within the epithelium and this variation differed for normal and cancerous tissue. For example, in the basal layers of normal tissue, the cells stained strongly for EGFR in the IHC section, which was reflected in the confocal images. However, in the superficial layers of normal tissue, there was very little EGFR staining while in samples of cancerous tissue, EGFR staining was strong throughout the epithelium. If the confocal imaging results followed the trend seen in the

EGFR IHC, it was assumed that the greatest differences in MFI between normal and cancerous tissue would be seen in the surface layer. Therefore, the MFI was classified by epithelial layer (basal, intermediate, or surface) to determine if this would reveal greater intensity differences between normal and cancerous tissue. Breaking down the MFI by epithelial layer revealed that the MFI of the surface layer separated cancer and moderate dysplasia from normal, hyperplasia, and hyperkeratosis the most effectively as demonstrated in Figure 4-7. The clinically abnormal biopsies from patients 8, 9, and 12 did not have any images from the surface layer and are therefore not shown in the plot. Patient 5 is also excluded because neither the clinically abnormal or clinically normal biopsies had images from the surface layer. Generally, the MFI of the surface layer was greater than 6 for the samples diagnosed as moderate dysplasia or cancer. The abnormal biopsy from patient 17, which had a pathological diagnosis of well-differentiated cancer, had a surface MFI of slightly less than 6. The abnormal biopsies with mixed pathological diagnoses of normal and cancer or normal and dysplasia also had a surface MFI of less than 6. In addition, all the abnormal biopsies with a pathological diagnosis of mild dysplasia had a surface MFI less than 6,

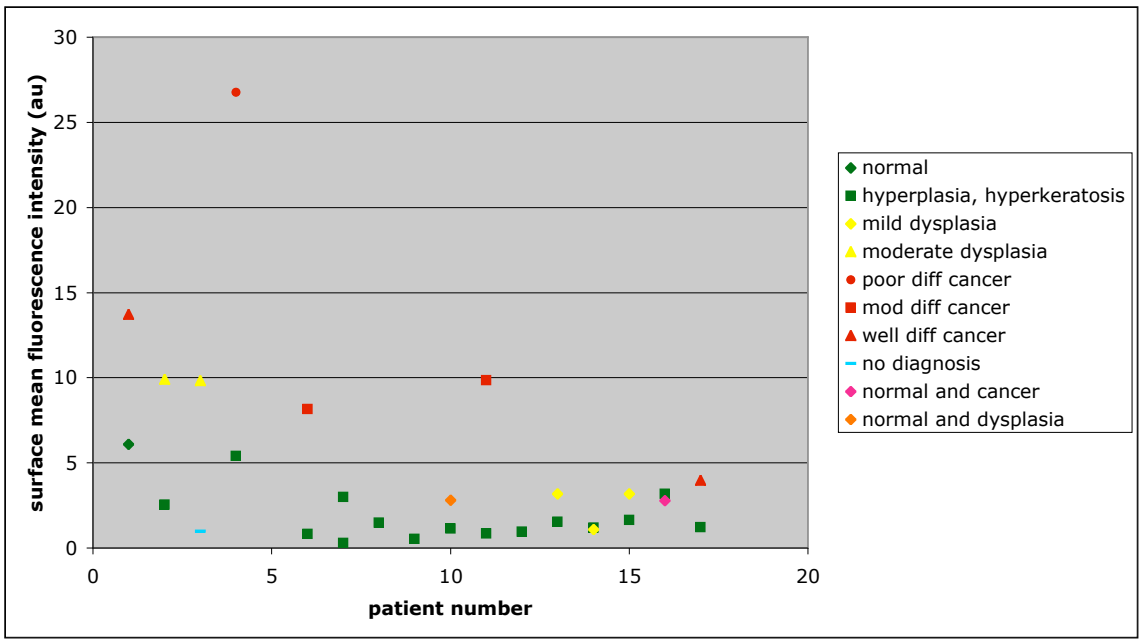

Figure 4-7 Diagnosis using the mean fluorescence intensity from the surface epithelium. In three cases, only one biopsy is shown per patient (patients 8,9, and 12). Both the clinically abnormal and clinically normal biopsies from patient 5 are also omitted.

The ratio of the MFI from the surface and basal layers versus the MFI for the entire epithelial is plotted in Figure 4-8 for biopsies diagnosed as normal, hyperplasia, hyperkeratosis, or dysplasia. Because there is no true superficial or basal epithelium in carcinoma tissue, this ratio was not calculated for samples diagnosed as cancer. Moderate dysplasia was well separated from the normal, hyperplasia, and hyperkeratosis samples, but mild dysplasia and the sample with a mixed diagnosis of normal and dysplasia did not separate well from the normal, hyperplasia, and hyperkeratosis.

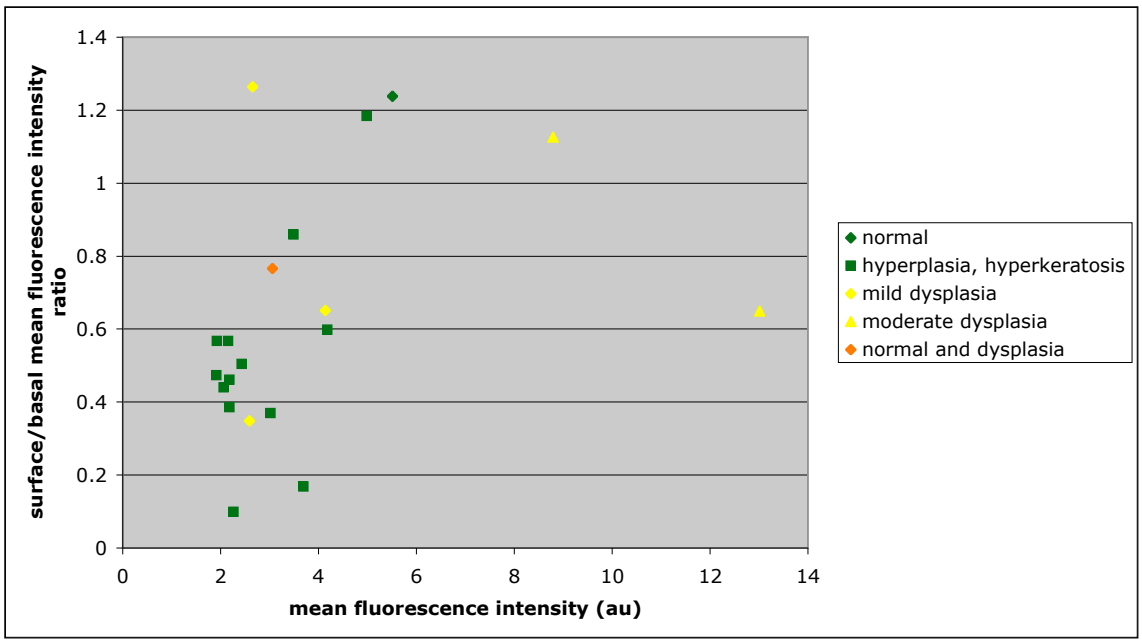

Figure 4-8 Plot of the ratio of the mean fluorescence intensity from the surface layer to basal layer versus the mean fluorescence intensity for the entire epithelium for normal, hyperplasia, hyperkeratosis, and dysplasia biopsies.

4.4 DISCUSSION

Epidermal growth factor receptor is a relatively well-established molecular marker that has demonstrated great promise for use as a target in diagnosing epithelial cancer. Other studies which have investigated correlation of EGFR expression and tumor staging have used traditional molecular biology or protein biochemistry techniques such as western blot or ligand assays which involve homogenization of the tissue sample to measure levels of EGFR expression (27-31). In contrast, we are interrogating EGFR expression in whole tissue sections such that expression by epithelial location can be investigated.

We have found that tissue slices taken from oral cavity biopsies can be labeled for EGFR using the fluorescence contrast agent. Fluorescence correlated well with EGFR IHC, indicating that the contrast agent was likely targeting EGFR as expected. EGFR expression was detected in normal tissue as well as the abnormal tissue; however, this was expected since EGFR is a growth factor that is expressed in any rapidly proliferating cell. In normal epithelial tissue, the basal layer is the source for new cells and is constantly dividing. Therefore, it is not surprising that the cells in the basal layer would express high levels of EGFR regardless of malignancy. As cells from the basal layer migrate upward and differentiate, proliferation decreases. This would be reflected in a decrease in expression of EGFR. One of the hallmarks of cancer is a failure of cells to differentiate and continual proliferation of cells throughout the epithelium, rather than in just the basal layer. So it would be expected that in cancerous tissue EGFR expression would be high throughout the epithelium rather than in just the basal layer. By using a fluorescence contrast agent to evaluate EGFR expression, intensity of the optical signal can be used to determine relative levels of EGFR expression. These patterns of EGFR expression were reflected in the fluorescence confocal imaging, where fluorescence was strong throughout the epithelium of abnormal tissue and in the basal layer of normal tissue but much lower or virtually non-existent in superficial layers of the normal tissue.

Overall, the MFI obtained from abnormal tissue was higher than the corresponding normal biopsy from the same patient. This is illustrated in the ratio of MFI of the clinically abnormal to clinically normal biopsy from a patient. Using a ratio

of 2, the majority of biopsies classified as moderate dysplasia or cancer can be separated from normal, hyperplasia, and hyperkeratosis. The biopsies with a mixed pathological diagnosis or mild dysplasia do not have a ratio greater than 2 and therefore do not separate from the normal pathological diagnoses. Figure 4-6 shows that it may be possible to use the ratio of the MFI of a clinically abnormal site to clinically normal site to diagnose moderate dysplasia or cancer. Eliminating interpatient variation by using the clinically abnormal to clinically normal MFI ratio from a single patient may be critical since EGFR levels may vary from patient to patient dependent on other factors such as tobacco and alcohol abuse. For example, EGFR expression in normal epithelia adjacent to tumor in patients who smoke or drink is higher than in patients who do not smoke or drink (35), so it is possible that pathologically normal tissue from a patient who smokes or drinks would have higher EGFR expression than pathologically abnormal tissue from a patient who does not smoke or drink. Assuming that the increase in EGFR expression is seen in all tissue, regardless of malignancy, for patients who smoke or drink, taking the ratio of their own abnormal to normal tissue would normalize for the increase in EGFR expression. This would then allow samples from different patients to be compared, regardless of the exposure to etiological agents such as tobacco and alcohol, so that a uniform demarcation could be used to identify a malignant diagnosis.

In addition to attempting to classify tissue based on the ratio of the MFI of the clinically abnormal to clinically normal, fluorescence by epithelial layer was also investigated. When considering the MFI from only the surface layers, biopsies classified

as moderate dysplasia or cancer generally had a much higher MFI than those classified as normal, hyperplasia, or hyperkeratosis. This is not surprising, since in normal tissue the superficial layer likely expresses very little EGFR. Mild dysplasia also had a lower surface MFI than moderate dysplasia or cancer. In mild dysplasia, abnormal cells only occupy the lower one-third of the epithelium, so the superficial layers do not contain abnormal cells which would have high levels of EGFR expression. The superficial layer of mild dysplasia resembles normal tissue, therefore the cells in the surface layer of mild dysplasia probably express very little EGFR. This probably explains why mild dysplasia cannot be separated from normal, hyperplasia, or hyperkeratosis using the surface MFI. Biopsies with a mixed pathological diagnosis of normal and cancer or normal and dysplasia also had a lower surface MFI than moderate dysplasia and cancer. This may be due to the presence of normal tissue, which would reduce the overall surface MFI of the clinically abnormal biopsy.

Plotting the ratio of MFI of the surface layer to the basal layer against the MFI of all epithelial layers provided fairly good separation between moderate dysplasia and normal, hyperplasia, or hyperkeratosis. Mild dysplasia could not be separated from normal, hyperplasia, or hyperkeratosis using this method. Again, this is likely the result of the superficial layers of mild dysplasia resembling normal tissue. In addition, the basal layer of mild dysplasia probably resembles normal tissue with respect to EGFR expression since the basal layers of normal tissue is comprised of rapidly proliferating cells with high levels of EGFR expression. Therefore, the lack of a difference between

mild dysplasia and normal tissue when looking at the ratio of the MFI of the surface to basal layer is not unexpected.

It may be more clinically relevant to use only the surface layers of the epithelium for diagnostic purposes. Mild dysplasia, which affects the lower one-third of the epithelium, is not highly indicative of an early malignant process and has the potential to resolve without treatment (13). In contrast, severe dysplasia, which affects the entire epithelium, can be considered early malignancy rather than pre-cancer because it often coexists with carcinoma *in situ* (13). In order to avoid overtreatment, which may result in unnecessary surgery for the patient and increases the cost of healthcare, it may be better to focus on diagnosing moderate to severe dysplasia as early indicators of cancer. In moderate to severe dysplasia, only the upper one to two thirds of the epithelium will contain possibly malignant cells, so targeting the superficial layers of the epithelium may be more specific for more advanced stages of dysplasia.

Figure 4-7 and Figure 4-8 demonstrate that the use of the surface MFI or ratio of MFI from the surface to basal layer can be used to separate moderate dysplasia and cancer from normal, hyperplasia, and hyperkeratosis. While mild dysplasia cannot be separated from normal tissue, it may not be important to be able to diagnose mild dysplasia since it is of less clinical concern than advanced stages of dysplasia or cancer.

With advances in optical technology, the optical signal can even be detected *in vivo* using spectroscopy or confocal microscopy. Numerous studies have investigated the use of *in vivo* fluorescence spectroscopy to diagnose malignancy in the oral cavity based

on autofluorescence (55, 58, 79, 81, 82, 84, 85). The techniques implemented in these studies could easily be adapted to the use of an exogenous contrast agent by modifying the excitation source and emission filters. Further, the contrast agent may even be better suited to *in vivo* use due to its longer excitation wavelength, which avoids many of the absorbers and scatterers present in the tissue at the optimal wavelengths for autofluorescence (300-440 nm) (58, 81-85). Also, the quantum yield of the contrast agent is higher than that of the endogenous fluorophores, resulting in a better optical signal. *In vivo* confocal imaging has been achieved using fiber-based probes (88-93). Fluorescence *in vivo* confocal microscopes are also commercially available from OptiScan Imaging Limited (Victoria, Australia) and Mauna Kea Technologies (Paris, France).

Optical techniques *in vivo* may even be enhanced by using the fluorescence intensity of the contrast agent in the superficial layers of tissue rather than throughout the entire epithelium as a diagnostic criteria. Angled illumination geometry can be used for depth-dependent spectroscopy measurements (109, 110), allowing measurements from only the superficial layer. *In vivo* microscopy requires that the images be acquired *en face*, but the depth of *in vivo* confocal microscopy can also be controlled, and the most superficial layers would be the first to be imaged and should also be the easiest to image. In both cases, signal should be relatively high from the superficial layer due to penetration limitations into the tissue.

Classifying by MFI did not have 100% success in separating dysplasia and cancer from the normal biopsies in any of the three methods used for diagnostic classification. This could be due to the focal nature of oral cancer, where malignancy can coexist with normal tissue in a very small area as was seen with three of the patients in the study. In these cases, the abnormal biopsy did not classify well. However, pathology confirmed that the sections contained both normal and malignant tissue, which may have resulted in a lower overall MFI.

This study reveals that it may be important to look at EGFR expression by epithelial layer rather than expression from a gross tissue sample. Because of the optical nature of the contrast agent, *in vivo* application and interrogation is feasible and would allow for depth-dependent measurements. In combination with fluorescence spectroscopy or confocal microscopy, the contrast agent has possibilities to be implemented as a screening tool for oral cancer.

Chapter 5

A Simple and Inexpensive Fluorescence Spectroscopy System Capable of Detecting a Molecular-Specific Contrast Agent for Diagnosis of Oral Neoplasia

5.1 INTRODUCTION

Fluorescence spectroscopy has shown promise in distinguishing malignancy in the oral cavity based on autofluorescence. A number of studies in *in vitro* cell models, *ex vivo* tissue samples, and *in vivo* in patients have interrogated the ability to use changes in autofluorescence as a distinguishing characteristic of malignancy. These studies have found that differences in the fluorescence spectra between abnormal and normal tissue can be used as a criteria to diagnose malignancy (55, 58, 79, 81). In the oral cavity, the optimal excitation wavelengths for distinguishing oral neoplasia range from 300-400 nm (58, 81-85).

Despite the promise of utilizing autofluorescence as a means of detecting neoplasia, there are some drawbacks. While it is generally believed that the tissue autofluorescence is due to endogenous fluorophores such as the reduced form of nicotinamide adenine dinucleotide (NADH), flavins (FAD^+, FMN, and riboflavin), aromatic amino acids (tryptophan, tyrosine, and phenylalanine), collagen crosslinks, and elastin crosslinks, the exact fluorophores contributing to fluorescence at a particular excitation and emission wavelength are not necessarily known. In addition, the exact

biophysical and biochemical changes underlying the changes in autofluorescence between abnormal and normal tissue are not known, although changes in tissue architecture, such as thickening of the mucosa or loss of layered structure (55, 56) and/or changes in both the concentration, form, and distribution of endogenous fluorophores and the absorption properties of normal versus neoplastic tissue (55, 57, 58) are likely to be underlying causes of the differences in fluorescence spectra. In addition to uncertainty about the biological nature of autofluorescence, the optimal excitation and emission wavelengths for distinguishing neoplasia tend to be relatively short, limiting penetration depth into the tissue due to increased scattering and absorption. Autofluorescence signals also tend to be relatively weak, photobleach rapidly, and are subject to low signal-to-noise ratio (SNR). Finally, the algorithms with the highest sensitivity and specificity in distinguishing cancer and dysplasia from normal tissue generally involve multiple excitation and emission wavelengths. For example, Wang *et al* found that a classification scheme which used two excitation wavelengths outperformed the single excitation wavelength classification scheme in specificity and positive predictive value (56). Heintzelman *et al* used an algorithm based on three excitation wavelengths and four emission intensities to achieve 90% specificity and 90% sensitivity(58). Because of the multiple excitation and emission wavelengths required for the classification algorithms, the spectroscopy systems associated with autofluorescence diagnosis are often large, complicated, and expensive to construct, on the order of $75,000 for optical components alone.

One alternative to the shorter-wavelength emission fluorophores is the red fluorescence of porphyrins, which has been observed in oral cancer and can be used as a distinguishing characteristic of malignancy (111). In addition, 5-aminolevulinic acid (ALA) can be used to bypass the normal feedback control of production of protoporpphyrin IX (PPIX), a precursor to the endogenous fluorophore protoporphyrin IX (PP IX) that accumulates in certain premalignant tissues (49, 59), thereby increasing the concentration of PP IX and increasing SNR. Malignant tissues convert ALA to PP IX at different rates and intensities than normal tissue (59) and tend to accumulate PP IX at a higher rate than normal tissue. While porphyrins and PP IX emit in the 600 nm range, they excite in the 450 nm range, limiting penetration depth of the excitation light. In addition, hemoglobin absorption, which is strongest at 420, 540, and 580 nm, could attenuate the excitation light. Further, Heintzelman *et al* found that while PP IX was associated with a larger number of abnormal samples, it was not diagnostically useful for discriminating neoplastic tissue in the oral cavity (58).

The efficacy of fluorescence spectroscopy can be improved by coupling with molecular-specific contrast agents. Use of an exogenous contrast agent has some advantages over relying on endogenous fluorescence. First, the optical properties of the fluorophore can be carefully chosen, to avoid wavelength regions where there is strong absorption, scattering, or autofluorescence in tissue and to increase SNR. Second, because the target of the molecular-specific contrast agent is known, the biological mechanism being targeted is known. Finally, because an exogenous contrast agent is

being used, the optimal excitation and emission wavelengths are known and a simple spectroscopy system and algorithm can be used for distinguishing abnormal from normal tissue.

Previously, we developed a molecular-specific contrast agent targeting epidermal growth factor receptor (EGFR), which is overexpressed in a number of human malignancies including bladder, breast, cervix and vulva, glioma, lung, and head and neck tumors (22-24), and demonstrated its efficacy in targeting oral squamous carcinoma cells of the buccal mucosa in monolayer, in multilayer tissue constructs, and in fresh tissue slices obtained from oral cavity biopsies (108). In this study, we have coupled the contrast agent with a simple fluorescence spectroscopy system to demonstrate the ability of an inexpensive, easily built, and easy-to-operate spectroscopy system to detect the optical signature of a molecular marker indicative of cancer progression.

5.2 MATERIALS AND METHODS

5.2.1 Spectroscopy System

The design of the spectroscopy system is illustrated in a block diagram in Figure 5-1. Figure 5-2 is a photograph of the actual system. The spectroscopy system consists of commercially obtainable components, the majority of which were purchased from Ocean Optics, Inc (Dunedin, FL). The S2000 spectrometer is equipped with a 600 lines/mm grating blazed at 400 nm with best efficiency (>30%) in the range of 250-800 nm, a detector collection lens, and a A/D board to allow USB or serial connection to a computer. The CCD of the spectrometer has 2048 elements at 12.5 μm x 200 μm per

element. The slit size of 100 μm gives a spectral resolution of 3.8 nm. As given by Ocean Optics, the spectral resolution is determined by the dispersion of the spectrometer (equation 1) and the resolution (equation 2) as shown in equation (3).

Dispersion (nm/pixel) = spectral range of grating (nm)/# of detector elements (pixel) **(1)**
Resolution (pixel) = value from slit size/fiber diameter chart given by Ocean Optics **(2)**
Spectral resolution (nm) = dispersion (nm/pixel) x resolution (pixel) **(3)**

The grating in the spectrometer has a spectral range of 650 nm and the CCD has 2048 elements, giving a dispersion of 0.31738 nm/pixel. The resolution for a 100 μm slit given by Ocean Optics is 12.0 pixels, giving a final spectral resolution of 3.8 nm.

For delivery and collection of light, the spectrometer is coupled to a R400-7 reflection probe, consisting of a 400 μm core collection fiber surrounded by six 400 μm core illumination fibers with a numerical aperture of 0.22. A filter holder is placed after the breakout in the collection fibers with a 695 nm bandpass filter with a 55 nm pass band (Omega Optical, Brattleboro, VT) to filter out extraneous excitation light and a 400 μm core patch fiber is used to connect the filter holder and spectrometer. Excitation light is provided by a 633 nm HeNe laser (output power 0.95 mW, JDS Uniphase, San Jose, CA), which is first focused to a spot size corresponding to the size of the illumination fibers using a plano-convex lens (efl 25 mm, Edmund Optics, Barrington, NJ) and passed through a 632.8 nm laser line filter (Edmund Optics) before coupling to the illumination fibers. The probe was held in an optical mount attached to a micrometer translation stage so that the separation distance between the probe and sample could be controlled.

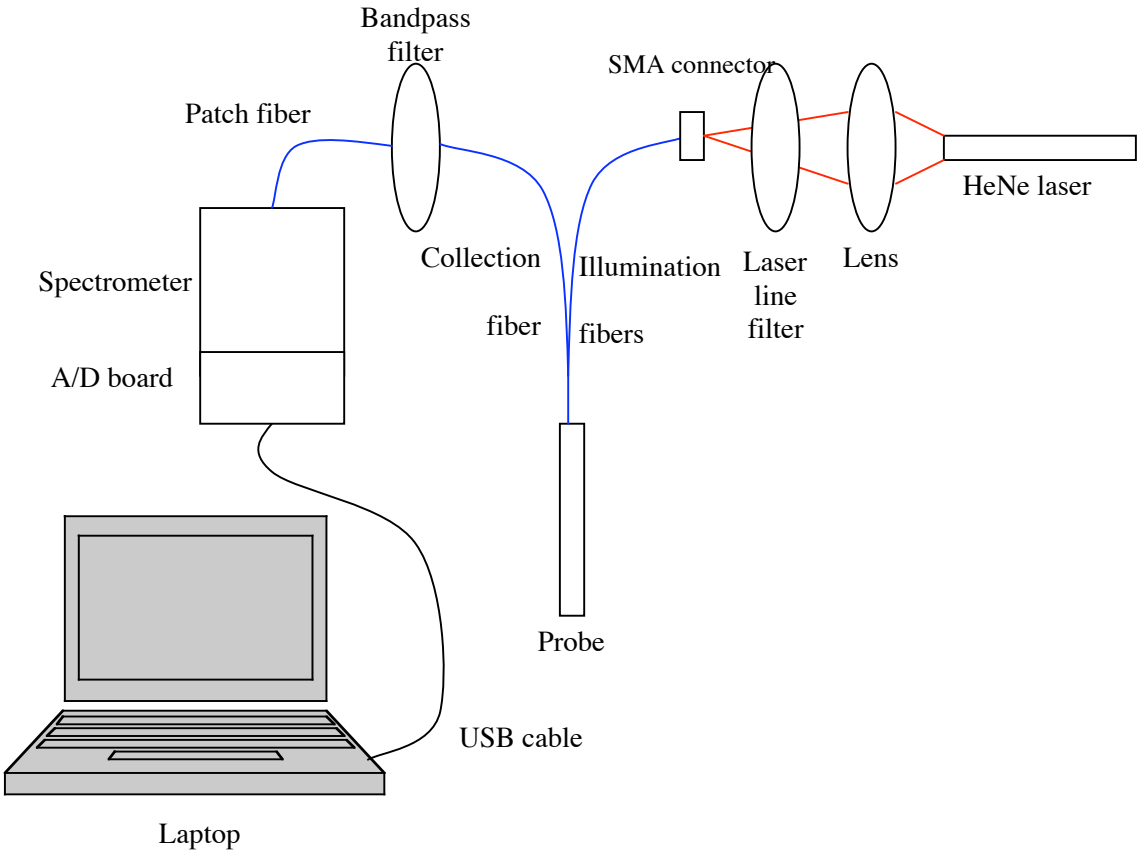

Figure 5-1 Block diagram of spectroscopy system.

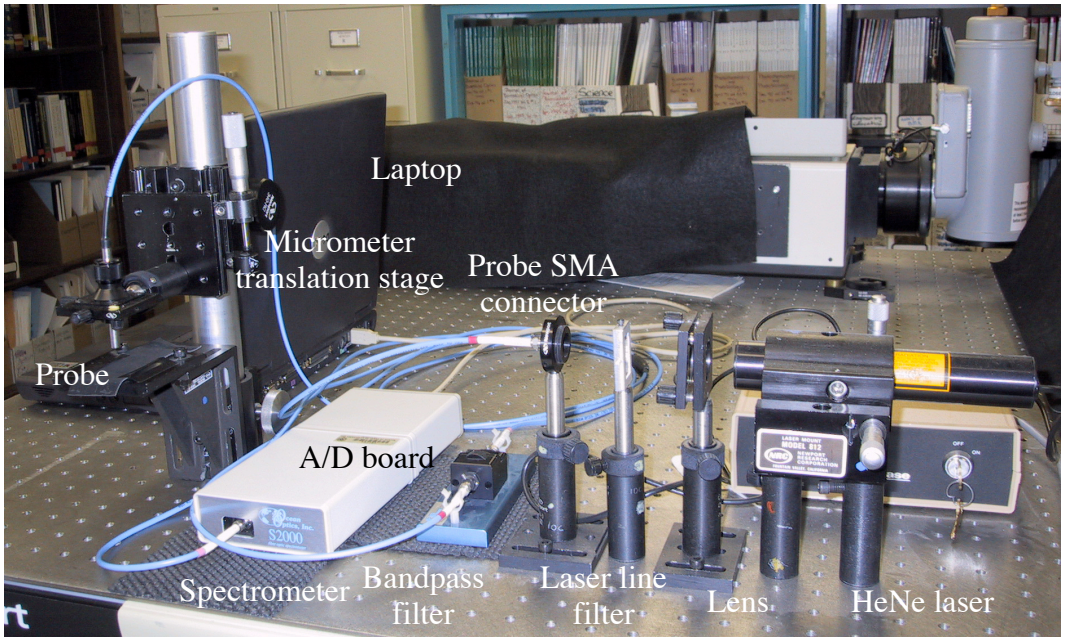

Figure 5-2 Photo of spectroscopy system.

5.2.2 Contrast Agent

The contrast agent is described in detail in (108), but will be briefly reviewed here. The antibody used in the contrast agent was a biotinylated mouse monoclonal anti-human EGFR (clone 111.6, 200 mg/ml, LabVision NeoMarkers, Fremont, CA). Alexa Fluor® 660 streptavidin (Molecular Probes, Eugene, OR) was used as the far-red fluorescent marker. Alexa Fluor® 660 streptavidin has a broad absorption peak with a maximum at 669 nm, but can also be excited at 633 nm or 647 nm. Its emission maximum is at 690 nm with a relative quantum yield of 0.88 compared to 7-hydroxy-9H-(1, 3-dichloro-9, 9-dimethylacridin-2-one) (DDAO). Alexa Fluor® 660 streptavidin has a degree of labeling of 4.7 moles of dye per mole of protein using an ε of 110,000 cm^{-1} M^{-1} at the absorbance maximum (all information on Alexa Fluor® 660 streptavidin as reported by Molecular Probes in the Certificate of Analysis for lot #65C1).

5.2.3 Pre-labeled Mutlilayer Tissue Constructs

Multilayer tissue constructs made up of Sq/CCY1 cells, a squamous carcinoma of the buccal mucosa (kindly provided by Reuben Lotan at the Univesity of Texas M.D. Anderson Cancer Center) already labeled with the contrast agent for EGFR were made to represent a tissue sample in which the entire epithelial layer is fluorescently tagged by the contrast agent. Cells were labeled in suspension as described in (108). After labeling, cells were formed into multilayer tissue constructs by resuspending the cells in solution of collagen (Roche Applied Science, Indianopolis, IN), reconstituted in 0.2% sterile acetic acide, 0.2 M HEPES, 10x phosphate buffered saline (PBS), and 1x PBS, final pH

7.4. The cell-collagen solution was pipetted into a 9 mm diameter, 2.5 mm depth silicone isolator (Grace Bio-Labs, Bend, OR) and allowed to solidify at 37ºC. The final thickness of the multilayer construct was approximately 2.5 mm and the final cell concentration was approximately 80 million cells/mL. In addition to the EGFR-labeled sample, three control samples were also prepared: cells labeled with a normal mouse IgG (Vector Laboratories, Burlinghame, CA), cells labeled with only the Alexa Fluor® 660 streptavidin dye, and unlabeled cells.

5.2.4 Multilayer Tissue Constructs Labeled in the Presence of Permeability-Enhancing Agents

We previously demonstrated that labeling of multilayer tissue constructs can be achieved to greater depths and with greater intensity in the presence of a permeability-enhancing solution of 5% dimethyl sulfoxide (DMSO) as compared to PBS. Multilayer tissue constructs of SqCC/Y1 cells were prepared in 6.5 mm diameter Costar Transwell inserts (VWR, West Chester, PA) as described in (108) and allowed to grow for 14-21 hours in a 37ºC incubator with 5% CO_2. Multilayer tissue constructs were labeled for EGFR or using the normal mouse IgG control in the presence of 5% DMSO or PBS as described in (108). An additional control of an unlabeled multilayer tissue construct was also prepared.

5.2.5 Fresh Tissue Slices

To test the ability of the spectroscopy system to detect optical signal in an actual tissue sample, tissue slices prepared from paired clinically abnormal and normal biopsy samples from the confocal imaging study described in Chapter 4 were also measured. The biopsies were obtained from consenting patients at the University of Texas M.D. Anderon Cancer Center with clinical protocols approved by the Institutional Review Boards at the University of Texas M.D. Anderson Cancer Center and the University of Texas at Austin. Tissue slices were prepared and labeled as described in (108).

5.2.6 Spectroscopy Measurements

Spectroscopy measurements were obtained using OOIBase32 Spectrometer Operating software provided by Ocean Optics. Before obtaining measurements, the HeNe laser was warmed up for at least 20 minutes, and the power was measured after the focusing lens, laser line filter, and probe using a Newport Optical power meter (model 1830-C, Irvine, CA). In addition, a global reference was taken with no sample in the path and a global dark was obtained using a dark background. Samples were transferred to a quartz slide for measurements.

For the multilayer tissue construct samples, five spectra were averaged with an integration time of 1.5 s each. Spectra were also corrected for electrical dark with the global dark subtracted. Measurements were taken with the probe touching the multilayer tissue construct and at distances 1, 2, 3, 4, and 5 mm away from the surface of the multilayer tissue construct. For the pair of tissue slices, a single spectra was obtained for each sample with a 5 s integration time with a separation distance of 3 mm from the

probe surface. Spectra were also obtained from the quartz slide and a frosted cuvette as controls.

5.2.7 Signal-to-Noise Ratio

SNR for each spectra was calculated using the method presented by Trujillo *et al* (112). The goal of this method is to separate the noise present in the measured spectrum from the true signal. To estimate the true spectrum, adjacent pixels are summed and the spectrum is resampled in a technique known as binning. A moving average window of 10 data points (approximately 3 nm) was applied to each spectrum, providing a binned signal which was subtracted from the original data, giving an estimate of the noise as shown in equation (4). A window of 3 nm was chosen because the data collected by the spectrometer was oversampled at approximately 0.3 nm while the true resolution of the system was only 3.8 nm. SNR was estimated by computing the local standard deviation of the noise, using the same moving window as used to calculate the binned spectra, and dividing the binned spectra by the local standard deviation as shown in equation (5).

$$N = P_{original} - P_{binned} \quad \textbf{(4)}$$

$$SNR = \frac{P_{binned}}{\sigma_{binned}} \quad \textbf{(5)}$$

5.3 RESULTS

5.3.1 System Characterization

As expected, there was a loss of power after each optical component in the system. From day to day, the power remained extremely constant. Table 5-1 gives the typical power after the lens, laser line filter, and probe.

Table 5-1 Power in system after each optical component.

Location in System	Power (mW)
After lens	0.8
After laser line filter	0.36
After probe	0.18

Power delivered to the sample is also a function of separation distance from the probe. This is due to the fact that the illumination light is delivered via six fibers. When the probe tip is close to the power meter, the illumination cones of the fibers do not overlap, resulting in a decrease in power. As the separation between the probe tip and the power meter increases, the illumination cones begin to overlap and the subsequent power increases, until the illumination cones fully overlap and the power remains relatively constant. Power as a function of separation distance from the probe is shown in Figure 5-3.

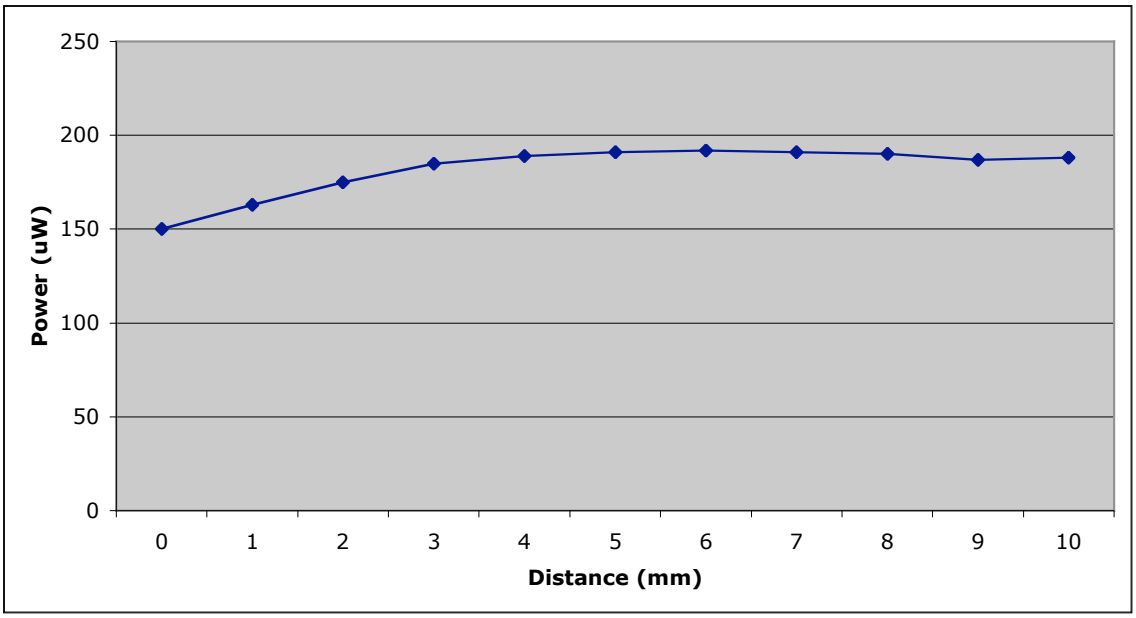

Figure 5-3 Power as a function of separation distance from the probe.

5.3.2 Spectroscopy Measurements of Pre-labeled Multilayer Tissue Constructs

The optical signal from the multilayer tissue constructs prepared using SqCC/Y1 cells labeled with the EGFR contrast agent was easily detectable compared to the IgG, Alexa Fluor® 660 only, and unlabeled controls. Figure 5-4 illustrates the spectra from the samples for the various separation distances. In all cases, the EGFR sample had a much stronger optical signal, 12-31x higher than the IgG sample, 8-23x higher than the dye only sample, and 13-32x higher than the unlabeled sample across all the separation distances. Minimal signal was obtained from the quartz slide or frosted cuvette at all separation distances. The signal from the EGFR sample was 9-27x higher than that from the quartz slide and 14-32x higher than that from the frosted cuvette. An overlay plot of the EGFR samples at the various separation distances is shown in Figure 5-5, along with

a plot of the maximum intensity at each separation distance. The maximum intensity occurs at approximately 690 nm at all separation distances. The intensity increases with increasing separation distance from touching to 2 mm, and then decreases again.

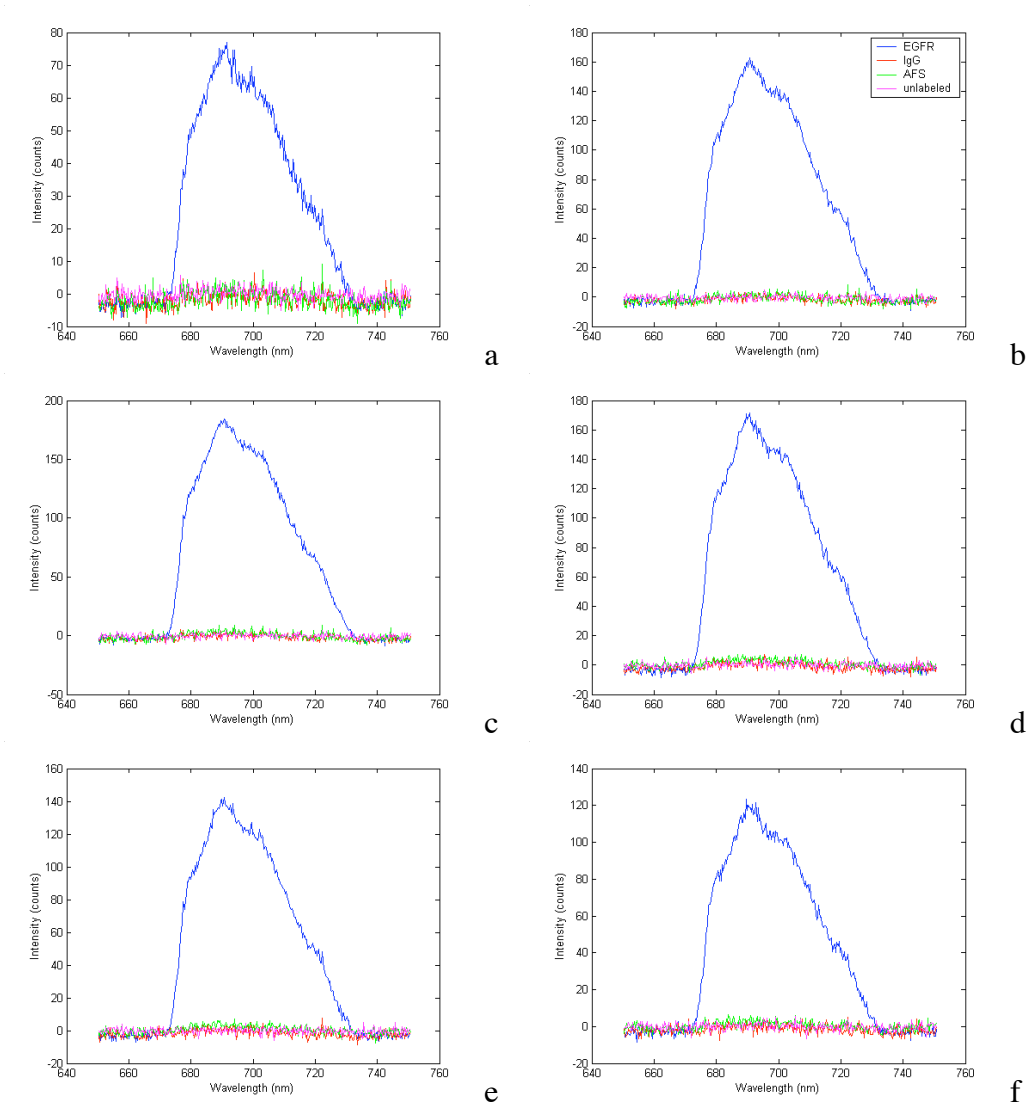

Figure 5-4 Spectra from multilayer tissue constructs prepared using SqCC/Y1 cells labeled using the EGFR contrast agent at various separation distances from the surface. Cells labeled using the EGFR contrast agent (blue) have a stronger optical signal than those labeled using the IgG control (red), Alexa Fluor® 660 (AFS) dye only (green), and unlabeled cells (pink), which have virtually no optical signal. (a) Probe touching surface (b) 1 mm separation between probe and surface (c) 2 mm (d) 3 mm (e) 4 mm and (f) 5 mm.

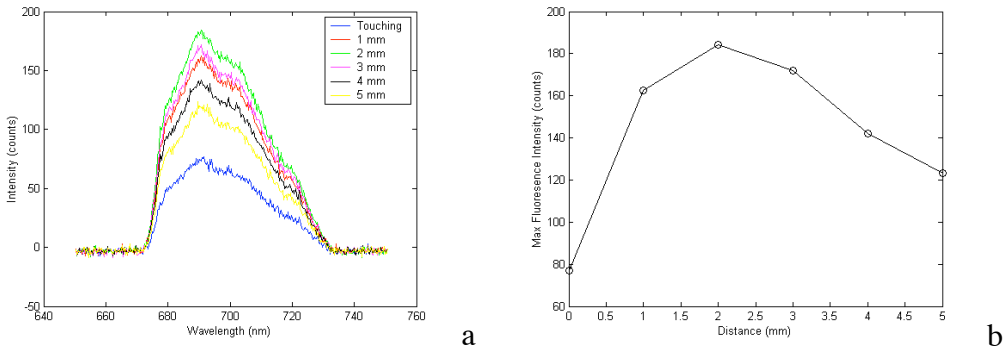

Figure 5-5 (a) Overlay plot of multilayer tissue constructs prepared using SqCC/Y1 cells labeled using the EGFR contrast agent. (b) Maximum intensity at each separation distance. Signal increases with increasing separation distance up to 2 mm and then decreases.

The smoothed spectra generated by binning in the SNR calculations and the SNR as a function of wavelength is shown in Figure 5-6. The separation distance with the strongest optical signal is shown in (a) and (b) and the weakest optical signal is shown in (c) and (d). At the maximum emission wavelength at a separation distance of 2 mm, the SNR is 67 while the maximum SNR is 108 (Figure 5-6 (b)). Even with decreased optical signal, the SNR is still approximately 20 at the peak emission wavelength with a maximum SNR of 46 (Figure 5-6 (d)).

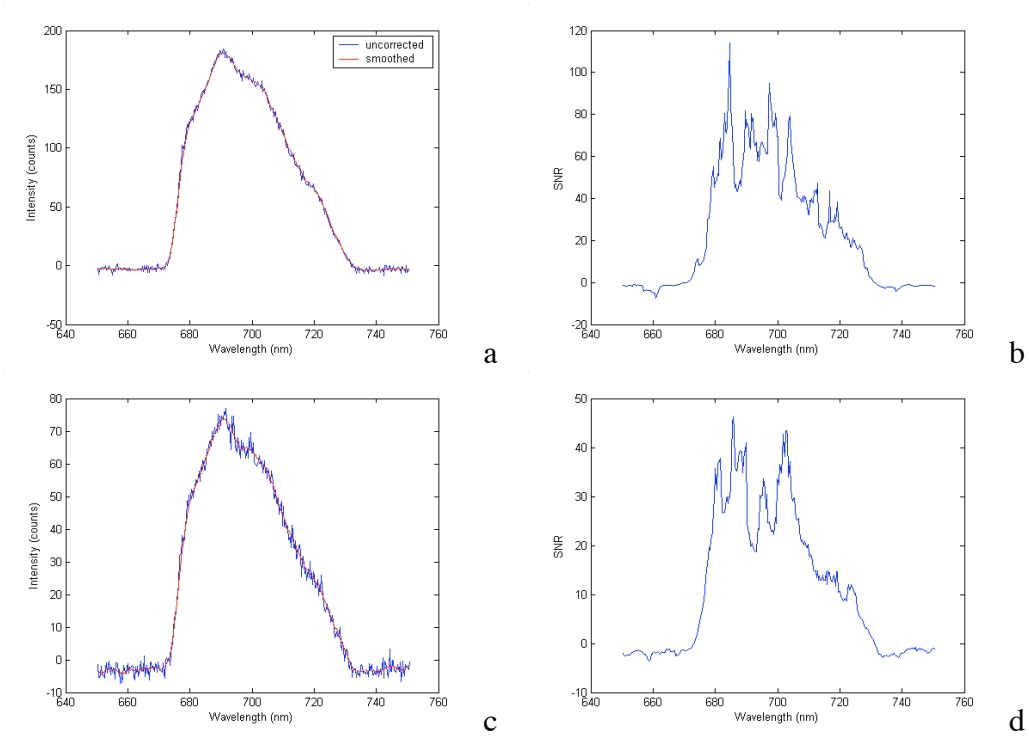

Figure 5-6 (a) and (c) Original (blue) and smoothed (red) spectra used to calculate SNR for multilayer tissue constructs prepared using SqCC/Y1 cells labeled using the EGFR contrast agent. (b) and (d) SNR as a function of wavelength. (a) and (b) are for a separation distance of 2 mm, which had the strongest optical signal. (c) and (d) are for the probe touching the multilayer tissue construct, which had the weakest optical signal.

5.3.3 Spectroscopy Measurements of Multilayer Tissue Constructs Labeled in the Presence of Permeability-Enhancing Agents

The spectra for multilayer tissue constructs labeled in the presence of permeability-enhancing agents at various separation distances are illustrated in Figure 5-7. As expected from previous confocal imaging results (108), the multilayer tissue construct labeled in the presence of 5% DMSO using the EGFR contrast agent had the strongest optical signal. While the signal from the sample labeled using the EGFR

contrast agent in PBS had a higher signal than the two IgG controls, it was 3-5x weaker than the 5% DMSO sample. The two IgG controls had about the same signal for both 5% DMSO and PBS. For the samples labeled in 5% DMSO, the EGFR sample had a signal 4-10x higher than the IgG sample. For the samples labeled in PBS, the EGFR sample had a signal 2-3x higher than the IgG sample. The unlabeled sample had very little signal, with the samples labeled using the EGFR contrast agent having a signals 7-35x and 3-9x higher respectively for 5% DMSO and PBS. In addition, the frosted cuvette had virtually no signal at all separation distances. The signal from the samples labeled with the EGFR contrast agent were 10-46x and 3-12x higher for 5% DMSO and PBS respectively. Figure 5-8 shows an overlay plot of the multilayer tissue constructs labeled using the EGFR contrast agent at the various separation distances and the maximum intensity at each separation distance. (a) and (b) were labeled in the presence of 5% DMSO and (c) and (d) were labeled in the presence of PBS. Again, the peak intensity occurs at a wavelength of approximately 690 nm at all separation distances for both 5% DMSO and PBS. In both cases, the maximum intensity occurs at a separation distance of 3 mm.

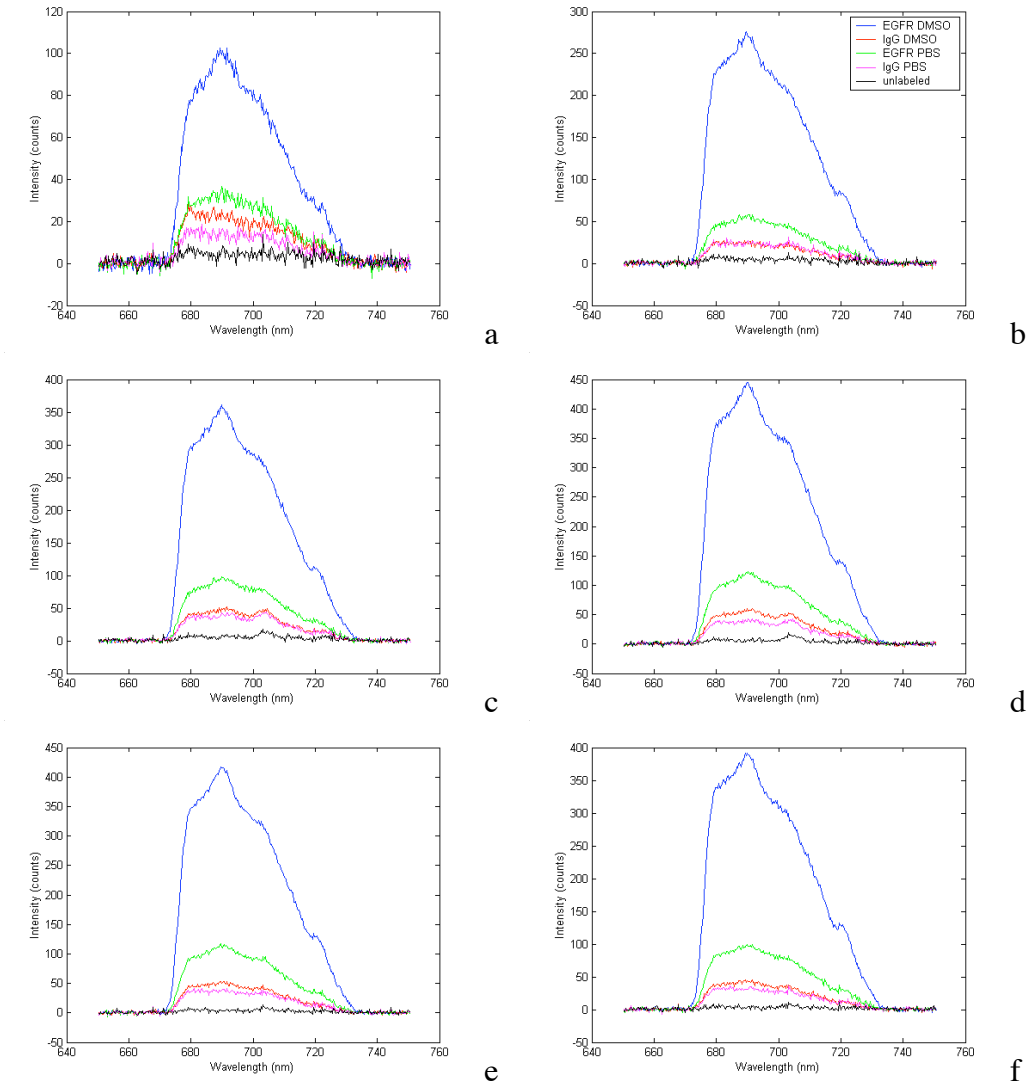

Figure 5-7 Spectra from multilayer tissue constructs labeled using in the presence of the permeability-enhancing agent, 5% DMSO. Multilayer tissue constructs were labeled using the EGFR contrast agent in the presence of 5% DMSO (blue) and PBS (green), using the IgG control in the presence of 5% DMSO (red) and PBS (pink), and left unlabeled (black). The optical signal from the two samples labeled using the EGFR contrast agent is higher than those labeled using the IgG control or left unlabeled, with the multilayer tissue construct labeled in the presence of 5% DMSO having a stronger signal than that labeled in the presence of PBS. (a) Probe touching surface (b) 1 mm separation between probe and surface (c) 2 mm (d) 3 mm (e) 4 mm and (f) 5 mm.

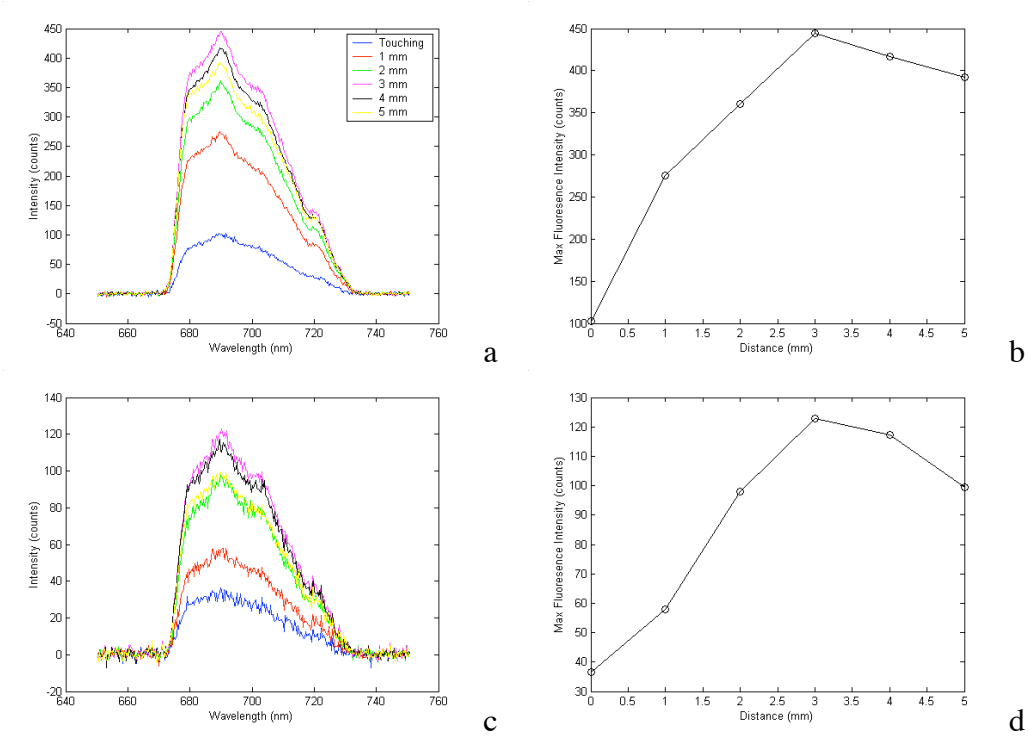

Figure 5-8 Overlay plot of multilayer tissue constructs labeled in the presence of 5% DMSO (a) and PBS (c) using the EGFR contrast agent. Maximum intensity at each separation distance for the 5% DMSO sample (b) and PBS sample (d). The signal increases until a separation distance of 3 mm and then decreases in both cases.

The smoothed spectra and SNR as a function of wavelength are illustrated in Figure 5-9 for 5% DMSO and in Figure 5-10 for PBS. In both figures (a) and (b) are from separation distance with the strongest optical signal while (c) and (d) are from the separation distance with the weakest optical signal. For a separation distance of 3 mm, the SNR is 110 at the peak emission wavelength with a maximum SNR of 169 for 5% DMSO (Figure 5-9 (b)) and 51 at the peak emission wavelength with a maximum of 113 for PBS (Figure 5-10 (b)). Even with the noisiest signal, the multilayer tissue construct labeled in PBS with the probe touching has an average SNR greater than 10, with an SNR

of 11 at the peak emission wavelength and a maximum SNR of 32 (Figure 5-10 (d)). The SNR of the weakest optical signal for 5% DMSO is 42 at the peak emission wavelength with a maximum of 77 (Figure 5-9 (d)).

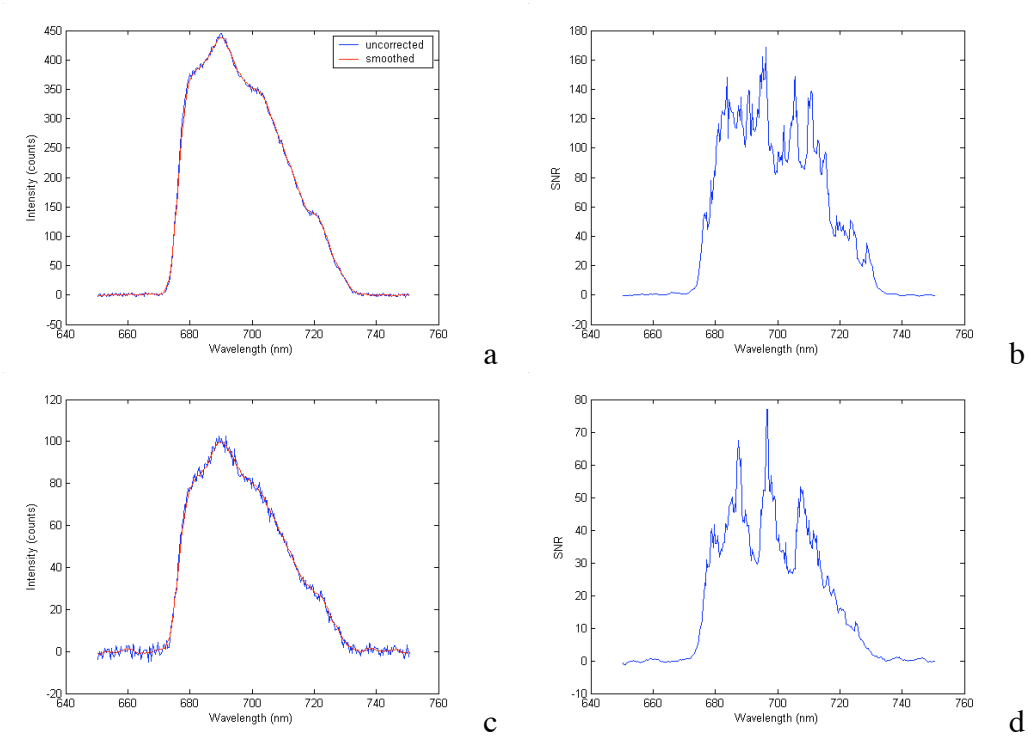

Figure 5-9 (a) and (c) Original (blue) and smoothed (red) spectra used to calculate SNR for multilayer tissue constructs labeled in the presence of 5% DMSO using the EGFR contrast agent. (b) and (d) SNR as a function of wavelength. (a) and (b) are for a separation distance of 3 mm, which had the strongest optical signal. (c) and (d) are for the probe touching the multilayer tissue construct, which had the weakest optical signal.

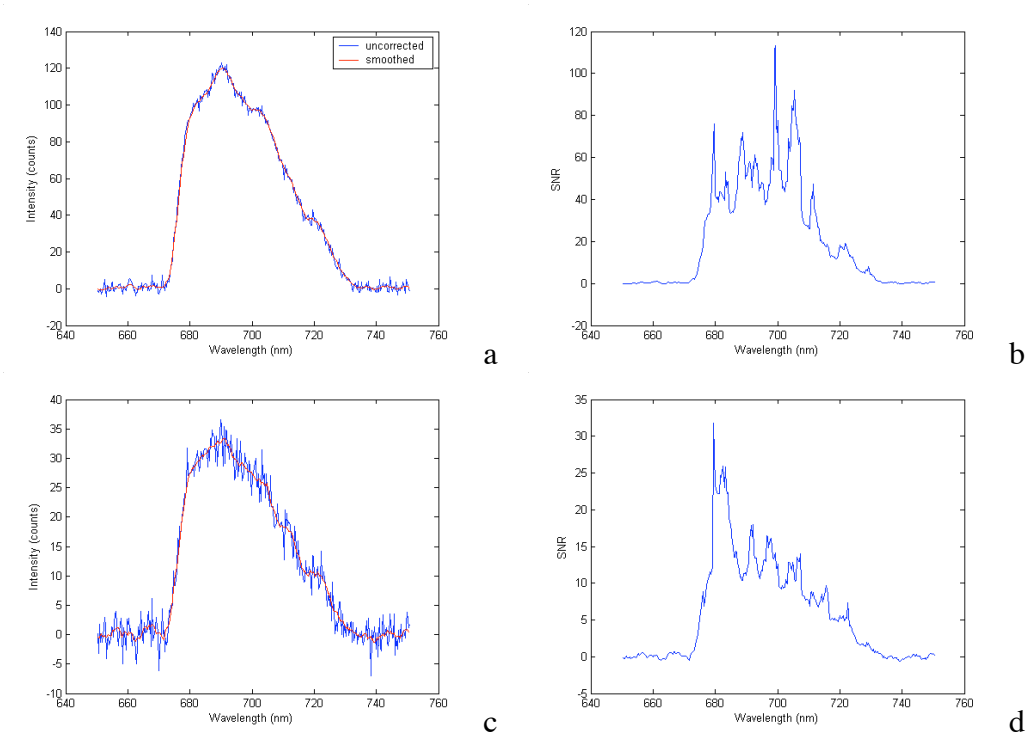

Figure 5-10 (a) and (c) Original (blue) and smoothed (red) spectra used to calculate SNR for multilayer tissue constructs labeled in the presence of PBS using the EGFR contrast agent. (b) and (d) SNR as a function of wavelength. (a) and (b) are for a separation distance of 3 mm, which had the strongest optical signal. (c) and (d) are for the probe touching the multilayer tissue construct, which had the weakest optical signal.

5.3.4 Spectroscopy Measurements of Fresh Tissue Slices

Spectra obtained from tissue slices prepared from a clinically abnormal and clinically normal biopsy pair are shown in Figure 5-11. The signal from the tissue slices labeled using the EGFR contrast agent is higher than that from the IgG control, though there is detectable fluorescence from both IgG controls. The pathological diagnosis for the clinically abnormal biopsy was a mixture of hyperkeratosis and mild to moderate dysplasia and the pathological diagnosis for the clinically normal biopsy was hyperplasia

and hyperkeratosis. The peak emission wavelength for both the EGFR samples is 690 nm. Figure 5-12 gives the smoothed spectra and SNR for the abnormal ((a) and (b)) and normal ((c) and (d)) tissue slices labeled using the EGFR contrast agent. The SNR is 51 and 41 for the abnormal and normal samples respectively at the peak emission wavelength (Figure 5-12 (b) abnormal and (d) normal).

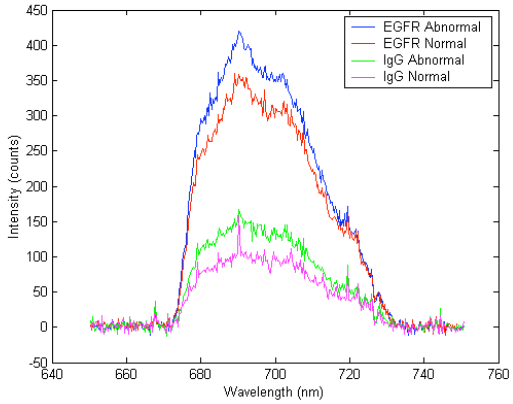

Figure 5-11 Spectra from tissue slices prepared from abnormal and normal biopsies from the oral cavity. Signal from both the abnormal (blue) and normal (red) tissue slices labeled using the EGFR contrast agent is higher than the IgG control samples from the abnormal (green) and normal (pink) tissue slices. Measurements taken at a 3 mm separation distance.

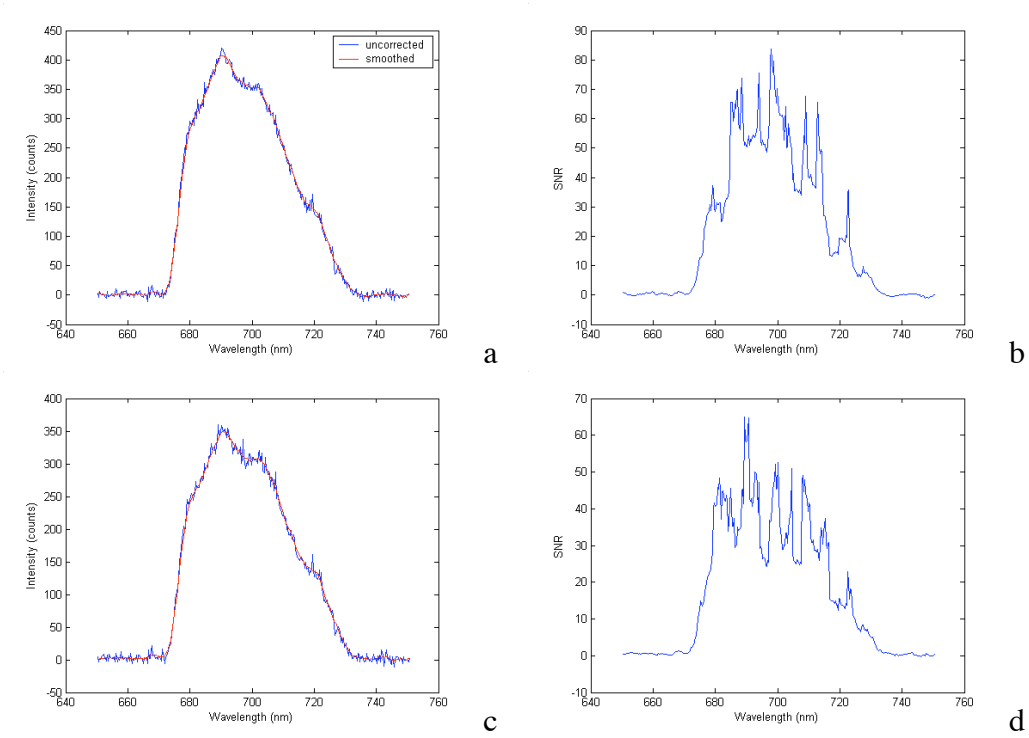

Figure 5-12 (a) and (c) Original (blue) and smoothed (red) spectra used to calculate SNR for abnormal and normal tissue slices using the EGFR contrast agent. (b) and (d) SNR as a function of wavelength. (a) and (b) are from the abnormal tissue slice. (c) and (d) are from the normal tissue slice.

5.4 DISCUSSION

The results presented here demonstrate that an inexpensive and simple spectroscopy system can be designed to detect the optical signal of a contrast agent targeted for a molecular maker that could potentially be used for detection of neoplasia with good SNR. The inherent advantages to this type of spectroscopy system are that at a cost of less than $5,000 for all the optical components, it is relatively inexpensive compared to systems designed to detect multiple excitation and emission wavelengths.

Further, the system is simple to build and maintain, and due to the size of the spectrometer and the minimal optical components to required couple the laser to the fiber probe and spectrometer, it can easily be made portable. However, there are also some disadvantages to the system which should be considered. Because it is designed to detect a specific contrast agent, it is limited to a single excitation wavelength and the components of the spectroscopy system must be tailored to the emission profile of the contrast agent. This limits the flexibility of the system, which is inherently present in multi-wavelength spectroscopy systems. In addition, the system is only interrogating the biological process targeted by the contrast agent, which limits the amount of information that can be collected. This may not necessarily be viewed as a disadvantage, because it is not easy to elucidate the sources of endogenous fluorescence, and targeting a contrast agent specific to a particular biological mechanism simplifies the interpretation of data. In weighing the advantages and disadvantages, the purpose of the spectroscopy system must be considered. While it clearly is not ideally suited to autofluorescence studies, which require multiple excitation and emission wavelengths to achieve good results, it does perform well in targeting an exogenous molecular-specific contrast agent.

To first test how the spectroscopy system would perform with a sample where the which was entirely labeled using the contrast agent, multilayer tissue constructs were prepared using cells pre-labeled with the contrast agent, in addition to IgG, dye only, and unlabeled controls. While the control samples had very little signal, the optical signature from the EGFR contrast agent was easily detectable. This demonstrates that a solid

tumor completely labeled by the contrast agent would be detectable by the spectroscopy system. However, it is possible that every cell in a tumor mass will not be targeted by the contrast agent, so to continue testing of the contrast agent, multilayer tissue constructs were labeled with the contrast agent applied from the top surface in the presence of 5% DMSO, a permeability-enhancing agent, and PBS as a control. Previous studies with confocal imaging revealed that the contrast agent is able to penetrate deeper into the multilayer tissue construct in the presence of 5% DMSO than in PBS and also has a stronger signal. Therefore, it was expected that the multilayer tissue construct labeled in the presence of 5% DMSO would have a stronger optical signal due to a greater number of labeled cells with greater intensity and the results obtained followed this assumption. In fact, the weakest optical signal from the multilayer tissue constructs labeled in the presence of 5% DMSO had an intensity only slightly less than the strongest optical signal from the multilayer tissue construct labeled in the presence of PBS. In both cases, the EGFR contrast agent had a greater intensity than the IgG controls and unlabeled samples. The IgG multilayer tissue constructs had nearly equivalent intensities at all separation distances, which is not surprising since regardless of the permeability-enhancing solution, there should only be minimal fluorescence from the IgG control. The fluorescence that is detected from the IgG controls is likely due to accumulation of dye at the surface of the multilayer tissue construct and not specific labeling, as shown in (108). Thee multilayer tissue constructs prepared using pre-labeled cells do not show significant fluorescence

with the IgG or dye only controls because the dye can be washed away easily before the cells are formed into the multilayer tissue construct.

In both types of multilayer tissue constructs, the intensity of the fluorescence signal is dependent on separation distance between the sample and probe. This is due to the design of the probe. With increasing separation, there is increase in the detected fluorescence to a certain separation distance and then a decrease in the detected fluorescence. This trend agrees with observations by other groups (113). With no or minimal separation between the probe and sample, there is no overlap between the illumination and collection fibers, such that light must propogate laterally to be detected by the probe (113). With increasing separation, there is an increase in the overlap between the illumination and collection areas and a subsequent increase in the fluorescence detected. However, with increasing separation, the collection efficiency also decreases approximately inversely proportional to the separation distance (113), which eventually leads to a reversal in the trend.

It has previously been shown that a probe geometry with overlapping illumination and collection areas is sensitive to fluorescence from the epithelial surface while a non-overlapping geometry is sensitive to sub-surface tissue layers (110). While it is generally believed that the non-overlapping geometry is more sensitive to the earliest changes associated with neoplasia (110, 113) and also has the advantage of avoiding collecting signal from the highly fluorescent keratin layer at the epithelial surface in oral mucosa (110), these observations were specifically for endogenous fluorescence. Using an

exogenous contrast agent with different optical properties than endogenous fluorophores will change the requirements for probing geometry in order to detect neoplasia. The fluorescence of keratin appears to be strongest in the 300 nm range (unpublished observations), and may therefore not cause increase noise in tissue labeled with the EGFR contrast agent. Cells at superficial layers may also show an increase in EGFR expression before displaying the metabolic changes which are detected using autofluorescence. Further, it may not always be desirable to probe sub-surface epithelial layers, particularly if the detection emphasis is on severe dysplasia and *in situ* carcinoma rather than mild dysplasia, which has the potential to reverse without treatment (13).

In order to test the spectroscopy system with an actual tissue sample, tissue slices labeled with the contrast agent for confocal imaging were also measured with the spectroscopy system. Fluorescence signal was obtained from both the abnormal and normal tissue slice, though there was not a significant difference in the intensities. However, the mixture of normal and dysplastic tissue types in the clinically abnormal biopsy may explain why the intensity of the abnormal tissue slice is not significantly greater than the normal tissue slice. In addition, labeling of the EGFR contrast agent in mild to moderate dysplasia is expected to be less than in cancer, so more significant differences in fluorescence intensity between a normal and cancer specimen may be seen.

As a sample for a spectroscopy system, tissue slices are not ideal because the sample is transversely sectioned thinly (200-250 μm) for confocal imaging. In a transverse section of biopsy sample, both the epithelial and stromal layers will be present.

Due to the small size of the section, and the inability to determine exact location in the tissue slice when obtaining a measurement, the optical signal from the entire tissue slice was obtained. Therefore, both specific labeling in the epithelial layer and non-specific stromal fluorescence was collected for each measurement. The thickness of the tissue slice is also thinner than some regions of oral mucosa, which could also lead to a comparative decrease in the amount of fluorescence that could be collected. A better tissue sample to use for spectroscopy measurements would be a whole biopsy, with spectroscopy measurements taken from the surface of the biopsy sample. However, due to a limitation in the number of biopsies that could be obtained from patients, it was not possible to dedicate a whole biopsy pair to the spectroscopy study. The use of tissue slices does demonstrate that the spectroscopy system can detect signal from a tissue sample. Further, it is likely that the fluorescence intensity from a whole biopsy would be greater than that from a tissue slice.

These results demonstrate that a simple spectroscopy system coupled with a molecular-specific fluorescence contrast agent has the ability to distinguish positively labeled malignant sample with good SNR. This is particularly compelling because it would greatly increase the ability to use a spectroscopy system for diagnosis of oral cancer in dental offices and clinics that might not be able to afford expensive diagnostic equipment.

Chapter 6

Considerations for *in vivo* Use of the Fluorescent Contrast Agent[2]

6.1 INTRODUCTION

The results presented in this dissertation have demonstrated the use of a molecular-specific fluorescence contrast agent for use in detection of oral cancer in *in vitro* biological models and *ex vivo* biopsy samples. However, to utilize the full potential of the contrast agent, it must have the ability to be used *in vivo*. The combination of the contrast agent with optical techniques such as fluorescence spectroscopy or confocal microscopy could result in a new diagnostic technique for oral cancer. However, to take advantage of the non-invasive nature of optical modalities, the contrast agent would need to be used *in vivo* in patients. Without *in vivo* use, the fluorescence contrast agent would not provide as much of a significant advantage over current diagnostic techniques, because biopsy and microscopic examination of the tissue would still be required.

When considering *in vivo* use of the contrast agent, a number of issues must be considered. First among these issues are toxic effects of the contrast agent, which would include possible cytotoxic effects of the Alexa Fluor® 660 streptavidin dye, immunogenic effects of the antibody, and the usage of a biotin-streptavidin system and

[2] Portions of this chapter have been published previously in Hsu, E.R., E.V. Anslyn, S. Dharmawardhane, R. Alizadeh-Naderi, J.S. Aaron, K.V. Sokolov, A.K. El-Naggar, A.M. Gillenwater, and R.R. Richards-Kortum, 2004. A far-red fluorescent contrast agent to image epidermal growth factor receptor expression. *Photochem. Photobiol.* **79(3)**, 272-279.

permeability-enhancing agents *in vivo*. In addition, optimal time for localization of the contrast agent to neoplasia and subsequent imaging and clearance of the contrast agent from the tissues must also be considered for optimal use of the contrast agent *in vivo*. Finally, the performance of the contrast agent under physiological conditions, most importantly temperature, must also be examined. Experiments were performed to assess the effects of the dye on cell growth, morphology, and viability and to evaluate the contrast agent under physiological temperatures, and will be described in the materials and methods section. The remaining issues will be discussed with respect to literature and current clinical practices in the discussion section.

6.2 MATERIALS AND METHODS

6.2.1 Cytotoxicity, Two Day Incubation

A preliminary cytotoxicity assay of Alexa Fluor® 660 streptavidin (Molecular Probes, Eugene, OR) was performed by incubating SqCC/Y1 cells with 1:10, 1:20, and 1:50 dilutions of the dye and no dye. A single plate of SqCC/Y1 cells was harvested, a viability count performed, and the plate split into 8 plates and allowed to set up for 2 days in Dulbecco's modified essential media/F12 (Invitrogen, Carlsbad, CA) with 5% fetal bovine serum (FBS) (Hyclone, Logan, UT), penicillin, streptomycin, and glutamine (Invitrogen). The media was then removed and replaced with media containing the appropriate dilution of dye for a total volume of 10 ml. Two plates of each sample were prepared. After two days, each plate was collected and a viability count performed using a hemacytometer and trypan blue (Sigma Aldrich, St. Louis, MO) staining.

6.2.2 Cytotoxicity, Eleven Day Incubation

To further test the cytotoxicity of Alexa Fluor® 660 streptavidin over a longer period of time, a similar experiment to the two day incubation was performed. A single plate of SqCC/Y1 cells was harvested and used to plate a 6 well tissue culture plate at a 1:8 split, ~200,000 cells/well. After setting up for one day, the media with the various dye dilutions was added. In addition to the dilutions used in the two day incubation study, 1:2 and 1:5 dilutions were added. At days three and seven, the cells were collected, a viability count performed, and the cells replated at a 1:4 split in media with the same dye concentration. On day eleven, the cells were collected and a viability count performed.

6.2.3 Cytotoxicity, Recovery After Exposure

A final cytotoxicity test was performed to assess the effects of long-term exposure to the dye without harvesting the cells and to assess the recovery of the cells after exposure to the dye. A single plate of SqCC/Y1 cells was harvested and used to plate a 6 well tissue culture plate at an low density, ~25,000 cells/well. After setting up for one day, the media with the dye concentrations used in the eleven day experiment was added. On day seven, the cells were collected, a viability count performed, and the cells replated at a 1:4 split in media with no dye. On day eight after replating in media with no dye, the cells were collected and a viability count performed.

6.2.4 Performance of Contrast Agent under Physiological Temperature

MDA-MB-468 and SqCC/Y1 cells were grown in monolayer as described in Chapter 3. Labeling was also performed as described in Chapter 3, at both room temperature and at 37° C. Cells were imaged using a Lecia TCS 4D laser scanning confocal microscopy with excitation at 647 nm and a 665 nm longpass filter.

6.3 RESULTS

6.3.1 Cytotoxicity of Alexa Fluor® 660 Streptavidin, Two Day Incubation

The Alexa Fluor® 660 streptavidin had no effect on the viability of the cells after the two day incubation period. All samples had a viability of 98% or higher as shown in Figure 6-1 (a). The cells grown in the presence of dye had a slightly lower cell count (Figure 6-1 (b)).

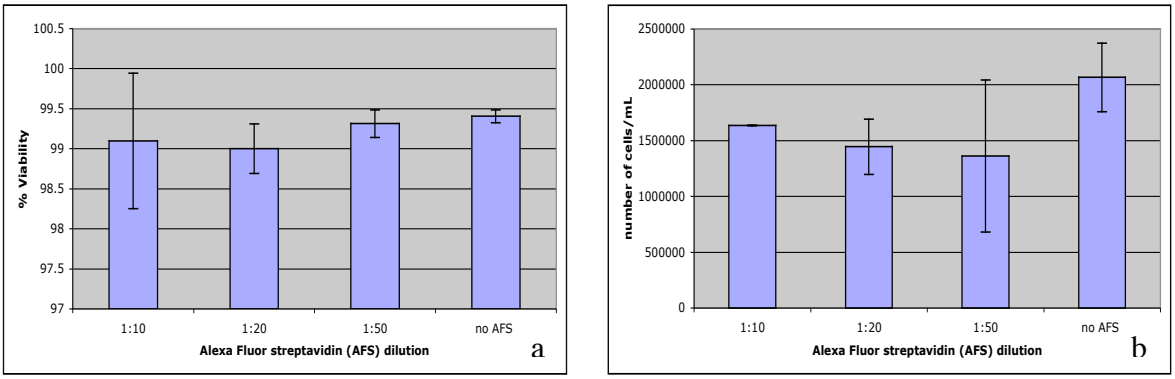

Figure 6-1 Results of two day cytotoxicity experiment. (a) Percent viability of the cells. (b) Concentration of cells in number of cells/mL.

6.3.2 Cytotoxicity, Eleven Day Incubation

When the incubation period was extended to eleven days, with the cells split and replated on days three and seven, the overall viability decreased. At day three, all samples had a viability of 94% or higher and a relatively comparable cell count as seen in Figure 6-2 (a) and (b). After replating, however, cells grown with the dye did not reattach as well as cells grown with no dye. At day seven, this was reflected in the overall cell count, with cells grown in the presence of dye having a cell count 2-7x less than cells grown with no dye (Figure 6-2 (d)). The viability of cells grown in the presence of dye had a viability of 80% or higher compared to 95% for the control cells as shown in Figure 6-2 (c). A similar situation was seen after the day seven split and viability count on day eleven (Figure 6-2 (e) and (f)).

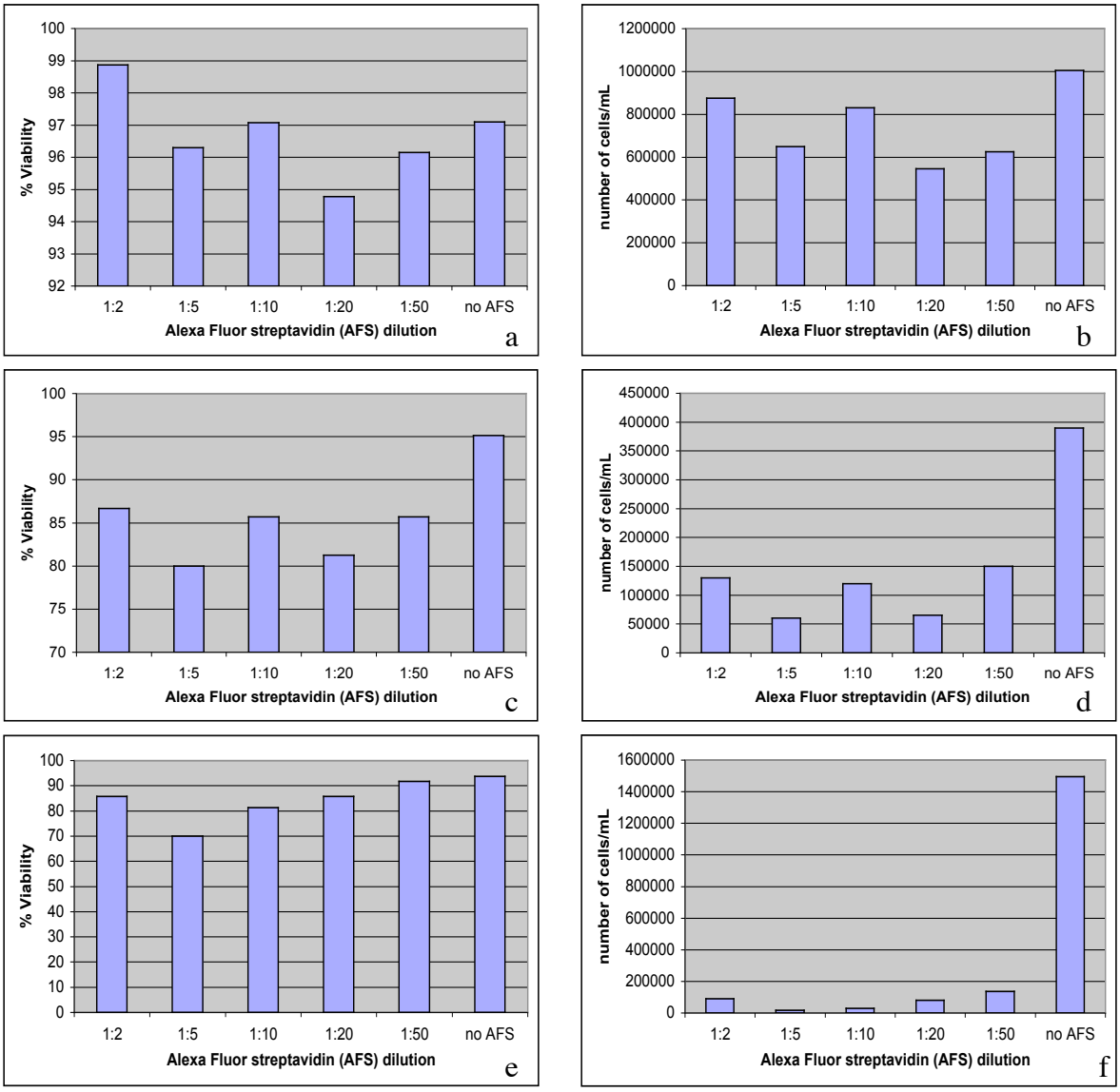

Figure 6-2 Results of eleven day cytotoxicity experiment. (a) Viability on day three, relatively comparable among all samples. (b) Cell concentration on day three. (c) Viability on day seven. (d) Cell concentration on day seven. Significantly lower for cells grown in the presence of dye. (e) Viability on day eleven. (f) Cell concentration on day eleven. The poor reattachment of cells grown with dye is reflected in the low cell count.

6.3.3 Recovery After Exposure

SqCC/Y1 cells were also grown in the presence of the dye over a seven day period without splitting to evaluate the effects of the dye without concern for cell reattachment. Through day four, all cells grew well with normal morphology. Between days five and seven, the morphology of the cells in the presence of dye began to change, with the cells exhibiting a more spindly and isolated morphology rather than continuous areas of confluent growth. In addition, there was a great deal of death between days five and seven. This was reflected in the cell count, where cells grown in the presence of dye had a cell count about 2x lower than the control cells (Figure 6-3 (b)). Overall, the viability of cells grown in the presence of dye was generally lower as well as seen in Figure 6-3 (a). In order to test the ability of cells to recover after exposure to the dye, these cells were split and grown in their normal media. The cells that had been grown with dye did not initially reattach well, which resulted in a low overall cell count after eight days of recovery compared to the control cells (Figure 6-3 (d)). The overall cell viability increased, however, with the 1:2 dilutions having the lowest viability at 88% and all other cells having a viability of 94% or higher (Figure 6-3 (c)).

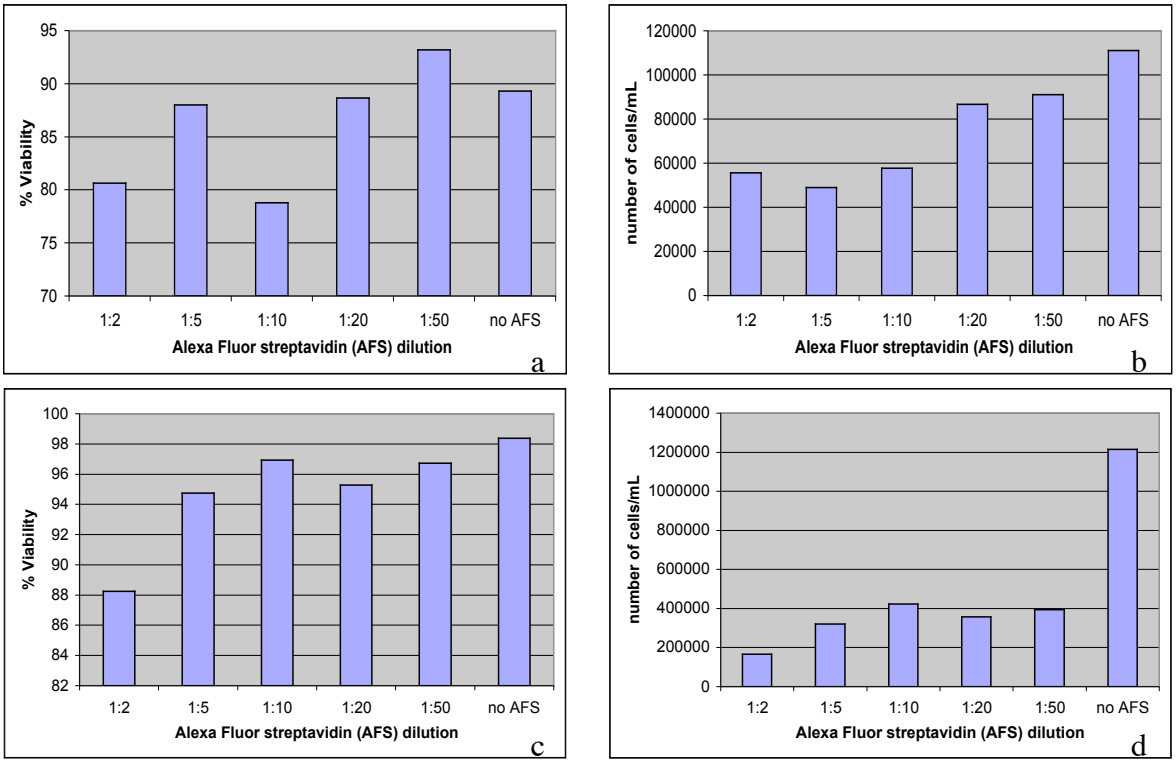

Figure 6-3 Results of recovery after exposure experiment. (a) Viability on day seven. (b) Cell concentration on day seven. (c) Viability on day eight after recovery. (d) Cell concentration on day eight after recovery.

6.3.4 Performance of Contrast Agent under Physiological Temperature

Fluorescence under both room temperature and at 37ºC for both cell lines labeled with the EGFR contrast agent was similar. SqCC/Y1 cells labeled using the contrast agent and IgG control are shown in Figure 6-4 along with the corresponding DIC transmitted images. Cells labeled at 37ºC (Figure 6-4 (c)) may show a little bit more internalization of the contrast agent than those labeled at room temperature (Figure 6-4 (a)), indicated by the small spots of more intense fluorescence. However, the periphery

of the cell still shows continuous labeling. In addition, the IgG control did not show any increase in fluorescence when labeling was performed either room temperature or 37°C (Figure 6-4 (e) and (g)).

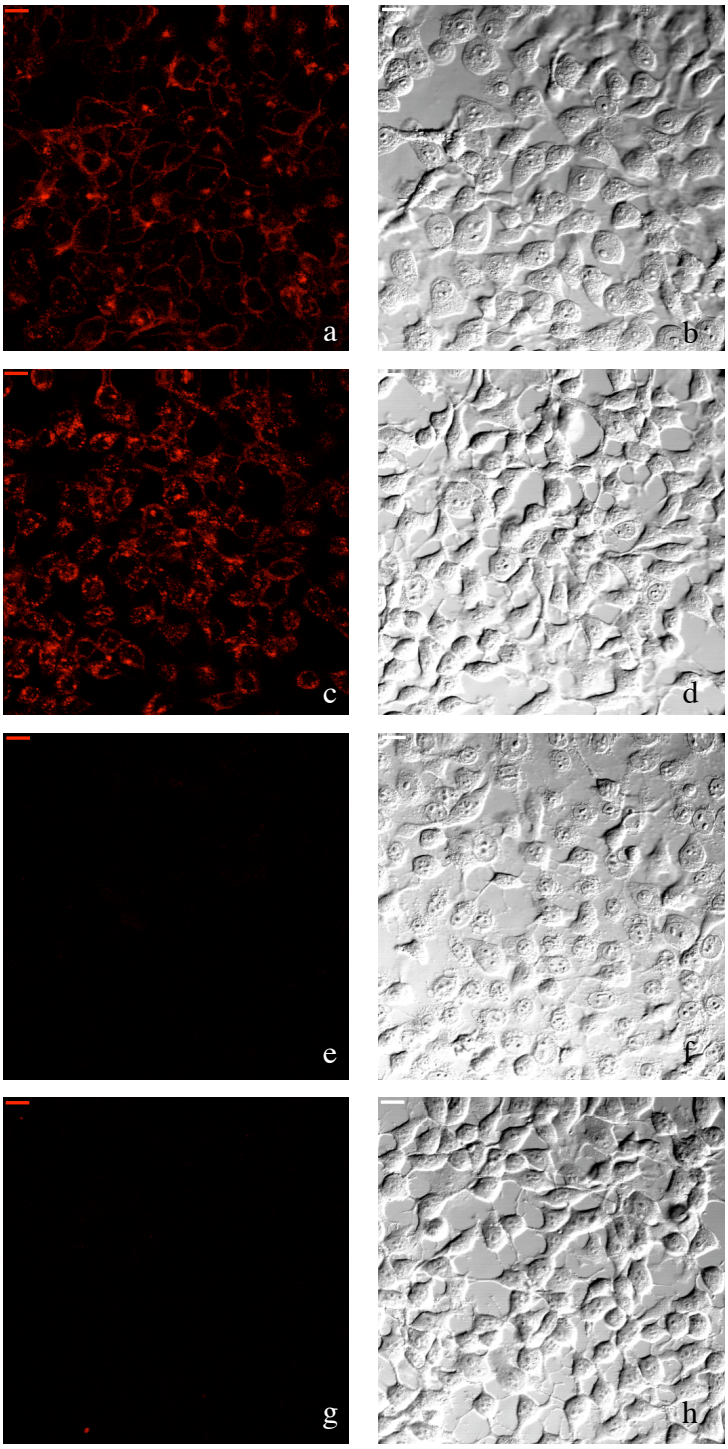

Figure 6-4 SqCC/Y1 cells labeled at room temperature and at 37ºC. Left column are fluorescence confocal images, right column are DIC transmitted images. (a) EGFR

contrast agent at room temperature, laser power 12 μW. (c) EGFR contrast agent at 37ºC, laser power 10 μW. (e) IgG control at room temperature, laser power 7 μW. (g) IgG control at 37ºC, laser power 9 μW.

6.4 DISCUSSION

Over a short period of time, the Alexa Fluor® 660 dye seems to have little effect on cell viability. As the incubation time is increased, however, the dye does have a detrimental affect on cell growth and viability. It appears that it may somehow interfere with how the cell attaches to the growth substrate due to changes in the cell morphology over time and the inability of cells to reattach effectively after splitting. An important caveat to the cytotoxicity studies performed here is that the cell concentration and cell viability was assessed using hemacytometer counting, which is not extremely accurate. However, the experiments do give a good general picture of the effects of the Alexa Fluor® 660 dye on cell growth and viability. Growing the cells in a 3D matrix such as Matrigel™ instead of in plastic tissue culture dishes might reveal whether the effects of the dye are due primarily to interference with cell adhesion. A 3D matrix is also more representative of the environment a cell would experience *in vivo* and the types of attachments the cell would need to form with its environment. Recovery experiments demonstrated that cells which did survive exposure to the dye eventually recovered and were able to grow normally after removal of the dye. Further toxicity studies should include animal testing to further assess the effects of the Alexa Fluor® 660 streptavidin dye. While detrimental effects of the Alexa Fluor® 660 streptavidin dye are evident in

cells exposed for longer than four days, this is considerably longer exposure than would be necessary for *in vivo* labeling.

Increased temperature will increase the rate of receptor internalization. Since previous *in vitro* and *ex vivo* experiments were performed at room temperature, the effects of labeling at 37ºC were evaluated. Increased receptor internalization could result in a decrease in labeling, if the receptor is internalized before targeting by the contrast agent, or increased fluorescence internally and a decrease in fluorescence in the cell membrane, if the receptor is internalized after targeting by the contrast agent. Very few differences were seen in the labeling at room temperature and at 37ºC, though bright spots of fluorescence were more evident in the cells labeled at 37ºC than at room temperature. These spots could represent vesicles of receptors that have been endocytosed by the cell or dense areas of receptors which are beginning the endocytosis process. However, there is not an associated decrease with labeling of the cell membrane. The lack of labeling at 37ºC with the IgG control indicates that the cell is not non-specifically taking up the Alexa Fluor® 660 dye, which would result in an increased background. These results are encouraging because they imply that there would be no decrease in fluorescence intensity or increase in non-specific background fluorescence with *in vivo* labeling.

Immunogenic effects of the antibody in the contrast agent can be minimized through the use of low antibody concentrations. In the studies presented in preceding chapters of this dissertation, a 1:10 dilution of the EGFR antibody resulted in a

concentration of 20 μg/ml and the Alexa Fluor® 660 streptavidin dye was used at a concentration of 31.25 μg/ml. 100 μl of each, or 2 μg of the antibody and 3.1 μg of the dye, was used in order to label the multilayer tissue constructs, which consisted of approximately 32 million cells. A precancer with a 1 mm radius and 300 μm depth consists of approximately 10^6 cells, so the amounts of antibody and dye used to label the multilayer tissue constructs are theoretically sufficient for detecting a precancerous lesion. Cetuximab is an EGFR antibody produced by ImClone Systems (Somerville, NJ) which is currently in clinical trials for treatment of several types of solid tumors, including head and neck. The current recommended dosage is an initial loading dose of 400 mg/m^2 and maintenance doses of 200 mg/m^2 (114). The body surface area of a man using the average height and weight statistics given by the CDC is 2 m^2, resulting in a Cetuximab loading does of 800 mg and maintenance does of 400 mg. Drug dosage is difficult to directly compare to the amounts of antibody used in this study because the goal of the Cetuximab treatment is cancer therapy rather than diagnosis and dosage is given in terms of body surface area, but it is clear that the amounts of EGFR antibody required for diagnostic imaging are considerably less than the amounts administered for therapeutic reasons with tolerable side effects. While the number of cells in the multilayer tissue construct cannot be extrapolated directly to the number of cells in an *in vivo* solid tumor, these numbers indicate that the concentrations of antibody and dye being used here are not unreasonable for clinical use.

With respect to *in vivo* use of the contrast agent, questions concerning the use of the biotin-(strept)avidin system and the various permeability enhancing agents must also be addressed. The high affinity biotin-(strept)avidin system has been used *in vivo* in radio-applications, including radioimmunodetection and therapy of cancer in humans (115) and immunotargeting of cytotoxic molecules and cells to tumor cells (96, 116-119). The possible drawbacks to using streptavidin for *in vivo* applications are that it tends to be sequestered quickly by the kidneys (120), which could limit the amount of the streptavidin-conjugated compound delivered to the target, and it cannot be humanized, potentially making it more immunogenic. Streptavidin has been modified in order to improve its *in vivo* sequestration characteristics (120), however kidney localization of the stretpavidin-labeled dye before tumor targeting is not likely to be a problem with topical application of the contrast agent. Further, streptavidin is an analog of avidin, which has better immunogenic characteristics but a much shorter circulatory half-life (115) and could replace streptavidin in the contrast agent for biotin-binding.

The presence of endogenous biotin could result in false-positive staining due to endogenous avidin-binding activity (EABA). Studies which investigated the levels of background EABA in tissue sections from various organ sites found levels to be high only in tissues known to contain large biotin stores, which include liver, adipose tissue, mammary gland, and kidney (121). We are therefore hopeful that in the oral cavity, EABA levels will be low and not contribute significant background.

Topical application would be ideal for *in vivo* use in targeting epithelial cancers to minimize systemic exposure to the contrast agent. We have demonstrated that the use of permeability-enhancing agents such as dimethyl sulfoxide (DMSO) and polyvinylpyrooliodone (PVP) have the potential to enhance topical application. However, the use of a permeability-enhancing agent adds an additional substance whose biocompatibility must be considered. Clinically, DMSO has been approved by the FDA for use in treatment of interstitial cystitis and is delivered as a 50% solution or in a DMSO cocktail which contains 50 cc of 50% DMSO (122). According to FDA toxicological data for class 3 solvents, the permitted daily exposure of DMSO is 50 mg/day or approximately 500 mol/day. 500 μl of a 5% solution of DMSO contains only 0.35 mmol of DMSO. In addition, PVP has been approved by the FDA as an excipient in topical formulations and is used in a povidone-iodine solution ranging from 1-20% in drugs from various pharmaceutical companies (information from the FDA Center for Drug Evaluation and Research website).

Two pharmokinetic issues which should be considered for *in vivo* use of the contrast agent are localization time to the tumor before imaging and clearance of the contrast agent from tissue. Most target-specific fluorescent contrast agents that have demonstrated localization to tumors in animal models are delivered via i.v. or i.p. injection (37, 62, 65-67). In the case of i.v. or i.p. injection, localization time to the tumor before imaging is critical because the contrast agent is generally being delivered systemically through the bloodstream. There will therefore be some delay before the

contrast agent can be circulated to the site of the tumor. In addition, the contrast agent may also be taken up by other organs, such as the liver and kidney, when injected into the bloodstream. Some time for clearance of the contrast agent after localization to the tumor may also be necessary to avoid background fluorescence from circulating contrast agent. In the case of topical application, time for localization and clearance may not be as critical. In one scenario for use of the contrast agent as a diagnostic tool for oral cancer, the contrast agent would be applied directly to a suspicious lesion. Therefore, there would be no time delay in waiting for the contrast agent to reach the tumor site. Also, because less tissue is exposed to the contrast agent in topical application, there may not be as much background fluorescence from non-specific interactions.

Clearance of the contrast agent from the tissue after obtaining measurements may also be important in order to reduce the length of exposure to the contrast agent. Contrast agent administered through i.v. injection that does not localize to a tumor and is circulating in the bloodstream should be cleared by the body naturally. It is also assumed that if the contrast agent does localize to a tumor, that the tumor would be removed, eliminating the contrast agent at the same time. However, contrast agent which is taken up non-specifically by other organs may remain in the body for a longer period of time.. Topical application would eliminate systemic exposure of the body to the contrast agent, minimizing many of these concerns. Finally, our contrast agent targets epithelial cancers in the oral cavity, which should also eliminate many of the concerns regarding clearance from the tissue. It is very unlikely that through topical application, the contrast agent

would be able to pass through the entire epithelial layer and portions of the stroma and endothelial vessel walls to infiltrate into the bloodstream, so the contrast agent should remain fairly localized to the epithelial layers of the oral cavity. Also, there tends to be faster overturn of epithelial cells, which may result in natural clearance of the contrast agent through cell death and removal.

Clearly, there are somewhat complicated issues which must be addressed before the contrast agent can be used *in vivo*. However, while careful consideration must be taken with all the issues discussed here, it is evident that *in vivo* use of the contrast agent is not an unreasonable prospect. Further studies will need to be performed to evaluate the contrast agent before it can be used *in vivo*, but the experiments performed thus far and the relevant literature review in similar areas reveal that the contrast agent has *in vivo* potential.

Chapter 7

Summary and Conclusions

7.1 SUMMARY OF RESULTS

The results presented in this dissertation demonstrate the use of a molecular-specific fluorescent contrast agent in combination with fluorescence spectroscopy and confocal microscopy. The contrast agent is targeted against epidermal growth factor receptor (EGFR), which is often overexpressed in oral cancer and is expressed in the early stages of cancer, making it a good molecular target for early detection of cancer. Currently, diagnosis of oral cancer relies on visual detection and suspicion by the treating clinician. Therefore, oral cancer is generally not diagnosed until it has reached advanced stages, when morbidity and mortality is high. The contrast agent could potentially be used as a diagnostic tool, particularly in conjunction with a noninvasive optical technique such as fluorescence spectroscopy.

In the third chapter of this dissertation, the contrast agent was evaluated in *in vitro* biological models as a first step in testing its potential for use in diagnosis of oral cancer. The ability of the contrast agent to image EGFR in cancer cell lines was demonstrated, with detectable fluorescence signal using a range of antibody dilutions and incubation times. The ability to penetrate through 500 μm thick multilayer epithelial tissue constructs when applied topically with permeability-enhancing agents was also demonstrated.

The fourth chapter expanded evaluation of the contrast agent to testing in *ex vivo* biopsy samples, using fresh tissue slices from paired clinically abnormal and clinically normal biopsy samples obtained from consenting patients. These experiments revealed that the biggest difference in fluorescence intensity between the abnormal and normal samples was seen in the surface layer of the epithelium, which had decreased EGFR expression in normal tissue due to lack of cellular proliferation. Within a patient, a pathologically abnormal biopsy had a greater fluorescence intensity than a pathologically normal biopsy, which was reflected in the ratio of the mean fluorescence intensity of the abnormal to normal. Both the abnormal and normal ratio and the mean fluorescence intensity of the surface layer of the epithelium provided fairly good separation between normal and moderate dysplasia or cancer.

Expansion of the use of the contrast agent in conjunction with fluorescence spectroscopy was explored in chapter five. A simple fluorescence spectroscopy system was built and designed to detect the optical signal of the contrast agent. This ability of this system to detect multilayer tissue constructs labeled using the contrast with good signal-to-noise ratio (SNR) was demonstrated. The potential of the spectroscopy system to detect labeled tissue was also explored using fresh tissue slices. With increased integration time, the spectroscopy system was able to detect the optical signal of the contrast agent in a tissue sample with good SNR.

Chapter six explored the issues which must be considered for *in vivo* use of the contrast agent. In order to fully utilize the potential of the contrast agent as a diagnostic

tool in the oral cavity in conjunction with a noninvasive optical technique, it must be used *in vivo*. While the Alexa Fluor® 660 streptavidin dye did appear to negatively effect cells over a long period of exposure, cells grew well in the presence of dye for up to four days. Labeling at physiological temperature rather than room temperature also did not appear to have a significant effect on labeling. Other considerations, such as immunogenic effects of the antibody, the use of the biotin-streptavidin system and permeability-enhancing agents, optimal time for localization, and clearance of the contrast agent from tissue, were discussed in relation to relevant literature. Altogether, it appears that *in vivo* use of the contrast agent without detrimental effects is possible.

The research presented in this dissertation lays the groundwork for the development of a tool that could be used in diagnosis of oral cancer. The specificity of the contrast agent for EGFR was demonstrated using *in vitro* biological models, along with the ability to penetrate into multiple layers of epithelial cells. The ability to use fluorescence intensity as a diagnostic criteria was demonstrated in *ex vivo* biopsy samples. Finally, the use of a simple spectroscopy system in conjunction with the contrast agent was demonstrated, which would be ideal as an inexpensive diagnostic tool that could be used without specialized training.

7.2 FUTURE DIRECTIONS

While the research presented here provides a solid basis for the development of a diagnostic tool for the early detection of oral cancer, further research must be performed to fully evaluate the use of a fluorescence contrast agent and spectroscopy system as a

diagnostic tool. More samples in the *ex vivo* biopsy study must be obtained to ensure that fluorescence intensity of the contrast agent can be used as a diagnostic criteria. Ideally, enough samples would be obtained to determine a demarcation in the abnormal to normal ratio or surface fluorescence intensity that separates normal from cancer and dysplasia with good sensitivity and specificity. This study could also be expanded to evaluate the ability of the contrast agent to aid in detection of tumor margins using both confocal microscopy and fluorescence spectroscopy. If the fluorescence intensity of the contrast agent can be used to demarcate a relatively clear border for a tumor, it could be used to determine if a tumor has been entirely resected during surgery in near real-time rather than having to wait for a biopsy sample to be prepared for microscopic examination.

The permeability-enhancing agents have shown the ability to penetrate multiple layers of epithelial cells in tissue constructs, but they must also be tested in actual tissue samples to determine the depth of labeling which can be achieved. This could be tested using whole biopsies, by immobilizing the biopsy in agar or gelatin and applying the contrast agent and permeability-enhancing agent on top, or possibly in an animal model. It would also be ideal to determine if the permeability-enhancing agents were increasing transport of the contrast agent intra- or intercellularly; in other words, if the permeability-enhancing solution is permitting the contrast agent to pass through the cell itself or between cell-cell junctions.

Further testing with the spectroscopy system also needs to be performed to validate its use as a simple diagnostic tool. If the contrast agent shows the ability to

discriminate between normal and dysplasia and cancer with good sensitivity and specificity based on mean fluorescence intensity, then it could easily be used in conjunction with the spectroscopy system as a diagnostic tool. In order to determine the performance of the spectroscopy system in tissue, it should be tested with whole *ex vivo* biopsies labeled with the contrast agent and possibly in an animal model as well. Ultimately, if the contrast agent is approved for *in vivo* use, the combination of the contrast agent and spectroscopy system as a diagnostic tool for oral cancer could be tested in an *in vivo* pilot study.

In addition to the spectroscopy system, the contrast agent could also be used in combination with fluorescence confocal microscopy. The contrast agent would improve the optical signal, making it easier to visual with confocal microscopy, and also would provide an indicator for early disease. To truly utilize the advantages of optical techniques, an *in vivo* fluorescence confocal microscope would need to be developed. Current fiber-based confocal microscopes either target reflectance or fluorescence at 488 nm only, while the contrast agent requires excitation at 633-660 nm. Adapting a 488 nm fiber-based confocal microscope for excitation at 633-660 nm should be a relatively straightforward change, the primary alterations consisting of a different excitation light source and emission filters.

Clearly, more research needs to be performed to assess both the contrast agent and spectroscopy system. However, the foundations presented in this dissertation are extremely promising and exciting for a fluorescence contrast agent that could be used as

diagnostic tool for early detection of cancer in the oral cavity. In particular, combining the contrast agent with a simple spectroscopy system would provide a simple diagnostic tool at relatively low cost that could be used by personnel without specialized training to identify suspicious lesions in the oral cavity. The development of a true diagnostic tool in the oral cavity that does not rely purely on the clinician's expertise would hopefully increase early detection of oral cancer and ultimately result in a decrease in the morbidity and mortality associated with oral cancer.

References

1. American Cancer Society, (2003) *Cancer Facts and Figures*. Vol. 02-20M-No. 5008.03. American Cancer Society, Inc., Atlanta.

2. Sciubba, J. J. (2001) Oral Cancer: The Importance of Early Diagnosis and Treatment. *Am. J. Clin. Dermatol.* **2**(4), 239-251.

3. Crawford, W. H. (2002), *Mucosa: Cancer and Premalignant Diseases*, in *Oral Pathology*, W. H. Crawford, Editor. p. 245-266. Health-Soft-Edu: Los Angeles.

4. Barasch, A., M. Safford and E. Eisenberg (1998) Oral Cancer and Oral Effects of Anticancer Therapy. *Mt. Sinai J. Med.* **65**(5&6), 370-377.

5. GLOBOCAN 2000, *Cancer Incidence, Mortality, and Prevalence*. 2000.

6. Sexton, J. (2000) Surgical Pathology of the Oral Cavity. *Clin. Dermatol.* **18**, 601-611.

7. American Cancer Society, *Cancer Reference Information*. 2003.

8. Yeole, B. B., A. V. Ramanakumar and R. Sankaranarayanan (2003) Survival from Oral Cancer in Mumbai (Bombay), India. *Cancer Causes Control*. **14**, 945-952.

9. Martini, F. H., M. J. Timmons, M. P. McKinley, W. C. Ober, C. W. Garrison, K. Welch and R. T. Hutchings, (2000) *Human Anatomy*. 3 ed, ed. P. F. Corey. Vol. 3. Prentice-Hall, Upper Saddle River, NJ.

10. de Veld, D. C. G., M. Skurichina, M. J. H. Witjes, R. P. W. Duin, D. J. c. M. Sterenborg, W. M. Star and J. L. N. Roddenburg (2003) Autofluorescence Characteristics of Health Oral Mucosa at Different Anatomical Sites. *Lasers Surg. Med.* **32**, 367-276.

11. Winning, T. A. and G. C. Townsend (2000) Oral Mucosal Embryology and Histology. *Clin. Dermatol.* **18**, 499-511.

12. Silverman, S. and P. B. Sugerman (2000) Oral Premalignancies and Squamous Cell Carcinoma. *Clin. Dermatol.* **18**, 563-568.

13. Mashberg, A. (2000) Diagnosis of Early Oral and Oralpharyngeal Squamous Carcinoma: Obstacles and Their Amelioration. *Oral Oncol.* **36**, 253-255.

14. Walker, D. C., B. H. Brown, A. D. Blackett, J. Tidy and R. H. Smallwood (2003) A Study of the Morphhological Parameters of Cervical Squamous Epithelium. *Physiol. Meas.* **24**, 121-135.

15. Papadimitrakopoulou, V. A., D. M. Shin and W. K. Hong (1996) Molecular and Cellular Biomarkers for Field Cancerization and Multistep Process in Head and Neck Tumorigenesis. *Cancer Metastasis Rev.* **15**, 53-76.

16. Srinivas, P. R., B. S. Kramer and S. Srivastava (2001) Trends in Biomarker Research for Cancer Detection. *Lancet Oncol.* **2**, 698-704.

17. Caldas, C. (1998) Molecular Assessment of Cancer. *Br. Med. J.* **316**, 1360-1363.

18. Rose, B. R., C. H. Thompson, M. H. Tattersall, C. J. O'Brien and Y. E. Cossart (2000) Squamous Carcinoma of the Head and Neck: Molecular Mechanisms and Potential Biomarkers. *Aust. N. Z. J. Surg.* **70**, 601-606.

19. Salesiotis, A. N. and K. J. Cullen (2000) Molecular Markers Predictive of Response and Prognosis in the Patient with Advanced Squamous Cell Carcinoma of the

Head and Neck: Evolution of a Model Beyond TNM Staging. *Curr. Opin. Oncol.* **12**, 229-239.

20. Abraham, M. T., M. A. Kuriakose, P. G. Sacks, H. Yee, L. Chiriboga, E. L. Bearer and M. D. Delacure (2001) Motility-Related Proteins as Markers for Head and Neck Squamous Cell Cancer. *The Laryngoscope*. **111**, 1285-1289.

21. Todd, R. and D. T. W. Wong (1999) Epidermal Growth Factor Receptor (EGFR) Biology and Human Oral Cancer. *Histol. Histopathol.* **14**, 491-500.

22. Ke, L. D., K. Adler-Storthz, G. L. Clayman, A. W. K. Yung and Z. Chen (1998) Differential Expression of Epidermal Growth Factor Receptor in Human Head and Neck Cancers. *Head Neck*, 320-327.

23. Nouri, A. M. E., C. Thompson, H. Cannell, M. Symes, S. Purkiss and Z. Amirghofran (2000) Profile of Epidermal Growth Factor Receptor (EGFr) Expression in Human Malignancies: Effects of Exposure to EGF and its Biological Influence on Established Human Tumour Cell Lines. *Int. J. Mol. Med.* **6**, 495-500.

24. Carpenter, G. (1987) Receptors for Epidermal Growth Factor and Other Polypeptide Mitogens. *Annu. Rev. Biochem.* **56**, 881-914.

25. Eisbruch, A., M. Blick, J. S. Lee, P. G. Sacks and J. Gutterman (1987) Analysis of the Epidermal Growth Factor Receptor Gene in Fresh Human Head and Neck Tumors. *Cancer Res.* **47**, 3603-3605.

26. Reiss, M., E. B. Stash, V. F. Vellucci and Z.-l. Zhou (1991) Activation of the Autocrine Transforming Growth Factor α Pathway in Human Squamous Carcinoma Cells. *Cancer Res.* **51**(23 Pt 1), 6254-6262.

27. Ishitoya, J., M. Toriyama, N. Oguchi, K. Kitamura, M. Ohshima, K. Asano and T. Yamamoto (1989) Gene Amplification and Overexpression of EGF Receptor in Squamous Cell Carcinomas of the Head and Neck. *Br. J. Cancer*. **59**, 559-562.

28. Christensen, M. E., F. Engbaek, M. H. Therkildsen, P. Bretlau and E. Nexø (1995) A Sensitive Enzyme-Linked Immunosorbent Assay Used for Quantitation of Epidermal Growth Factor Receptor Protein in Head and Neck Carcinomas: Evaluation, Interpretations and Limitations. *Br. J. Cancer*. **72**, 1487-1493.

29. Scambia, G., P. B. Panici, F. Battaglia, G. Ferrandina, G. Almadori, G. Paludetti, M. Maurizi and S. Mancuso (1991) Receptors for Epidermal Growth Factor and Steroid Hormones in Primary Laryngeal Tumors. *Cancer*. **67**, 1347-1351.

30. Kawamoto, T., K. Takahashi, M. Nishi, T. Kimura, T. Matsumura and S. Taniguchi (1991) Quantitative Assay of Epidermal Growth Factor Receptor in Human Squamous Cell Carinomas of the Oral Region by an Avidin-Biotin Method. *Jpn. J. Cancer Res*. **82**, 403-410.

31. Santini, J., J.-L. Formento, M. Francoual, G. Milano, M. Schneider, O. Dassonville and F. Demard (1991) Characterization, Quantification, and Potential Clinical Value of the Epidermal Growth Factor Receptor in Head and Neck Squamous Cell Carcinomas. *Head Neck*. **13**, 132-139.

32. Kannan, S., P. Balaram, G. J. Chandran, M. R. Pillai, B. Mathew and M. K. Nair (1994) Co-Expression of ras p21 and Epidermal Growth Factor Receptor during Various Stages of Tumour Progression in Oral Mucosa. *Tumor Biol.* **15**, 73-81.

33. Shintani, S., T. Matsumura, R. E. Alcalde and Y. Yoshihama (1996) Sequential Expression of *myc-, ras-,* Oncogene Products and EGF Receptor during DMBA-induced Tongue Carcinogenesis. *Int. J. Oncol.* **8**, 821-826.

34. Shin, D. M., J. Y. Ro, W. K. Hong and W. N. Hittelman (1994) Dysregulation of Epidermal Growth Factor Receptor Expression in Premalignant Lesions during Head and Neck Tumorigenesis. *Cancer Res.* **54**, 3153-3159.

35. van Oijen, M. G. C. T., G. Rijksen, F. W. ten Broek and P. J. Slootweg (1998) Increased Expression of Epidermal Growth Factor Receptor in Normal Epithelium Adjacent to Head and Neck Carcinomas Independent of Tobacco and Alcohol Abuse. *Oral Dis.* **4**, 4-8.

36. Ang, K. K., B. A. Berkey, X. Tu, H.-Z. Zhang, R. Katz, E. H. Hammond, K. K. Fu and L. Milas (2002) Impact of Epidermal Growth Factor Receptor Expression on Survival and Pattern of Relapse in Patients with Advanced Heand and Neck Carcinoma. *Cancer Res.* **62**, 7350-7356.

37. Soukos, N. S., M. R. Hamblin, S. Keel, R. L. Fabian, T. F. Deutsch and T. Hasan (2001) Epidermal Growth Factor Receptor-targeted Immunophotodiagnosis and Photoimmunotherapy of Oral Precancer *in Vivo*. *Cancer Res.* **61**, 4490-4496.

38. Osborn, M. and K. Weber (1983) Tumor Diagnosis by Intermediate Filament Typing: A Novel Tool for Surgical Pathology. *Lab. Invest.* **48**(4), 372-394.

39. Sawaf, M. H., J. P. Ouhayoun and N. Forest (1991) Cytokeratin Profiles in Oral Epithelia: A Review and a New Classification. *J. Biol. Buccale*. **19**, 187-198.

40. Ogden, G. R., D. M. Chisholm, M. Adi and E. B. Lane (1993) Cytokeratin Expression in Oral Cancer and its Relationship to Tumor Differentation. *J. Oral Pathol. Med.* **22**, 82-86.

41. Morgan, P. R., P. J. Shirlaw, N. W. Johnson, I. M. Leigh and E. B. Lane (1987) Potential Applications of Anti-Keratin Antibodies in Oral Diagnosis. *J. Oral Pathol. Med.* **16**, 212-222.

42. Vaidya, M. M., A. M. Borges, S. A. Pradhan, R. M. Rajpal and A. N. Bhisey (1989) Altered Keratin Expression in Buccal Mucosal Squamous Cell Carcinoma. *J. Oral Pathol. Med.* **18**, 282-286.

43. Xu, X. C., J. S. Lee, S. M. Lippman, J. Y. Ro, W. K. Hong and R. Lotan (1995) Increased Expression of Cytokeratins CK8 and CK19 is Associated with Head and Neck Carcinogenesis. *Cancer Epidemiology, Biomarkers, and Prevention*. **4**, 871-876.

44. Cema, I., B. Stengel and H. Nizze (1998) Expression of Cytokeratins in Oral Dysplasias and Squamous Cell Carcinoma. *Proceedings of the Latvian Academy of Sciences*. **52**(3/4), 119-125.

45. Kannan, S., P. Balaram, G. J. Chandran, M. R. Pillai, B. Mathew, K. R. Nalinakumari and M. K. Nair (1994) Differential Expression of Cytokeratin Proteins During Tumour Progression in Oral Mucosa. *Epithelial Cell Biol.* **3**, 61-69.

46. van der Velden, L.-A., H. E. Shaafsma, J. J. Manni, F. c. S. Ramaekers and W. Kuijpers (1993) Cytokeratin Expression in Normal and (Pre)Malignant Head and Neck Epithelia: an Overview. *Head Neck*. **15**, 133-146.

47. Ogden, G. R., D. M. Chisholm and E. B. Lane (1996) The Utility of Cytokeratin Profiles for Detecting Oral Cancer Using Exfoliative Cytology. *Br. J. Oral Maxillofac. Surg*. **34**, 461-466.

48. Ogden, G. R., E. B. Lane, D. V. Hopwood and D. M. Chisholm (1993) Evidence for Field Change in Oral Cancer Based on Cytokeratin Expression. *Br. J. Cancer*. **67**, 1324-1330.

49. Bornhop, D. J., C. H. Contag, K. Licha and C. J. Murphy (2001) Advances in Contrast Agents, Reporters, and Detection. *J. Biomed. Opt*. **6**(2), 106-110.

50. Piffkò, J., À. Bànkfalvi, U. Joss, D. Öfner, M. Krassort and K. W. Schmid (1999) Immunophenotypic Analysis of Normal Mucosa and Squamous Cell Carcinoma of the Oral Cavity. *Cancer Detect. Prev*. **23**(1), 45-46.

51. Bergers, G. and L. M. Coussens (2000) Extrinsic Regulators of Epithelial Tumor Progression: Metalloproteinases. *Curr. Opin. Genet. Dev*. **10**, 120-127.

52. Ziober, B. L., M. A. Turner, J. M. Palefsky, M. J. Banda and R. H. Kramer (2000) Type I Collagen Degradation by Invasive Squamous Cell Carcinoma. *Oral Oncol.* **36**, 365-372.

53. Gillenwater, A., X.-C. Xu, A. K. El-Naggar, G. L. Clayman and R. Lotan (1996) Expression of Galectins in Head and Neck Squamous Cell Carcinoma. *Head Neck.* **18**, 422-432.

54. Gillenwater, A., X.-C. Xu, Y. Estrov, P. G. Sacks, D. Lotan and R. Lotan (1998) Modulation of Galectin-1 Content in Human Head and Neck Squamous Carcinoma Cells by Sodium Butyrate. *Int. J. Cancer.* **75**, 217-224.

55. Wagnières, G. A., W. M. Star and B. C. Wilson (1998) *In Vivo* Fluorescence Spectroscopy and Imaging for Oncological Applications. *Photochem. Photobiol.* **68**(5), 603-632.

56. Wang, C.-Y., H. K. Chiang, C.-T. chen, C.-P. Chiang, Y.-S. Kuuo and S.-N. Chow (1999) Diagnosis of Oral Cancer by Light-Induced Autofluorescence Spectroscopy Using Double Excitation Wavelengths. *Oral Oncol.* **35**, 144-150.

57. Gillenwater, A., R. Jacob and R. Richards-Kortum (1998) Fluorescence Spectroscopy: A Technique with Potential to Improve the Early Detection of Aerodigestive Tract Neoplasia. *Head Neck.* **20**, 556-562.

58. Heintzelman, D. L., U. Utzinger, H. Fuchs, A. Zuluaga, K. Gossage, A. M. Gillenwater, R. Jacob, B. Kemp and R. R. Richards-Kortum (2000) Optimal Excitation

Wavelengths for *In Vivo* Detection of Oral Neoplasia Using Fluorescence Spectroscopy. *Photochem. Photobiol.* **72**(1), 103-113.

59. van der Breggen, E. W. J., A. I. Rem, M. M. Christian, C. J. Yang, K. H. Calhoun, H. J. C. M. Sterenborg and M. Motamedi (1996) Spectroscopic Detection of Oral and Skin Tissue Transformation in a Model for Squamous Cell Carcinoma: Autofluorescence versus Systemic Aminolevulinic Acid-Induced Fluorescence. *IEEE Journal of Selected Topis in Quantum Electronics.* **2**(4), 997-1007.

60. Onofre, M. A., M. R. Sposto and C. M. Navarro (2001) Reliability of Toluidine Blue Application in the Detection of Oral Epithelial Dysplasia and *In situ* and Invasive Squamous Cell Carcinomas. *Oral Surgery, Oral Medicine, Oral Pathology, Oral Radiology and Endodontics and Endodontics.* **91**(5), 535-540.

61. Warnakulasuriya, K. A. A. S. and N. W. Johnson (1996) Sensitivity and Specificity of OraScan® Toluidine Blue Mouthrinse in the Detection of Oral Cancer and Precancer. *J. Oral Pathol. Med.* **25**, 97-103.

62. Sevick-Muraca, E. M., J. P. Houston and M. Gurfinkel (2002) Fluoresence-enhanced, Near Infared Diagnostic Imaging with Contrast Agents. *Curr. Opin. Chem. Biol.* **6**, 642-650.

63. Malicka, J., I. Gryczynski, C. D. Geddes and J. R. Lakowicz (2003) Metal-enhanced Emission from Indocyanine Green: A New Approach to *In Vivo* Imaging. *J. Biomed. Opt.* **8**(3), 472-478.

64. Haglund, M. M., M. S. Berger and D. W. Hochman (1996) Enhanced Optical Imaging of Human Gliomas and Tumor Margins. *Neurosurgery*. **38**(2), 308-317.

65. Becker, A., C. Hessenius, K. Licha, B. Ebert, U. Sukowski, W. Semmier, B. Wiedenmann and C. Grötzinger (2001) Receptor-targeted Optical Imaging of Tumors with Near-Infrared Fluorescent Ligands. *Nature Biotechnology*. **19**, 327-331.

66. Bugaj, J. E., S. Achilefu, R. B. Dorshow and R. Rajagopalan (2001) Novel Fluorescent Contrast Agents for Optical Imaging of *In Vivo* Tumors Based on a Receptor-targeted Dye-Peptide Conjugate Platform. *J. Biomed. Opt.* **6**(2), 122-133.

67. Ballou, B., G. W. Fisher, T. R. Hakala and D. L. Farkas (1997) Tumor Detection and Visualization Using Cyanine Fluorochrome-Labeled Antibodies. *Biotechnol. Prog.* **13**, 649-658.

68. Licha, K., C. Hessenius, A. Becker, P. Henklein, M. Bauer, S. Wisniewski, B. Widenmann and W. Semmler (2001) Synthesis, Characterization, and Biological Properties of Cyanine-Labeled Somatostatin Analogues as Receptor-Targeted Fluorescent Probes. *Bioconjug. Chem.* **12**, 44-50.

69. Weissleder, R., C.-H. Tung, U. Mahmood and A. B. Jr. (1999) In Vivo Imaging of Tumors with Protease-Activated Near-Infrared Fluorescent Probes. *Nature Biotechnology*. **17**, 375-378.

70. Bruchez, M., M. Moronne, P. Gin, S. Weiss and A. P. Alivisatos (1998) Seminconductor Nanocrystals as Fluorescent Biological Labels. *Science*. **281**, 2013-2016.

71. Chan, W. C. W. and S. Nie (1998) Quantum Dot Bioconjugates for Ultrasensitive Nonisotropic Detection. *Science*. **281**, 2016-2018.

72. Cantor, S. B., M. F. Mitchell, G. Torotolero-Luna, C. S. Bratka, D. C. Bodurka and R. Richards-Kortum (1998) Cost-Effectiveness Analysis of Diagnosis and Management of Cervical Squamous Intraepithelial Lesions. *Obstet. Gynecol*. **91**, 270-277.

73. Collier, T., A. Lacy, R. Richards-Kortum, A. Malpica and M. Follen (2002) Near Real-Time Confocal Microscopy of Amelanotic Tissue: Detection of Dysplasia in *ex Vivo* Cervical Tissue. *Acad. Radiol*. **9**, 504-512.

74. White, W. M., M. Rajadhyaksha, S. Gonzalez, R. L. Fabian and R. R. Anderson (1999) Noninvasive Imaging of Human Oral Mucosa in Vivo by Confocal Reflectance Microscopy. *The Laryngoscope*. **109**, 1709-1717.

75. Sokolov, K., R. Drezek, K. Gossage and R. Richards-Kortum (1999) Reflectance Spectroscopy with Polarized Light: Is it Sensitive to Cellular and Nuclear Morphology? *Optics Express*. **5**(13), 302.

76. Utzinger, U., M. Brewer, E. Silva, D. Gersheson, R. C. B. Jr., M. Follen and R. Richards-Kortum (2001) Reflectance Spectroscopy for *In Vivo* Characterization of Ovarian Tissue. *Lasers Surg. Med*. **28**, 56-66.

77. Sacks, P. G., H. E. Savage, J. Levine, V. R. Kolli, R. R. Alfano and S. P. Schantz (1996) Native Cellular Fluorescence Identifies Terminal Squamous Differentiation of

Normal Oral Epithelial Cells in Culture: A Potential Chemoprevention Biomarker. *Cancer Lett*. **104**, 171-181.

78. Kolli, V. R., A. R. Shaha, H. E. Savage, P. G. Sacks, M. A. Casale and S. P. Schantz (1995) Native Cellular Fluorescence Can Identifiy Changes in Epithelial Thickness In-Vivo in the Upper Aerodigestive Tract. *The American Journal of Sugery*. **170**, 495-598.

79. Gillenwater, A., R. Jacob, R. Ganeshappa, B. Kemp, A. K. El-Naggar, J. L. Palmer, G. Clayman, M. F. Mitchell and R. Richards-Kortum (1998) Noninvasive Diagnosis of Oral Neoplasia Based on Fluorescence Spectroscopy and Native Tissue Autofluorescence. *Archives of Otolaryngology--Head and Neck Surgery*. **124**, 1251-1258.

80. Pitts, J. D., R. d. Sloboda, K. H. Dragnev, E. Dmitrovsky and M.-A. Mycek (2001) Autofluorescence Characteristics of Immortalized and Carcinogen-transformed Human Bronchial Epithelial Cells. *J. Biomed. Opt*. **6**(1), 31-40.

81. Ramanujam, N. (2000) Fluoresence Spectroscopy of Neoplastic and Non-Neoplastic Tissues. *Neoplasia*. **2**(1-2), 89-117.

82. Müller, M. G., T. A. Valdez, I. Georgakoudi, V. Backman, C. Fuentes, S. Kabani, N. Laver, Z. Wang, C. W. Boone, R. R. Dasari, S. M. Shapshay and M. S. Feld (2003) Spectroscopic Detection and Evaluation of Morphologic and Biochemical Changes in Early Human Oral Carcinoma. *Cancer*. **97**(7), 1681-1692.

83. Svistun, E., R. Alizadeh-Naderi, A. El-Naggar, R. Jacob, A. Gillenwater and R. Richards-Kortum (2004) Vision Enhancement System for Detection of Oral Cavity Neoplasia Based on Autofluorescence. *Head Neck*. **26**(3), 205-215.

84. Schantz, S. P., V. Kolli, H. E. Savage, G. Yu, J. P. Shah, D. E. Harris, A. Katz, R. R. Alfano and A. G. Huvos (1998) *In Vivo* Native Cellular Fluorescence and Histological Characteristics of Head and Neck Cancers. *Clinical Cancer Research*. **4**, 1177-1182.

85. Betz, C. S., M. Mehlmann, K. Rick, H. Stepp, G. Grevers, R. Baumgartner and A. Leunig (1999) Autofluorescence Imaging and Spectroscopy of Normal and Malignant Mucosa in Patients with Head and Neck Cancer. *Lasers Surg. Med.* **25**, 323-334.

86. Dhingra, J. K., D. F. Perrault, K. McMillan, E. E. Rebeiz, S. Kabani, R. Manoharan, I. Itzkan, M. S. Feld and S. M. Shapshay (1996) Early Diagnosis of Upper Aerodigestive Tract Cancer by Autofluorescence. *Arch. Otolaryngol. Head Neck Surg.* **122**(11), 1181-1186.

87. Kulapaditharom, B. and V. Boonkitticharoan (1998) Laser Induced Fluorescence Imaging in Localization of Head and Neck Cancers. *Ann. Otol. Rhinol. Laryngol.* **107**(3), 241-246.

88. Sung, K. B., C. Liang, M. Descour, T. Collier, M. Follen, A. Malpica and R. Richards-Kortum (2002) Near Real Time *in vivo* Fibre Optic Confocal Microscopy: Sub-cellular Structure Resolved. *J. Microsc.* **207 (Pt) 2**, 137-45.

89. Sung, K. B., C. Liang, M. Descour, M. Follen and R. Richards-Kortum (2002) Fiber Optic Confocal Microscope with Miniature Objective for *in-vivo* Imaging. *IEEE Trans. Biomed. Eng.* **49**(10), 1168-1172.

90. Anikijenko, P., L. T. Vo, E. R. Murr, J. Carrasco, W. J. McLaren, Q. Chen, S. G. Thomas, P. M. Delaney and R. G. King (2001) *In Vivo* Detection of Small Subsurface Melanomas in Athymic Mice Using Noninvasive Fiber Optic Confocal Imaging. *J. Invest. Dermatol.* **117**, 1442-1448.

91. Gmitro, A. F. and D. Aziz (1993) Confocal Microscopy Through a Fiber-Optic Imaging Bundle. *Opt. Lett.* **18**(8), 565-567.

92. Juˇskaitis, R. and T. Wilson (1992) Imaging in Reciprocal Fibre-Optic Based Confocal Scanning Microscopes. *Optics Communications*. **92**, 315-325.

93. Swindle, L. D., S. G. Thomas, M. Freeman and P. M. Delaney (2003) View of Normal Human Skin *In Vivo* as Observed Using Fluorescent Fiber-Optic Confocal Microscopic Imaging. *J. Invest. Dermatol.* **121**, 706-712.

94. Clark, A. L., A. M. Gillenwater, T. G. Collier, R. Alizadeh-Naderi, A. K. El-Naggar and R. R. Richards-Kortum (2003) Confocal Microscopy for Real-Time Detection of Oral Cavity Neoplasia. *Clinical Cancer Research*. **9**, 4714-4721.

95. Watson, T. F., W. M. Petroll, H. D. Cavanagh and J. V. Jester (1992) *In Vivo* Confocal Microscopy in Clinical Dental Research: An Initial Appraisal. *J. Dent.* **20**(6), 352-358.

96. Yu, Z.-W. and P. J. Quinn (1998) The Modulation of Membrane Structure and Stability by Dimethyl Sulphoxide. *Mol. Membr. Biol.* **15**, 59-68.

97. Yu, Z.-W. and P. J. Quinn (1994) Dimethyl Sulphoxide: A Review of its Applications in Cell Biology. *Biosci. Rep.* **14**(6), 259-281.

98. Viegas, T. x., A. H. Hikal and R. W. Cleary (1998) Formulation of Penetration Enhancers in Polymers. *Drug Dev. Ind. Pharm.* **14**(6), 855-866.

99. Krishna, G., K.-J. Chen, C.-C. Lin and A. A. Nomeir (2001) Permeability of Lipophilic Compounds in Drug Discovery using *In-Vitro* Human Absorption Model, Caco-2. *Int. J. Pharm.* **222**, 77-89.

100. Andersson-Engels, S., C. a. Klinteberg, K. Svanber and S. Svanber (1997) *In Vivo* Fluorescence Imaging for Tissue Diagnostics. *Phys. Med. Biol.* **42**, 815-824.

101. Ferris, D. G., R. A. Lawhead, E. D. Dickman, N. Holtzapple, J. A. Miller, S. Grogan, S. Bambot, A. Agrawal and M. L. Faupel (2001) Multimodal Hyperspectral Imaging for the Noninvasive Diagnosis of Cervical Neoplasia. *Journal of Lower Genital Tract Disease*. **5**(2), 65-72.

102. Gurjar, R. S., V. Backman, L. T. Perelman, I. Georgakoudi, K. Badizadegan, I. Itzkan, R. R. Dasari and M. S. Feld (2001) Imaging Human Epithelial Properties with Polarized Light-Scattering Spectroscopy. *Nature Medicine*. **7**(11), 1245-1248.

103. Sokolov, K., M. Follen and R. Richards-Kortum (2002) Optical Spectroscopy for Detection of Neoplasia. *Curr. Opin. Chem. Biol.* **6**, 651-658.

104. Sokolov, K., J. Galvan, A. Myakov, A. Lacy, R. Lotan and R. Ricards-Kortum (2002) Realistic Three-Dimensional Epithelial Tissue Phantoms for Biomedical Optics. *J. Biomed. Opt.* **71**(1), 148-156.

105. Anido, J., P. Matar, J. Albanell, M. Guzmán, F. Rojo, J. Arribas, S. Averbuch and J. Baselga (2003) ZD1839, a Specific Epidermal Growth Factor Receptor (EGFR) Tyrosine Kinase Inhibitor, Induces the Formation of Inactive EGFR/HER2 and EGFR/HER3 Heterodimers and Prevents Heregulin Signaling in HER2-overexpression Breast Cancer Cells. *Clinical Cancer Research*. **9**, 1274-1283.

106. King, I. and A. C. Sartorelli (1989) Epidermal Growth Factor Receptor Gene Expression, Protein Kinase Activity, and Terminal Differentation of Human Malignant Epidermal Cells. *Cancer Res*. **49**(20), 5677-5681.

107. Sokolov, K., M. Follen, J. Aaron, I. Pavlova, A. Malpica, R. Lotan and R. Richards-Kortum (2003) Real Time Vital Optical Imaging of Pre-cancer Using Anti-EGF Receptor Antibodies Conjugated to Gold Nanoparticles. *Cancer Res*. **63**(9), 1999-2004.

108. Hsu, E. R., E. V. Ansyln, S. Dharmawardhane, R. Alizadeh-Naderi, J. S. Aaron, K. V. Sokolov, A. K. El-Naggar, A. M. Gillenwater and R. R. Richards-Kortum (2004) A Far-red Fluorescent Contrast Agent to Image Epidermal Growth Factor Receptor Expression. *Photochem. Photobiol.* **79**(3), 272-279.

109. Nieman, L., A. Myakov, J. Aaron and K. Sokolov (2004) Optical Sectioning Using a Fiber Probe with an Angled Illumination-Collection Geometry: Evaluation in Engineering Tissue Phantoms. *Applied Optics*. **43**(6), 1308-1319.

110. Skala, M. C., G. M. Palmer, C. Zhu, Q. Liu, K. M. Vrostsos, C. L. Marsek-Stone, A. Gendron-Fitzpatrick and N. Ramanujam (2004) Investigation of Fiber-Optics Probe Designs for Optical Spectroscopic Diagnosis of Epithelial Pre-Cancers. *Lasers Surg. Med.* **34**, 25-38.

111. Inaguma, M. and K. Hashimoto (1999) Prophyrin-Like Fluorescence in Oral Cancer. *Cancer*. **86**(11), 2201-2211.

112. Trujillo, E. V., D. R. Sandison, U. Utzinger, N. Ramanujam, M. F. Mitchell and R. Richards-Kortum (1998) Method to Determine Fluorescence Efficiency *in Vivo* and Predict Signal-to-Noise Ratio for Spectrometers. *Applied Spectroscopy*. **52**(7), 943-951.

113. Pfefer, T. J., K. T. Schomacker, M. N. Ediger and N. S. Nishioka (2002) Multiple-fiber Probe Design for Fluoresence Spectroscopy in Tissue. *Applied Optics*. **41**(22), 4712-4721.

114. Baselga, J. (2001) The EGFR as a Target for Anticancer Therapy--Focus on Cetuximab. *Eur. J. Cancer*. **37**, S16-S22.

115. Boerman, O. c., F. G. v. Schaijk, W. J. G. Oyen and F. H. M. Corstens (2003) Pretargeted Radioimmunotherapy of Cancer: Progress Step by Step. *J. Nucl. Med.* **44**(3), 400-411.

116. Moro, M., M. Pelagi, G. Fulci, G. Paganelli, P. Dellabona, G. Casorati, A. G. Siccardi and A. Corti (1997) Tumor Cell Targeting wth Antibody-Avidin Complexes and Biotinylated Tumor Necrosis Factor α. *Cancer Res.* **57**, 1922-1928.

117. Reali, E., J. W. Greiner, A. Corti, H. J. Gould, F. Bottazzoli, G. Paganelli, J. Schlom and A. G. Siccardi (2001) IgEs Targeted on Tumor Cells: Therapeutic Activity and Potential in the Design of Tumor Vaccines. *Cancer Res.* **61**, 5517-5522.

118. Schechter, B., R. Arnon, M. Wilchek, J. Schlessinger, E. Hurwitz, E. Aboud-Pirak and M. Sela (1991) Indirect Immunotargeting of Cis-Pt to Human Epidermoid Carcinoma KB using the Avidin-Biotin System. *Int. J. Cancer.* **48**, 167-172.

119. Guttinger, M., F. Guidi, M. Chinol, E. Reali, F. Veglia, G. Viale, G. Paganelli, A. Corti and A. G. Siccardi (2000) Adoptive Immunotherapy by Avidin-driven Cytotoxic T Lymphocyte Tumor Bridging. *Cancer Res.* **60**, 4211-4215.

120. Wilbur, D. S., P. M. Pathare, D. K. Hamlin, P. S. Stayton, R. To, L. A. Klumb, K. R. Buhler and R. L. Vessella (1999) Development of New Biotin/Streptavidin Reagents for Pretargeting. *Biomol. Eng.* **16**, 113-118.

121. Wood, G. S. and R. Warnke (1981) Supression of Endogenous Avidin-binding Activity in Tissues and Its Relevance to Biotin-Avidin Detection Systems. *J. Histochem. Cytochem.* **29**(10), 1196-1204.

122. Moldwin, R. M. and G. R. Sant (2002) Interestitial Cystitis: A Pathophysiology and Treatment Update. *Clin. Obstet. Gynecol.* **45**, 259-272.

Vita

Elizabeth Rita Hsu was born in Abington, Pennsylvania on November 1, 1977, the daughter of An-Fei Hsu and Stephen C. Hsu. She was raised in the suburbs of Philadelphia and attended Upper Dublin High School, graduating in 1995. She then attended Stanford University, where she completed an Individually Designed Major in Bioengineering, earning her Bachelor of Science degree in 1999. In 2000, she received her Master of Science from Columbia University in Biomedical Engineering, concentrating in biomechanics. She entered the University of Texas at Austin to earn her doctorate in Biomedical Engineering in the fall of 2000.

Permanent Address: 1409 Ft. Washington Avenue, Ambler, Pennsylvania 19002

This dissertation was typed by the author.